

DISSERTATION

submitted to the

Combined Faculties for the Natural Sciences and for Mathematics

of the Ruperto-Carola University of Heidelberg, Germany

for the degree of

Doctor of Natural Sciences

presented by

Biologist Cristina Gabriela Sandu

born in Buzau, Romania

oral examination: 28.03.2006

The generation and the characterization of the  
TASK-3 knockout mice

Gutachter: Prof. Dr. Peter Seeburg  
Prof. Dr. Hannah Monyer

## Table of contents

<b>1 INTRODUCTION.....</b>	<b>1</b>
1.1 Membrane potential.....	2
1.2 Potassium channels.....	4
1.3 Two pore domain (K2P) potassium channels.....	5
1.3.1 Classification of the mammalian K2P genes.....	6
1.3.2 The expression of the K2P gene family in adult mouse brain.....	10
1.3.3 Functional Characteristics of the K2P gene family.....	13
1.4 TASK channel subfamily: TASK-1, TASK-3 and TASK-5.....	18
1.4.1 Distinguishing between TASK-1 and TASK-3 channels.....	18
1.4.2 Do TASK-1 and TASK-3 channels have a specific location on cells? Accessory proteins.....	20
1.5 K2P channels and their importance for medical pharmacology.....	22
1.5.1 K2P currents are a basis for modulation by neurotransmitters and peptides.....	22
1.5.2 Neuromodulation and TASK channels.....	23
1.5.3 Second messenger systems for modulating TASK-1 and TASK-3 channels.....	24
1.5.4 Endocannabinoids as agonists on TASK-1 and TASK-3.....	26
1.5.5 The pH sensitivity of TASK channels and their possible role in stimulating breathing during sleep.....	26
1.5.6 The role of K2P channels in homeostatic plasticity: cerebellar granule cells.....	27
1.5.7 Why are so many K2P channels expressed in the same neuronal cell?.....	28
1.5.8 K <sup>+</sup> -dependent neuronal apoptosis. A role for TASK-1 and TASK-3 channels?.....	29
1.5.9 TASK-3 gene amplified in some breast cancers.....	30
1.5.10 K2P channels and ischemia (stroke).....	31
1.5.11 K2P channels as targets for inhalational anesthetics.....	32
1.5.12 TASK-1 (and TASK-3?) channels could inhibit the spread of HIV in the brain.....	34
1.5.13 Contributions of TASK-1 and TASK-3 channels to the physiology of peripheral organs.....	34
1.6 Project aims with the TASK-3 knockout mice.....	37
<b>2 METHODS.....</b>	<b>39</b>
2.1 Generation of TASK-3 knockout mice.....	39
2.2 Breedings with deleter mice to remove neomycin gene insertions.....	41
2.3 Recombinant expression of mouse TASK-1 and TASK-3 cDNAs in HEK cells.....	41

2.3.1 Cloning of mTASK-3 cDNA .....	42
2.3.2 Cloning of mTASK-1 cDNA .....	42
2.4 In situ hybridization.....	43
2.5 Real-Time quantitative RT-PCR .....	43
2.6 Immunohistochemistry .....	44
2.7 Western blots .....	44
2.8 Electrophysiology experiments .....	45
2.8.1 Acute slice preparation .....	45
2.8.2 Patch-clamp recording from cerebellar granule cells.....	46
2.9 Behavioural studies.....	46
<b>3 RESULTS.....</b>	<b>48</b>
3.1. Expression of the TASK-1 and TASK-3 genes in the adult mouse .....	48
3.1.1 TASK-1 expression in the adult mouse brain .....	49
3.1.2 TASK-3 expression in the adult mouse brain .....	49
3.1.3 Mainly TASK-3 expressing areas/cells.....	50
3.1.4 Cell-types/areas expressing both TASK-1 and TASK-3 .....	50
3.1.5 Cell types with no detectable TASK-1 or TASK-3 expression .....	50
3.2 Electrophysiological properties of recombinant mouse TASK-1 and TASK-3 channels	58
3.3 Generation of TASK-3 knockout mice.....	60
3.3.1 Planned TASK-3 gene targeting strategy.....	61
3.3.2 Actual targeting of the TASK-3 gene: multiple targeting vector integration .....	61
3.4 Analysis of TASK-3 physiological functions using mitv-TASK3 mice .....	67
3.4.1 The mitv-TASK3 allele is not expressed: <i>in situ</i> hybridisation and real-time PCR.....	67
3.4.2 Attempts to confirm the absence of TASK-3 protein by western blotting and immunocytochemistry.....	70
3.4.3 No compensation at level of gene expression by other K2P family members for loss of TASK-3.....	72
3.4.4 Expression analysis of genes flanking the mitv-TASK3 locus.....	72
3.5 Behavioural studies of mitv-TASK3 mice .....	73
3.5.1 mitv-TASK3 mouse behaviour: motor skills .....	74
3.5.2 mitv-TASK3 mouse behaviour: acoustic startle reflex and prepulse inhibition .....	74
3.5.3 Mitv-TASK3 mouse behaviour: memory and motivation .....	75

3.6 Electrophysiological analysis of adult cerebellar granule cells lacking TASK-3 expression .....	77
<b>4 DISCUSSION .....</b>	<b>79</b>
4.1 Generation of TASK-3 knockout mice: technical considerations .....	80
4.2 Phenotype analysis of mitv-TASK3 knockout mice .....	81
4.3 Antibodies as immunohistochemical tools: knockouts as tests for antibody specificity ..	82
4.4 Dissecting the contribution of K2P channels to leak currents in vivo: cerebellar granule cells as an example .....	83
4.5 Electrophysiological properties of recombinant mouse TASK-1 and TASK-3 channels: Zn <sup>2+</sup> and ruthenium red as diagnostic agents to distinguish them .....	84
4.6 Comment on preliminary behaviour and electrophysiology data on mitv-TASK3 mice ..	85
4.7 Future plans .....	86
<b>5 APPENDIX .....</b>	<b>87</b>
5.1 “Fingerprinting” the TASK-3 BAC clones .....	87
5.2 Further details on construction of TASK-3 targeting vector .....	89
5.2.1. Shotgunning the 8Kb EcoRI exon-1 containing TASK-3 gene fragment from the BAC into pLitmus 38 .....	89
5.2.2 Changing the Sall site to a NotI site in pTASK-3EcoRI-8Kb .....	89
5.2.3 Insertion of loxP oligo into BclI site of pTASK-3EcoRI-8Kb-NotI .....	90
5.2.4 Insertion of lox-neo-lox-frt cassette into pTASK3-EcoRI-8Kb-loxP .....	90
5.3 Colony screening protocol for ligations .....	91
5.4 Southern blotting .....	91
5.4.1 Pulse-field gel electrophoresis .....	92
5.5 Southern blot membrane hybridization .....	92
5.6 Hybridization probes .....	92
5.6.1. 1 Kb intronic TASK-3 probe .....	92
5.6.2. 5’ external TASK-3 genomic probe .....	93
5.6.3. Neo probe .....	94
5.7. Mouse embryonic stem cell culture .....	94
5.8. Genotyping of mice .....	94
5.8.1. Preparation of mouse tail DNA .....	94
5.8.2. Mouse tail DNA digestion for Southern blotting .....	94
5.8.3. PCR genotyping of mice .....	95

5.9. Removal of the neomycin insertion from the mitv-TASK3 line reactivates the TASK-3 gene.....	97
5.10. List of primers .....	99
5.10.1 Sequencing primers used for targeting vector construction.....	99
5.10.2 Sequencing primers used for mTASK-3 and mTASK-1 cDNA.....	99
5.10.3 Probe primers .....	99
5.10.4 Primers for genotyping.....	100
5.11 In situ hybridization oligonucleotides .....	100
5.12 Real-time quantitative-PCR oligonucleotides .....	101
<b>6 ABBREVIATIONS .....</b>	<b>103</b>
<b>7 REFERENCES .....</b>	<b>107</b>

## 1 INTRODUCTION

A fundamental property of all living cells is the maintenance of a negative membrane potential. Signaling in electrically excitable cells depends on the existence of a polarized membrane potential in which the cell interior is negative with respect to the exterior. In neurons, the resting membrane potential controls excitability by setting the distance to the threshold for firing an action potential, the basis of communication in the nervous system.

Although it has been known for a long time that  $K^+$ -selective ion channels play a critical role in setting the resting membrane potential, the understanding of the molecular nature of these channels became clearer with the relatively recent cloning and expression of a new class of constitutively active  $K^+$  channels, the so called two-pore-domain (KCNK or K2P) potassium channels (North, 2000; Goldstein et al., 2001; Patel and Honoré, 2001a; Talley et al., 2003; Mathie and Clarke, 2002; Lesage, 2003; Franks and Honoré, 2004; Plant et al., 2005). K2P channels produce currents with all the characteristics of background (“leak”) or baseline conductances (these currents are time- and voltage-independent). Several members of the K2P gene family are highly expressed in the central and peripheral nervous systems. Detailed characterization of cloned channels revealed that they actively influence cell excitability and *in vivo* contribute directly to plasticity processes.

Two members of the K2P channel family, TASK-1 and TASK-3 were identified to be possibly involved in a long-term homeostatic regulation of cerebellar granule cell excitability (Brickley et al., 2001). This mechanism was observed in granule cells from GABA<sub>A</sub> receptor  $\alpha 6$  subunit knockout mice that do not express a tonic inhibitory membrane chloride conductance because they lack extrasynaptic GABA<sub>A</sub> receptors composed of  $\alpha 6\beta\delta$  subunits (Brickley et al., 2001). It was hypothesized that a compensatory upregulation of these TASK K2P channels leads to an adaptive regulation of cerebellar granule cell excitability (Brickley et al., 2001). Studying this compensatory mechanism is important for understanding principles of homeostatic regulation.

In the following Introduction, I first summarize briefly the basic biology of membrane potentials (section 1.1), and then concentrate on reviewing the K2P gene family (section 1.3) and the contributions of its different family members to animal physiology (sections 1.4 and 1.5); in the final part of the Introduction (section 1.6), I summarize the intentions and aims of my project regarding the generation and analysis of TASK-3 knockout mice.

## 1.1 Membrane potential

This section summarizes the core textbook knowledge on membrane potential; this knowledge, mostly gleaned from the squid giant axon, was already well worked out by the mid-1950s, culminating in Hodgkin & Huxley's work, which can be viewed truly as a foundation of the neuroscience field; accounts can be found in many books, for example "Cellular and Molecular Neurobiology" (Hammond, 2001), "Principles of Neural Sciences" (Kandel et al., 2000) and Hille's chapter "Classical Biophysics of the Squid Giant Axon" in his book "Ion Channels of Excitable Membranes" (Hille, 2001). The Hille chapter is particularly interesting for describing how this knowledge base was built up during the first 50 or so years of the twentieth century: Julius Bernstein in 1902 first postulated a selective potassium permeability in excitable cell membranes and according to Hille "may be credited with opening the road to the discovery of  $K^+$  channels"; Ludimar Hermann in 1905 formulated the concept of "Strömchen" (small currents) circulating in axons and made the correct suggestion that propagation is an electrical self-stimulation. Here I condense the key facts to set the scene for discussion of the  $K_2P$  channels in the later sections.

Nerve cells generate electrical signals that transmit information. Neurons have evolved elaborate mechanisms for generating electrical signals based on the flow of ions across their plasma membranes. The current flow is controlled by ion channels in the cell membrane. There are two types of ion channels: resting ("leak") and gated channels (Hille, 2001). The plasma membrane of nerve cells consists of a mosaic of lipids and proteins. The membrane is formed by a double layer of phospholipids in which are embedded the integral membrane proteins, including ion channels. Every neuron has a separation of charges across its cell membrane. At rest a nerve cell has an excess of negative charge on the inside. The charge separation gives rise to a difference of electrical potential (voltage) across the membrane called membrane potential. The membrane potential of a cell at rest is called the resting membrane potential. Its usual range in neurons is  $-60$  mV to  $-75$  mV. At the resting membrane potential the cell is not in equilibrium but rather in a steady state: there is a continuous passive influx of  $Na^+$  and efflux of  $K^+$  through resting ("leak") channels that is exactly counterbalanced by the  $Na^+ - K^+$  pump.  $Na^+$  and  $K^+$  leak channels allow ions to diffuse selectively down their respective concentration gradients whereas the  $Na^+ - K^+$  pump moves  $Na^+$  and  $K^+$  against their net electrochemical gradients: it extrudes three  $Na^+$  ions from the cell and takes in two  $K^+$  ions using the energy from the hydrolysis of one molecule of ATP. The unequal flux of  $Na^+$  and  $K^+$  ions causes the pump to generate a net outward ionic

current that tends to hyperpolarize the membrane to a more negative potential than that which would be achieved by the simple passive-diffusion alone. At rest, the membrane potential is close to the equilibrium potential for  $K^+$  (-75 mV), the ion to which the membrane is most permeable (Table 1).

<b>Species of ion</b>	<b>Concentration in cytoplasm (mM)</b>	<b>Concentration in extracellular fluid (mM)</b>	<b>Equilibrium potential (mV)</b>
$K^+$	150	5	-75
$Na^+$	5-15	145	+50
$Cl^-$	4-30	110	-60

*Table 1. Distribution of the major ions across a membrane at rest in the mammalian neuron (Kandel et al., 2000)*

When a neuron sends information down an axon an action potential occurs. Action potentials are mediated by sequential opening of voltage-gated  $Na^+$  and  $K^+$  channels. In the presence of a stimulus the membrane potential can depolarise to a threshold level. The voltage-gated  $Na^+$  channels can detect this change and open, initiating an action potential. During this depolarisation phase the membrane potential is driven towards the equilibrium potential for  $Na^+$  (+50 mV). At this point, voltage-gated  $Na^+$  channels start to close (inactivation) and the voltage-gated  $K^+$  channels open, causing an outflow of  $K^+$  ions. This restores the initial membrane potential (-75 mV) (repolarization phase). In most nerve cells the action potential is followed by a transient hyperpolarization, the after-potential. The resting membrane potential is then restored by the  $Na^+-K^+$  pump and leak channels.

Hodgkin and Huxley, in their models predicted the existence of a potassium leak current which was voltage-independent. Nevertheless, although starting in the late 1980s many potassium channels (e.g. voltage-gated channels) and many other ion channels were cloned so that Hodgkin's and Huxley's action potential model could be explained by actual identified channels (reviewed Hille, 2001, Chapter 3), the potassium channels that could explain the leak conductance remained elusive. According to North (North, 2000), people just either forgot about leak channels, or assumed that the leak potassium current was due to an already cloned channel family such as the inward rectifier potassium channels. True leak channels were not actually

cloned until the mid 1990s, thus representing the last major family of potassium channels to be characterized (see next section).

## 1.2 Potassium channels

Potassium channels are found in all phyla, including bacteria (Hille, 2001). Eukaryotic potassium channels are ubiquitous multisubunit membrane proteins that participate in a large number of cellular functions, from the epithelial transport in the kidney, the regulation of cardiac electrical patterns, to signal transduction pathways in neurons (Hille, 2001).  $K^+$  channels form the most diverse family of ion channels with 118 genes cloned or predicted from the human genome and 124 genes cloned or predicted from the mouse genome (<http://www.ncbi.nlm.nih.gov>). The  $K^+$  channel subunits can be grouped into three structural classes (Figure 1) made of two, four or six transmembrane domains (TM) (Hille, 2001; Patel and Honoré, 2001a). All  $K^+$  channel subunits can be recognized by the presence of a conserved motif (signature sequence) called the P domain. The P domain is the pore-forming region, a short amino-acid segment between two transmembrane helices that dips into the membrane without fully crossing it; a typical P loop consensus sequence is -TXXTXGYGD-, which is part of the  $K^+$  conduction pathway (Hille, 2001, Chapter 5). The residues TXGYG, repeated in the four subunits of a typical K channel, line the selectivity filter. In 1998 Roderick MacKinnon's laboratory crystallized and solved the structure of the bacterial KcsA K channel (Doyle et al., 1998), a major achievement as intact ion channels are notoriously difficult to crystallize and obtain structure from. According to Hille, "the importance of this structure cannot be underestimated, as it is the first direct view of the structural blueprint of a member of the Na-Ca-K superfamily of channels" (Hille, 2001, Chapter 5). The conducting pore of KcsA is an excellent model of eukaryotic  $K^+$  channels. In the crystal structure of KcsA, the P loop residues -TVGYG- line the narrowest part of the pore near the fourfold axis of symmetry. For this and subsequent work on  $K^+$  channel structure, MacKinnon was awarded the Nobel Prize in 2003. This group's latest achievement concerns solving the structure of voltage-gated  $K^+$  channels (Long et al., 2005).

In eukaryotes, the simplest potassium channel structure belongs to members of the Kir family, which generate  $K^+$  currents that are inwardly rectifying (they conduct current more effectively in the inward direction). Each subunit includes two transmembrane domains surrounding a P domain (Figure 1). These subunits form channels as tetramers, with four P domains combining to create a single ion-conducting aperture. Subunits from the KV family, which typically generate

voltage-gated currents, also form tetramers, with each subunit containing six transmembrane domains and one P domain (Figure 1) (Long et al., 2005). Some calcium-activated  $K^+$  channels ( $K_{Ca}$ ) have a similar structure but contain an extra transmembrane domain. As indicated by their name, two-pore-domain channel subunits contain two P domains (P1 and P2) and four transmembrane domains (TM1-TM4) (Figure 1); these subunits form channels by joining together as dimers. Most members of this third family generate currents with little voltage or time dependence, thus creating leak  $K^+$  channels. The abundance of leak currents in a given cell will determine important aspects of its excitability such as the resting membrane potential, the repolarizing effect, and the resistance to depolarization.

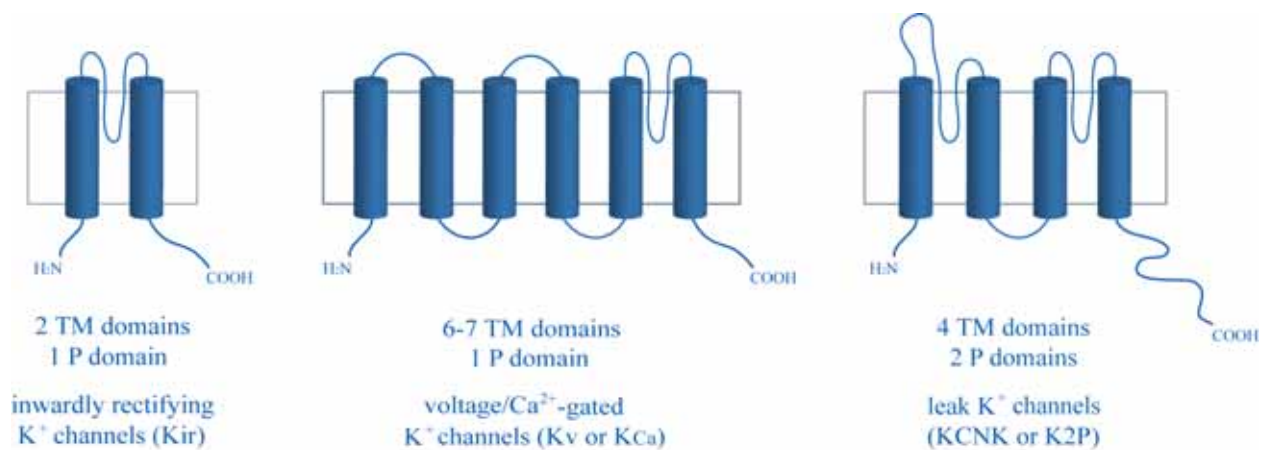


Figure 1. Topology of the three main structural classes of eukaryotic  $K^+$  channels (adapted from Talley et al., 2003)

### 1.3 Two pore domain (K2P) potassium channels

The first cloned  $K^+$  channel with electrophysiological properties resembling background  $K^+$  currents was the yeast  $K^+$  channel TOK1, “that contains two P domains within one continuous polypeptide”, identified by Steven Goldstein and collaborators (Ketchum et al., 1995). Subsequently, the same research group also isolated a *Drosophila* two-pore domain  $K^+$  channel, ORK1 (Goldstein et al., 1996). These channels produced pure leak currents and were different from the other previously identified  $K^+$  channels in having two pore-forming sequences (P domains) present within the primary amino acid sequence (the yeast TOK1 channel has a subunit

structure that so far is unique, because it has eight transmembrane domains instead of four (Ketchum et al., 1995). Another early report of two-pore domain K<sup>+</sup> channel genes came from the sequencing analysis of the nematode *Caenorhabditis elegans* genome (Wei et al., 1996): a total of 40 K2P genes has been identified in the worm, many more than in the vertebrates (section 1.3.1); in fact, K2P channel genes account for more than half of the K<sup>+</sup> channel genes in *C. elegans*; each worm K2P gene has a distinct expression pattern (Salkoff et al., 2001). Salkoff and collaborators concluded that “in *C. elegans* single neurons may serve the functional roles of millions of neurons (or even an entire brain region) in a higher animal. In mammals, it is of course not feasible to treat each neuron as a genetically discrete unit and assign a unique gene to each. *C. elegans* may maintain an exceptionally large inventory of these (K2P) channels as an adaptive mechanism to fine tune individual neurons, making the most of its limited circuitry (of 302 neurons)”.

### **1.3.1 Classification of the mammalian K2P genes**

Currently there are in use three nomenclature systems for the description of the mammalian K2P channels (Figure 2). One has been provided by the Human Genome Organization (HUGO) (<http://www.hugo-international.org>) which has assigned the prefix KCNK, followed by different numbers for each gene (KCNK<sub>x</sub>); these numbers resulted from the order in which each gene was discovered, so they do not reflect any classification by sequence or function. However, despite the fact that there are described 15 human genes encoding for two-pore domain K<sup>+</sup> channels, HUGO nomenclature numbering series, from KCNK1 to KCNK18, contains gaps.

A second nomenclature system was introduced by the International Union of Pharmacology (IUPHAR) by replacing the HUGO nomenclature system KCNK<sub>x</sub> with K2P<sub>x.1</sub> (<http://www.iuphar-db.org/iuphar-ic/>) (Gutman et al., 2003).

The most popular nomenclature system utilizes acronyms (e.g. TASK) that are derived from salient physical features of the cloned channels (Figure 2). The acronym nomenclature is actually by far the easiest to use, in spite of attempts by various senior investigators in the field to impose the K2P gene terminology; with an acronym one remembers what one is talking/reading about, whereas with the K2P nomenclature, and given the large size of this gene family with at least 15 members, it is easy to become confused with which particular K2P gene one is describing. Thus, other than “K2P” as a generic designator of the entire gene family, I mostly use the acronym terminology throughout this thesis.

The K<sub>2</sub>P channels can be grouped into six distinct subfamilies (Figure 2):

**TWIK:** tandem of P domains in a weak inwardly rectifying K<sup>+</sup> channel: 3 members

**THIK:** tandem pore domain halothane-inhibited K<sup>+</sup> channel: 2 members

**TREK:** TWIK-related K<sup>+</sup> channel: 3 members

**TASK:** TWIK-related acid-sensitve K<sup>+</sup> channel: 3 members

**TALK:** TWIK-related alkaline pH activated K<sup>+</sup> channel: 3 members

**TRESK:** TWIK-related spinal cord K<sup>+</sup> channel: 1 member

The family of human K<sub>2</sub>P channel subunit genes has 15 members (Gutman et al., 2003; Sano et al., 2003, Kang et al., 2004a) (Figure 2). A map of the human chromosomal localization of these genes is represented in Figure 3.

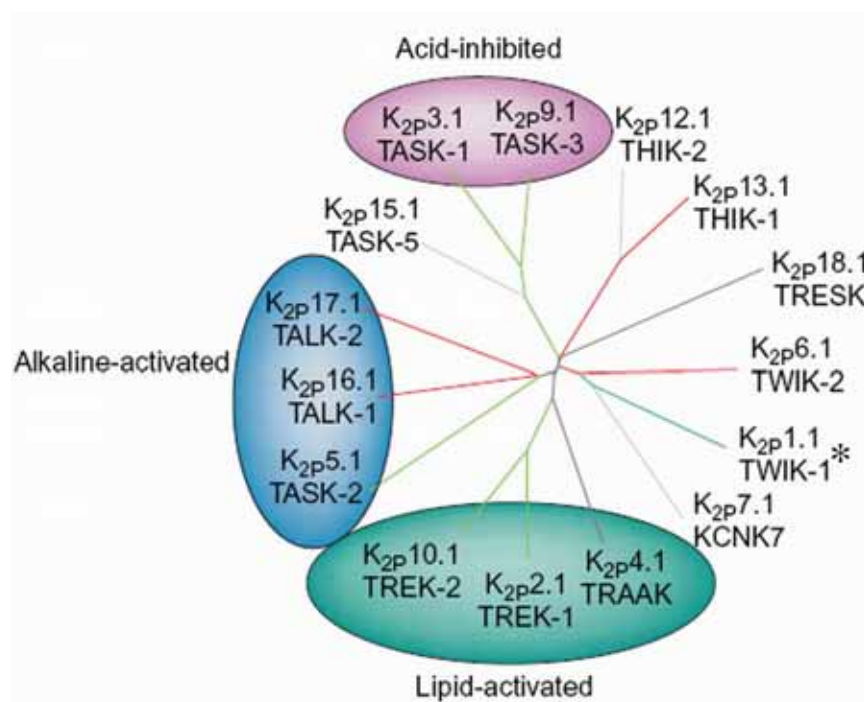


Figure 2: The human two-pore domain K<sup>+</sup> channel subfamilies

The 15 known human two-pore-domain K<sup>+</sup> channel genes are presented in a phylogenetic tree, demonstrating their division into six structural and functional subfamilies. The subgroups are represented in different colors; genes that have not produced functional channels are shown by gray connecting lines. \*TWIK-1 functions when unsumoylated (Rajan et al., 2005) (adapted after Franks and Honoré, 2004).

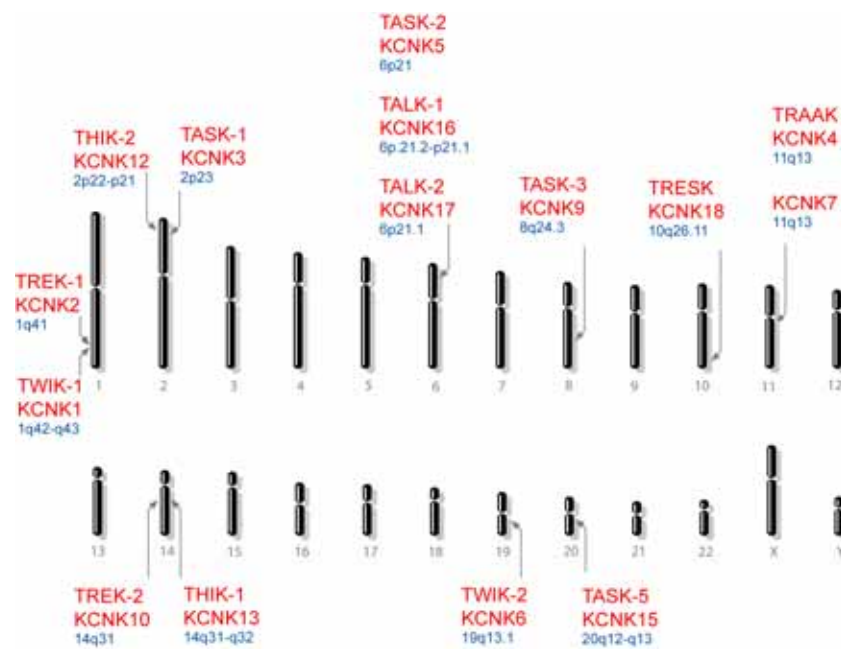


Figure 3. Chromosomal localisation of human K2P channel subunit genes

From the NCBI Genome Database, <http://www.ncbi.nlm.nih.gov>.

In the mouse genome, there are 14 K2P channel genes identified, an alignment that I made of their predicted peptide sequences is shown in Figure 4; in other vertebrate species such as Puffer fish (*Fugu rubripes*), putative orthologues are also identifiable (10 predicted genes).

Some genes such as TRESK are highly divergent between mammals, showing relatively poor sequence conservation (60% identity at the amino acid level). These genes have possibly been wrongly annotated by investigators, for example TRESK-2 (mouse) (Kang et al., 2004a) and TRESK-1 (human) (Sano et al., 2003), when in fact there is only one TRESK gene in each species. Further, from the human there are two TALK genes (TALK-1 and TALK-2), but in the mouse there seems to be only one.

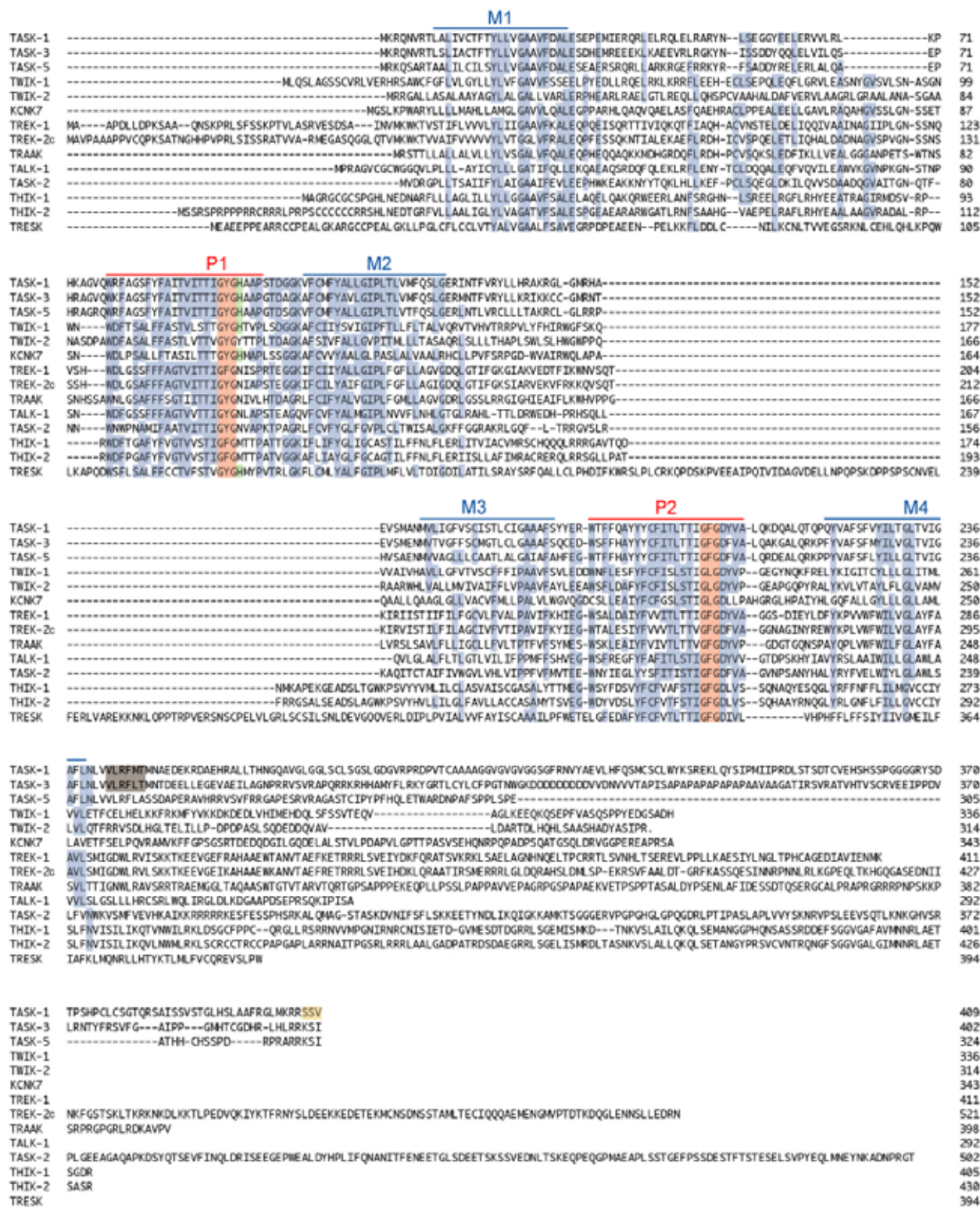


Figure 4. Amino acid alignment of the 14 known mouse K2P genes

The mouse K2P sequences were obtained from the NCBI Genome Database (<http://www.ncbi.nlm.nih.gov/genome/guide/mouse/>) and aligned with MegAlign. Transmembrane (M1-M2) and pore (P1 and P2) domains are indicated. Colours of filled boxes indicate as follows: blue, conserved amino acids, red, K<sup>+</sup> selectivity filter; dark green, pH sensitivity histidine residue; dark grey, anesthetic-responsive sequence; orange, p11 association motif

Considering the mammalian K2P subunits as a general class, these all share the same structural motif (Figure 1 and Figure 4) with four transmembrane domains (TM1-TM4), an extended TM1P1 extracellular loop, and both the amino- and carboxy-termini intracellular but low sequence identity is found outside the P domains (see also Figure 19 in the Results section). The amino acid motif that composes the classical selectivity filter of a potassium channel is GYG. The 2P domain K<sup>+</sup> channels present two motifs: P1 and P2. Most P1 domains contain a GYG motif, except TREK-1, THIK-1 and THIK-2, which contain a GFG motif. Most P2 domains contain a GFG, except TWIK-1, TWIK-2 and KCNK7 that contain an unusual GLG motif (Figure 4).

### 1.3.2 The expression of the K2P gene family in adult mouse brain

All channel members of the K2P family seem to associate as dimers (reviewed in Plant et al., 2005); whether most channels are homodimers (e.g. TWIK-1/TWIK-1) or are sometimes heterodimers (e.g. TASK-1/TASK-3) is an open question. Indeed, TASK-1 and TASK-3 can be physically expressed as a contiguous open reading frame (e.g. Czirják and Enyedi, 2002a; Clarke et al., 2004). The electrophysiological properties of the K2P channels are summarized in Table 2. Further details on channel function are found in section 1.3.3.

Within the K2P gene family, only certain members (TASK-1, TASK-3, TREK-1, TREK-2, TWIK-1, THIK-1, THIK-2 and TRAAK), as detected by *in situ* hybridisation with K2P gene-specific oligonucleotides, are expressed significantly in the adult mouse brain (Aller et al., 2005) (Figure 5) and rat brain (Talley et al., 2001). As is common with gene families of this type, each gene member is differentially transcribed depending on cell type, and thus there are overlapping but distinct patterns of expression for each gene (Figure 5). Thus some cell types, for example cerebellar granule cells express multiple K2P genes, giving rise to the possibility of heteromeric assembly among members. Other cell types seem to have mainly one type of K2P gene expressed, for example mainly TASK-3, and in these cell types one would expect TASK-3 homomeric channels to form.

Cerebellar granule cells are the primary sites of TASK-1 gene expression (Figure 5), followed by the raphe nuclei, the olfactory bulb granule cells and brainstem trigeminal motor nuclei with considerably weaker TASK-1 gene expression in neocortex and thalamus. TASK-3 mRNA is more widely distributed throughout the brain than TASK-1 with strong expression in cerebellar granule cells, hippocampal dentate granule cells, olfactory bulb granule cells and periglomerular cells, CA1 pyramidal cells, layers II and VI of neocortex, inferior colliculi, raphe nuclei, motor

Family	Subunits	Conductance (pS)	I/V curve in normal K <sup>+</sup>	I/V curve in symmetrical K <sup>+</sup>	General characteristic
TWIK	TWIK-1*	32	Outward rectifier	Outward rectifier	
	TWIK-2	<5	Inward rectifier	Inward rectifier	
	KCNK7	nonfunctional	-	-	
THIK	THIK-1		Outward rectifier	Weak inward rectifier	Halothane inhibited
	THIK-2	nonfunctional	-	-	
TREK	TREK-1	48	Outward rectifier	Saturating at negative potentials	Arachidonic acid Strech sensitive
	TRAAK	46	Outward rectifier	Linear	
	TREK-2	68	Outward rectifier	Linear / Outward rectifier	
TASK	TASK-1	14	Outward rectifier	Linear	Acid-inhibited
	TASK-3	27	Outward rectifier	Outward rectifier	
	TASK-5	nonfunctional	-	-	
TALK	TASK-2	15	Outward rectifier	Saturating at negative potentials	Alkaline-activated
	TALK-1		Outward rectifier	Linear	
	TALK-2		Outward rectifier	Saturating at negative potentials	
TRESK	TRESK		Outward rectifier	Saturating at negative potentials	-

Table 2. The electrophysiological properties of the K2P channels

\*TWIK-1 was initially characterized as an inward rectifier (Lesage et al., 1996b), with a unitary conductance of 19pS. The studies of Rajan et al., 2005, showed that unsumoylated TWIK-1 has properties of a typical background K<sup>+</sup> channel.

nuclei, and large interneurons (putative cholinergic) in the caudate-putamen (a detailed mapping of the expression of TASK-1 and TASK-3 genes is shown in Results chapter, section 3.1 “Expression of the TASK-1 and TASK-3 genes in the adult mouse brain”).

TREK-2 and THIK-2 genes have expression patterns broadly similar to TASK-1 in the mouse brain, with their highest sites of expression occurring in cerebellar granule cells, followed by olfactory bulb granule cells (Figure 5). However, there are clear differences in the expression of these genes. For example, TREK-2 and THIK-2 are not clearly evident in the raphe or motor nuclei although TASK-1 and TASK-3 have strong expression in these areas. TREK-1 has its highest expression in the caudate-putamen, with a striking lateral to medial expression gradient in that structure, and two marked expression layers in the neocortex (Figure 5). THIK-1 is specifically expressed in the white matter tracts of the cerebellum, and possibly in other brain regions, at about the same low intensity as its expression in cerebellar granule cells (THIK-1’s highest expression in mouse brain is the olfactory bulb granule cells).

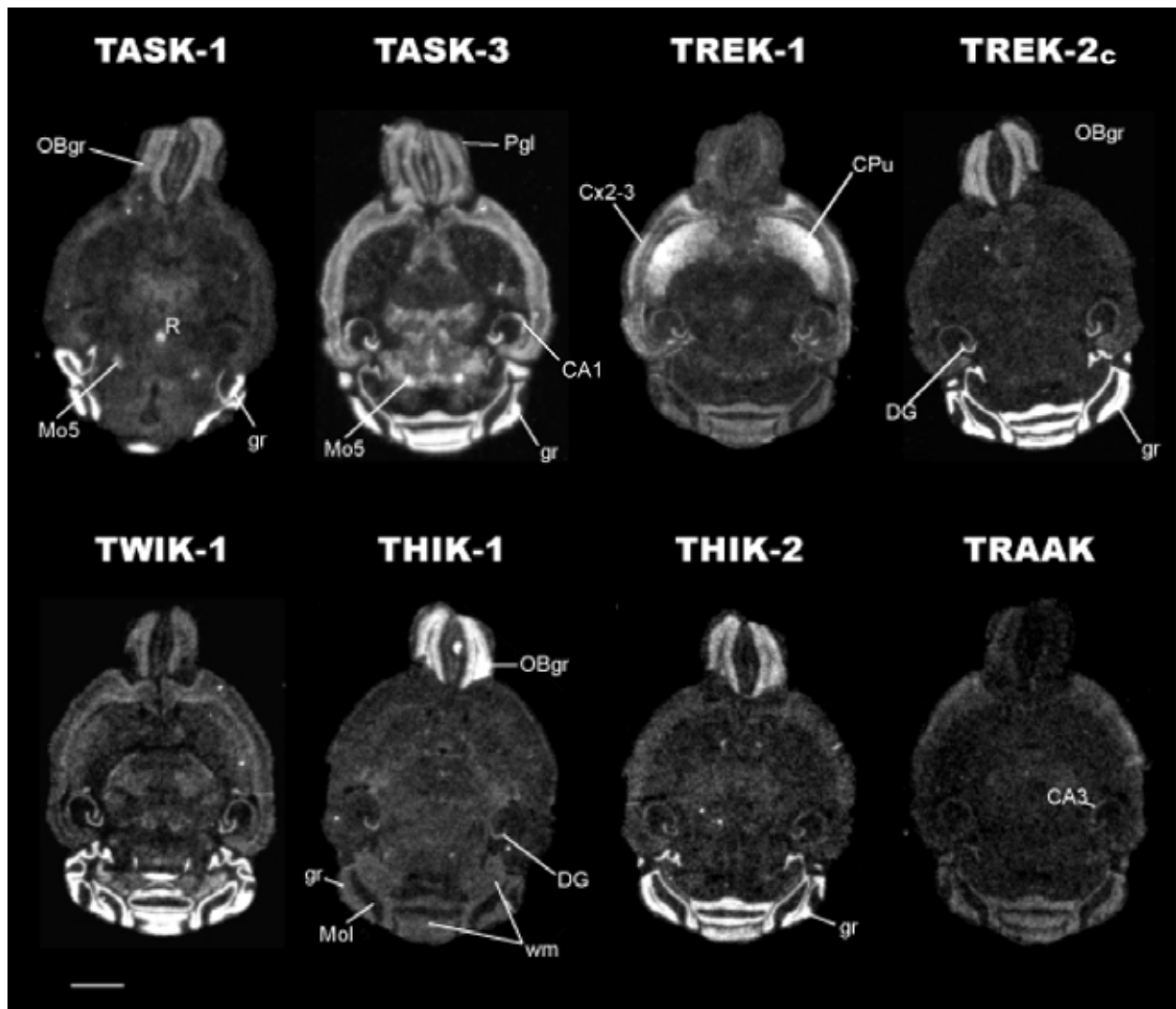


Figure 5. *In situ* hybridization of K2P gene family members expressed in the adult mouse brain TASK-1, TASK-3, TREK-1, TREK-2, TWIK-1, THIK-1, THIK-2 and TRAAK.

X-ray film autoradiographs indicating CA1- CA1 pyramidal cells, CA3- CA3 pyramidal cells, CPu- caudate-putamen, Cx2-3- layers II and III of neocortex, DG- hippocampal dentate granule cells, gr- cerebellar granule cells, Mo5- motor nucleus V, OBgr- olfactory bulb granule cells, Pgl- olfactory bulb periglomerular cells, R- raphe nuclei, wm- white matter. The TRAAK signal was obtained after three times longer exposure. Only TREK-2c isoform is detected in the brain. Scale bar, 2 mm. (adapted from Aller et al., 2005)

Another feature worth noting for the mouse brain is that TASK-3 expression is quite similar to TWIK-1 (a possibility of heteromeric association), with the notable exceptions of the caudate-putamen and septum. Relative to the other K2P genes described here, the TRAAK gene seems barely expressed in the mouse brain, with expression mainly at a low level in CA3 pyramidal

cells (Figure 5), a quite different expression profile from that reported for the rat (Talley et al., 2001).

### 1.3.3 Functional Characteristics of the K2P gene family

#### **TWIK channel subfamily: TWIK-1, TWIK-2 and KCNK7**

TWIK-1 (KCNK1) was the first mammalian K2P family member to be described in 1996 by Lesage and collaborators, with a high expression in the brain and in the heart (Lesage et al., 1996b). TWIK-1 and the related TWIK-2 (KCNK6) were described to generate inwardly rectifying currents at the whole-cell level (Lesage et al., 1996b; Chavez et al., 1999; Patel et al., 2000). TWIK channels are widely distributed in human tissues; TWIK-1 mRNA is particularly abundant in cerebellar granule cells (Talley et al., 2001; Aller et al., 2005) (Figure 5) whereas TWIK-2 expression is almost absent in the brain (Chavez et al., 1999). KCNK7, another member of this structural subfamily, is mainly expressed in the human brain (Salinas et al., 1999). This subunit gene is alternatively spliced into five mRNAs that code for three protein forms with truncated cytoplasmic carboxyl termini; none of these isoforms can generate channel activity by themselves. A site for Ca<sup>2+</sup> calmodulin kinase II at the cytoplasmic N-terminal tail could confer to KCNK7 an indirect regulation by Ca<sup>2+</sup> (Salinas et al., 1999).

An interesting controversy has arisen concerning the properties of TWIK-1. Various groups were unable to reproduce the original functional data of Lesage et al., 1996b, and it was considered a non-expressing channel at least in *Xenopus* oocytes or HEK cells (Rajan et al., 2005). However, recently TWIK-1 was found to be a target of the small ubiquitin-related modifier protein called SUMO (Rajan et al., 2005). Sumoylation, the covalent modification of substrate proteins with SUMO on lysine residues, is a reversible, posttranslational modification that was initially observed with nuclear proteins and implicated in nuclear import/export and transcriptional activity (Muller et al., 2001; Melchior et al., 2003). This process, originally thought to be active only in the nucleus, occurs at the plasma membrane to control TWIK-1 channel function (Rajan et al., 2005). Briefly, sumoylation is a three-step process (Figure 6) (Marx, 2005). The SUMO pathway begins with a SUMO-activating enzyme (E1), which carries out an ATP-dependent activation of the SUMO C-terminus and then transfers activated SUMO to a SUMO-conjugating enzyme (E2), e.g. Ubc-9. SUMO is then transferred from Ubc9 to the substrate with the assistance of a SUMO-protein ligase (E3). Yeast-two-hybrid analysis, immunohistology and biochemical studies showed that the TWIK-1 channel interacts with Ubc-9 at the plasma membrane (Rajan et al., 2005). TWIK-1 is modified by SUMO only at the  $\epsilon$ -amino group of

lysine residue (K274). Also, the covalent linkage of SUMO to K274 can be reversed by the specific desumoylating protease SENP1 (Rajan et al., 2005).

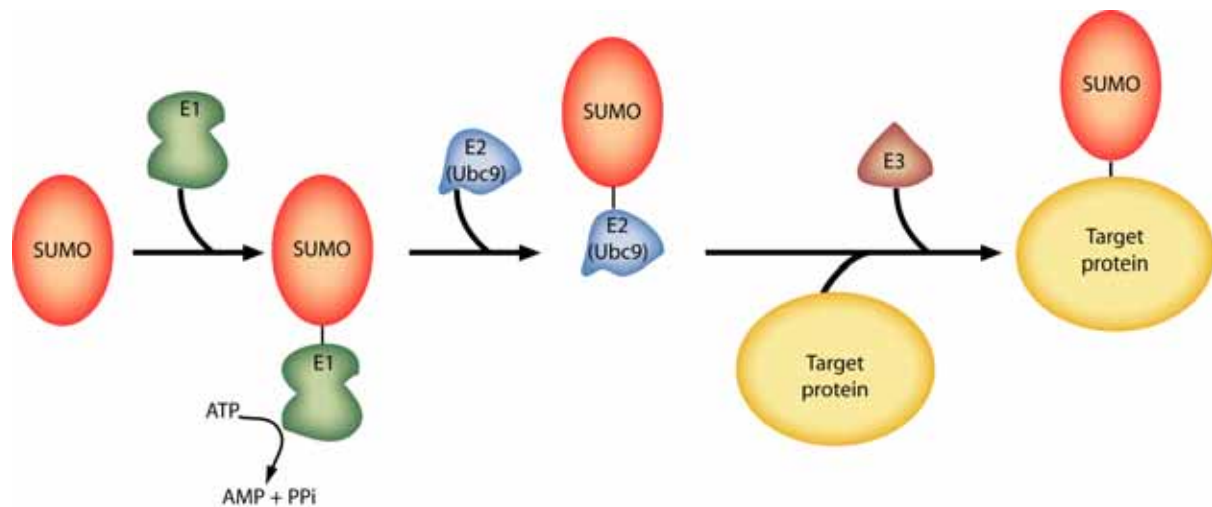


Figure 6. Sumoylation process

In the first step SUMO is attached to the E1 activating enzyme. Then SUMO is transferred to the E2 conjugating protein (Ubc9) and from there an E3 ligase directs it to its target protein (e.g. TWIK-1). (adapted after Marx, 2005)

*Xenopus* oocyte studies revealed that TWIK-1 channels are silent when sumoylated and active when SUMO is absent. The active TWIK-1 channel generates large outward currents under physiological conditions and functions as a typical background  $K^+$  channel (32pS unitary conductance).

### **THIK channel subfamily: THIK-1 and THIK-2**

THIK-1 (KCNK13) and THIK-2 (KCNK12) were cloned in 2001 by Rajan and collaborators, showing 58% identity at the amino acid level (Rajan et al., 2001). The whole-cell current induced by heterologous expression of THIK-1 in *Xenopus* oocytes displayed outward rectification at physiological external  $K^+$  and weak inward rectification with symmetrical  $K^+$  concentrations (Rajan et al., 2001). Also, as indicates its name (see page 7), THIK-1 is inhibited by halothane (Rajan et al., 2001). The other member of this subfamily, THIK-2 did not functionally express (Rajan et al., 2001; Girard et al., 2001). Although both THIK-1 and THIK-2 are targeted to the outer membrane, co-injection of THIK-2 mRNA in *Xenopus* oocytes does not affect the currents induced by THIK-1, indicating that the two channel subunits do not form

heterodimers (Rajan et al., 2001). *In situ* hybridization shows little overlap between THIK-1 and THIK-2 mRNA expression in the brain, which also argues against heteromerization (Rajan et al., 2001; Aller et al., 2005) (Figure 5). The recently described sumoylation of TWIK-1 (Rajan et al., 2005) suggests that THIK-2 might also be a target of a SUMO protein that silences the channel. If so, desumoylation could turn THIK-2 into a functional channel and its electrophysiological properties could be revealed.

### **TREK channel subfamily: TREK-1, TREK-2 and TRAAK**

TREK-1 (KCNK2) was cloned by Fink et al., 1996, and shares most of the properties of the *Aplysia* S-type  $K^+$  channel (Patel et al., 1998). The TREK-1 gene has two paralogues, TREK-2 (KCNK10) (Bang et al., 2000; Lesage et al., 2000b) and TRAAK (TWIK-related arachidonic acid-stimulated K<sup>+</sup> channel) (KCNK4) (Fink et al., 1998; Lesage et al., 2000a, Maingret et al., 1999a). The TREK-1 channel is inhibited by fluoxetine (an antidepressant drug, commercially known as Prozac) and its active metabolite norfluoxetine (Kennard et al., 2005). TREK subfamily channels are activated by polyunsaturated fatty acids (PUFA) (Fink et al., 1998; Kim et al., 2001a; Kim et al., 2001b), lysophospholipids (LPL) (Maingret et al., 2000; Chemin et al., 2005) and increased membrane tension (Maingret et al., 1999a; Maingret et al., 1999b; Patel et al., 1998; Bang et al., 2000). TREK-1 and TREK-2c splice form are the principal family members expressed in brain (Figure 5) The TREK-2 channel gene has three alternatively N-terminal spliced isoforms (TREK-2a, TREK-2b and TREK-2c) with clearly distinct expression patterns (TREK-2b is expressed in kidney and pancreas and TREK-2c is mainly expressed in the cerebellar granule cells) (Gu et al., 2002; Aller et al., 2005)) (Figure 5). Heterologous expression studies on TREK-2a (Lesage et al., 2000b) and TREK-2b and TREK-2c (Gu et al., 2002) showed that their physiological characteristics are similar. It is possible that TREK-1 and TRAAK also have N-terminal splice variants. TREK-1 and TREK-2, unlike TRAAK, are strongly inhibited by protein kinase C (PKC) stimulation (Fink et al., 1996; Maingret et al., 2000; Gu et al., 2002).

Modulation of TREK-1 via protein kinase A (PKA) changes the electrophysiological properties of this channel: TREK-1 reversibly interconverts between a leak and voltage-dependent channel (Bockenhauer et al., 2001, Plant et al., 2005). Thus, TREK-1 is an open rectifier when the PKA site (serine 348) is not phosphorylated or is mutated to alanine, passing large currents both inward and outward in symmetrical  $K^+$  conditions and larger outward currents under physiological conditions. Conversely, phosphorylated channels and those altered to aspartate at the PKA site, pass more outward current even in symmetrical  $K^+$  because of voltage-dependent changes in open probability. This phenotypic conversion, if it occurs *in vivo*, should enhance

excitability because less  $K^+$  leak enables depolarization to reach the firing threshold, whereas activation at supra-threshold potentials facilitates recovery and repetitive re-firing (Bockenhauer et al., 2001; Plant et al., 2005).

TREK-1 might play important roles during metabolically stressed conditions when intracellular levels of free fatty acids and protons are elevated, and cell swelling occurs. This idea is supported by on TREK-1 knockout mice (Heurteaux et al., 2004). TREK-1 knockout mice have an increased sensitivity to epilepsy and brain and spinal cord ischemia (the neuroprotective action of polyunsaturated fatty acids is hypothesized to be lost), whereas TRAAK knockout mice showed no increased sensitivity to ischemia or epilepsy (Heurteaux et al., 2004), most likely because TRAAK is little expressed in the mouse brain (Figure 5).

### **TALK channel subfamily: TALK-1, TALK-2 and TASK-2**

“TWIK-related alkaline pH activated  $K^+$  channel” describes the group of K2P channels which generate background  $K^+$  currents that are increased by external alkalization in the physiological range of pH. This subfamily includes TASK-2 (KCNK5) (Reyes et al., 1998), TALK-1 (KCNK16), and TALK-2/TASK-4 (KCNK17) (Girard et al., 2001). The TALK channels are not expressed in the brain, but seem to be mainly expressed in pancreas; the human TALK genes have a binary organization; the 3' end of the TALK-1 channel open reading frame is separated by less than 1 Kb from the 5' end of the TALK-2 open reading frame; this tight clustering suggests that their transcription will be under the control of common promoter elements, and that TALK-1 and TALK-2 assemble heteromerically (Girard et al., 2001). As mentioned above, in the mouse there appears to be only one TALK gene.

TASK-2 is not expressed significantly in the brain by RNA analysis such as RT-PCR (Reyes et al., 1998), Northern blot analysis (Warth et al., 2004) and *in situ* hybridization (Aller et al., 2005) or lacZ expression from a TASK-2 gene trap (Aller et al., 2005), although an antibody of unproven specificity has indicated its strong expression in brain (Gabriel et al., 2002) (see Discussion section 4.3 “Antibodies as immunohistochemical tools: knockouts as tests for antibody”). TASK-2 is strongly expressed in kidney and liver (Reyes et al., 1998; Warth et al., 2004). Evidence concerning the roles of TASK-2 channel came from *in vivo* and *in vitro* studies on TASK-2 knockout mice (Gerstin et al., 2003; Barriere et al., 2003; Warth et al., 2004) which were generated by gene trapping. As well as extracellular alkaline pH, TASK-2 is activated by cell swelling and is involved in volume regulation of native renal proximal tube cells, being the main  $K^+$  conductance involved in the regulatory volume decrease in proximal convoluted tubule cells (Barriere et al., 2003). Warth and collaborators investigated the effects of TASK-2 on ion

transport in the kidney. In primary cultured proximal tube cells (involved in renal bicarbonate reabsorption) TASK-2 is responsible for a large  $K^+$  conductance during activation of bicarbonate transport (Warth et al., 2004). The TASK-2 knockout mice have a reduced arterial blood pressure that could be caused by enhanced renal salt loss. The acid-base status of TASK-2 knockout mice was similar to that in patients suffering from isolated proximal renal tubular acidosis (Warth et al., 2004).

### **TRESK channel subfamily: TRESK**

**TRESK** (TWIK-related spinal cord  $K^+$  channel) (KCNK18) is a K2P channel expressed primarily in spinal cord (Sano et al., 2003). By RT-PCR and real-time PCR TRESK can also be weakly detected in other brain regions (Czirjak et al., 2004; Kang et al., 2004a; Aller et al., 2005), but we could not detect its expression by *in situ* hybridization (Aller et al., 2005). TRESK shows outward rectification and functions as a typical background  $K^+$  channel (Sano et al., 2003; Czirjak et al., 2004; Kang et al., 2004a). Its currents can be inhibited by unsaturated fatty acids and extreme acidification (40% inhibition at pH 5.6) (Sano et al., 2003). TRESK is activated by cytoplasmatic  $Ca^{2+}$  through calcineurin (calcium/calmodulin-dependent protein phosphatase) (Czirjak et al., 2004). Thus may hyperpolarize the membrane potential in response to different stimuli increasing the cytoplasmic calcium concentration.

Mammalian TRESK genes show relatively poor sequence conservation (60%). The non-conservation of amino acid sequence between rodent and human would suggest either that the TRESK gene is important, and has undergone a positive selection pressure accounting for differences in function, for example, of primate and rodent nervous systems; or, alternatively, that this is an unimportant gene, as there has been no selection pressure to conserve the gene sequence and it is drifting in sequence space, on the way to becoming a dead pseudogene.

In the next sections of the Introduction, I devote the most space to reviewing the TASK-1 and TASK-3 channels, these being the subject of my thesis

#### **1.4 TASK channel subfamily: TASK-1, TASK-3 and TASK-5**

TASK-1 (KCNK3) was discovered by Duprat et al., 1997. In 2000, Kim et al. cloned the rat TASK-3 (KCNK9) channel from a cerebellum cDNA library. The deduced protein shares 54% sequence identity with TASK-1 (Duprat et al., 1997). The other mammalian TASK family member is the as yet non-functional (in recombinant systems) TASK-5 (KCNK15), which has 51% amino acid sequence identity with TASK-1 and TASK-3 (Kim et al., 2001; Ashmole et al., 2001; Karschin et al., 2001). The TASK-1 and TASK-3 channel genes have stayed highly conserved in animal evolution with putative orthologues recognizable in *C. elegans*: the worm TASK-1 orthologue (n2P20) and TASK-3 orthologue (n2P38) are both expressed in nerve and muscle (Salkoff et al., 2001). [On the subject of TASK channel evolution, one exotic fact to emerge recently concerns “molecular piracy”: the N-terminal region of TASK-1 is 56% identical with the HIV accessory protein Vpu-1 (Hsu et al., 2004), with the conservation stretching from the N-terminus through to the end of TM1. TASK-1 and Vpu-1 physically interact in cultured cells and AIDS lymphoid tissues; it could be that an evolving HIV virus “stole” part of the host TASK-1 gene (Hsu et al., 2004)]

TASK-1 and TASK-3 channels can sense physiologically relevant changes in extracellular pH. The channels form, either as homo or heterodimers, a constitutively active pore. The TASK-1 and TASK-3 subunits contain structural features characteristic of the K2P channel family, including the canonical GYG/GFG sequences within the two channel pore regions. In the human TASK-5 gene a single nucleotide polymorphism was identified at the position 95 in the P1 domain giving rise to two different selectivity filter sequences, GYG and EYG (Kim et al., 2001); other three putative polymorphisms were identified at codons 260 (CCC or ACC), 261 (CAC or CCC) and 323 (CTT or CCT) (Karschin et al., 2001).

##### **1.4.1 Distinguishing between TASK-1 and TASK-3 channels**

The TASK-3 single conductance is 27 pS and external divalent cations block channel activity at negative membrane potentials (Rajan et al., 2000; Kim et al., 2000). The unitary conductance of TASK-3 channels is double that of the TASK-1 channel (14 pS), although the macroscopic currents arising from these two TASK channels are similar in terms of kinetics and voltage dependence (Duprat et al., 1997; Kim et al., 1998; Leonoudakis et al., 1998; Kim et al., 2000; Rajan et al., 2000; Lopes et al., 2000).

TASK-3 is inhibited reversibly at acidic extracellular pH with a pK of 6.5–6.7, more acidic by about 0.5 pH units than TASK-1 (Chapman et al., 2000; Rajan et al., 2000; Kim et al., 2000; Meadows and Randall 2001). The inhibition of TASK channel activity by protons appears to be an effect on channel-open probability (gating) rather than blockade of the pore, and involves interaction with a histidine residue (His98) that immediately follows the GYG motif (in other K<sup>+</sup> channels this histidine residue is occupied by aspartate) (Figure 4). Mutation of this residue to asparagines or glutamate abolishes pH sensitivity (Rajan et al., 2000). Because this same histidine residue appears in both TASK channels, other determinants must account for the differential pH sensitivity of TASK-3 and TASK-1. The TASK-1/TASK-3 heterodimers have an intermediate pH sensitivity compared with homodimeric TASK channels (Czirjak and Enyedi, 2002).

The cationic dye ruthenium red ( $[(\text{NH}_3)_5\text{RuORu}(\text{NH}_3)_4\text{ORu}(\text{NH}_3)_5]\text{Cl}_6$ ) blocks homomeric TASK-3 channels, but not heteromeric TASK-1/TASK-3 or homomeric TASK-1 channels. Homomeric TASK-3 channels are blocked by ruthenium red in the range of low micromolar concentrations (Figure 7) (Czirjak and Enyedi, 2003). The negatively charged residue Glu70 in the P1 pore domain, absent in TASK-1, is responsible for ruthenium red inhibition of TASK-3 (Czirjak et al., 2003). A single polycationic ruthenium red molecule binds simultaneously to Glu 70 of both TASK-3 subunits, and this explains as well why ruthenium red does not inhibit heterodimeric TASK-1/TASK-3 channels (Figure 7) (Czirjak et al., 2003). Although ruthenium red is not specific for K<sub>2</sub>P channels (it affects the intermediate and large conductance Ca<sup>2+</sup>-activated K<sup>+</sup> channels (Wu et al., 1999), the non-specific cation channel vanilloid receptor (Dray et al., 1990) and other ion transport mechanisms (Cibulsky and Sather, 1999; Hirano et al., 1998)) it is remarkably selective within the TASK subfamily.

Inhibition by zinc has been also proven to be a good tool to discriminate TASK-1 from TASK-3 channels. Zinc inhibits selectively TASK-3 channels and has no effect on TASK-1 channels and on TASK-1/TASK-3 heterodimers (Clarke et al., 2004; Aller et al., 2005).

Volatile anesthetic sensitivity of the leak K<sup>+</sup> current can also be used to distinguish between homomeric and heteromeric TASK channels (see footnote 1, page 33).

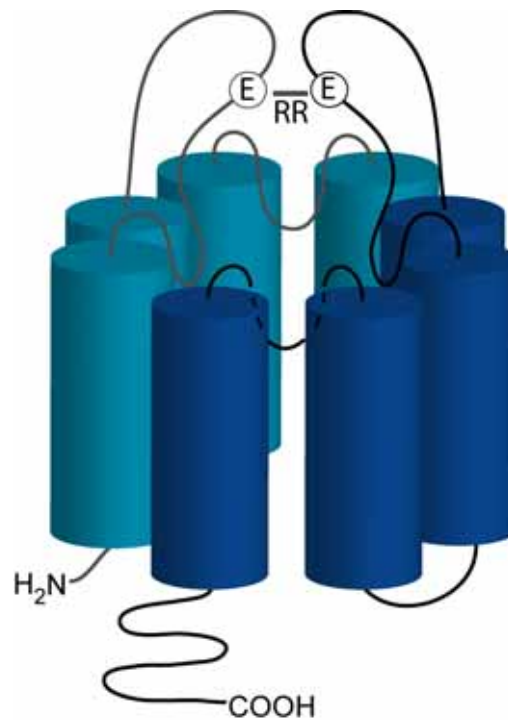


Figure 7. The model of TASK-3 homodimer inhibition by ruthenium red

Ruthenium red (RR) interconnects glutamate 70 (E) located in the first extracellular loop of the TASK-3 subunits. The two TASK-3 subunits are drawn in different shades of blue (adapted from Czirjak and Enyedi, 2003)

#### 1.4.2 Do TASK-1 and TASK-3 channels have a specific location on cells? Accessory proteins.

The subcellular distribution of TASK-1 and TASK-3 channels on neurons is not known. There are no good TASK-specific antibodies to tackle this issue (see section 4.3 in the Discussion chapter). However, a number of TASK-interacting proteins have been identified, although these proteins (e.g. 14-3-3 and p11) seem to have more to do with the general assembly, export and trafficking of generic transmembrane domain proteins rather than being something specific (Girard et al., 2002; O’Kelly et al., 2002; Rajan et al., 2002).

The first auxiliary protein for a K<sub>2</sub>P channel, called p11, associates with TASK-1 but not TASK-3 channels (Girard et al., 2002). p11, the small subunit of annexin II, belongs to a protein family (S100) involved in the regulation of a number of physiological processes, such as protein phosphorylation, inflammatory response, cAMP signaling pathways, dynamics of cytoskeleton components, and cell proliferation and differentiation. p11 association with TASK-1 requires the presence of the C-terminal sequence SSV of TASK-1 (Figure 4). This SSV motif does not exist

in TASK-3 (Figure 4). The association of p11 with TASK-1 masks the endoplasmic reticulum retention signal KRR, located immediately upstream of the key SVV sequence, a masking necessary for normal trafficking to the plasma membrane and expression of the channel activity (Girard et al., 2002).

TASK-1 and TASK-3 channels interact with members of another protein family, 14-3-3, which are implicated in many cellular processes including regulation of protein kinases, cell cycle control, apoptosis, and transfer of signalling molecules between nucleus and cytosol. (Rajan et al., 2002). A pentapeptide motif RRX(S/T)X in C-terminal tail of TASK channels (see Figure 4) is essential for this interaction, promoting the assembly and/or the trafficking to the surface membrane and functional expression of TASK-1 and TASK-3 channels. Co-immunoprecipitation of TASK-1 and 14-3-3 was found in rat synaptic membrane extracts and postsynaptic density membranes, indicating that interaction between 14-3-3 and TASK channels might occur *in vivo*. The pentapeptide motif RRX(S/T)X that is essential for 14-3-3 binding to TASK-1 represents a consensus PDZ binding site. TASK-3 and TASK-5 do not possess a consensus PDZ binding motif, so it is unlikely that PDZ binding is involved in the localization of TASK channels to the surface membrane. It was hypothesized that association of 14-3-3 with TASK-1 and TASK-3 is required to enable the binding of an accessory protein that facilitates trafficking of the assembled dimeric channel proteins from the endoplasmic reticulum to the surface membrane. Alternatively, the binding of 14-3-3 may mask a retention/retrieval motif and thus prevent the binding of an accessory protein that mediates retention in the endoplasmic reticulum (Rajan et al., 2002). Indeed, the interaction of 14-3-3 with the C-terminal domain of TASK overcomes retention of the channel in the ER by dibasic sites binding to  $\beta$ -COP, a  $\beta$ -coatamer protein. Moreover, phosphorylation of the C terminal motif (SS<sup>P</sup>V) enables 14-3-3, suppresses  $\beta$ -COP association and enables forward trafficking of correctly assembled channels to the plasma membrane (O'Kelly et al., 2002; Plant et al., 2005).

It remains an important issue where exactly on the cell particular K2P channels are located; for example, are they enriched on dendrites or the soma or evenly distributed? If a K2P channel is mainly on the dendrites, then this will impact more on dendritic inhibition for example by particular neuromodulators. Are K2P channels part of signalling scaffolds?

## 1.5 K2P channels and their importance for medical pharmacology

Any evaluation of the biology of K2P channels in a whole animal context (e.g. of a global knockout) must consider multiple systems as K2P channels are probably expressed in every tissue type. Here I consider aspects especially relevant for the TASK-1 and TASK-3 channels: neuromodulation and homeostatic plasticity of neural responses, inhalational anesthetic action, secretion of aldosterone from the adrenal gland, oxygen sensing in the carotid, a possible protective or pathological involvement in brain ischemia (stroke), a possible role in HIV infections, a possible role in the modulation of cell division (breast cancer) and in neural development (apoptosis).

### 1.5.1 K2P currents are a basis for modulation by neurotransmitters and peptides

One might get the impression that K2P channels provide only essential housekeeping functions but the dynamic modulation of K2P channels is likely to be a key endpoint for the way many neuromodulator transmitters and peptides produce some of their important effects on neuronal excitability. Neuromodulation entails slow effects of transmitters that are distinct from fast actions of ligand-gated ion channels, and it has been well established that up- and down modulation of  $K^+$  currents are among the primary ionic mechanisms for this process (Nicoll et al., 1990). In particular,  $K^+$  channel inhibition in neurons often involves channels with linear or weakly rectifying voltage dependence, and it seems likely that K2P channels provide molecular substrates for many of these effects.

One of the early and classic descriptions of neuromodulation within a behavioral context involved the inhibition of a background  $K^+$  conductance in sensory neurons of the sea slug *Aplysia californica*, which occurs during sensitization of the gill withdrawal reflex. This is a simple form of adaptation that was the starting point for a host of studies on more complex behavioral changes (Byrne and Kandel., 1996). In *Aplysia*, gill-withdrawal is a defensive reflex that is potentiated following a noxious stimulus to a different part of the body, such as the tail. The potentiation is mediated in part by serotonergic inhibition of a resting  $K^+$  channel, which was designated the *S* channel because of its modulation by serotonin. The intracellular mechanism for *S* channel inhibition involves activation of protein kinase A (PKA) and likely entails direct phosphorylation of the channel. Although the molecular identity of this *Aplysia* channel is unknown, it has properties that are remarkably similar to the mammalian two-pore-domain  $K^+$  channels TREK-1 and TREK-2 (Patel et al., 1998). To date, only one K2P subunit,

*AcK2p1*, has been identified in the CNS of *Aplysia californica* (Jezzini et al., 2004). Functional data have not yet been obtained for this protein but its deduced amino acid sequence is homologous to the channels of the mammalian THIK subfamily (Jezzini et al., 2004).

### 1.5.2 Neuromodulation and TASK channels

In mammals, inhibition of TASK channels is a prominent mechanism for neuromodulation in a variety of neurons such as motor neurons (Talley et al., 2000), thalamocortical relay neurons (Meuth et al., 2003) and cerebellar granule neurons (Millar et al., 2000). Usually a transmitter modulator binds its receptor and closes a TASK channel, leading to depolarization of the cell. This mechanism has been well documented in motor neurons, where TASK channel closure is induced by multiple transmitters, including serotonin, norepinephrine, substance P (SP), thyrotropin-releasing hormone (TRH), and glutamate (Rekling et al., 2000, Talley et al., 2000). The thalamocortical neuronal network provides another example of the predicted involvement of TASK-1 and TASK-3 channels (Meuth et al., 2003) (Figure 8). The thalamocortical system is characterized by two different states of activity: the rhythmic burst activity during sleep and tonic single-spike activity during the awake state.

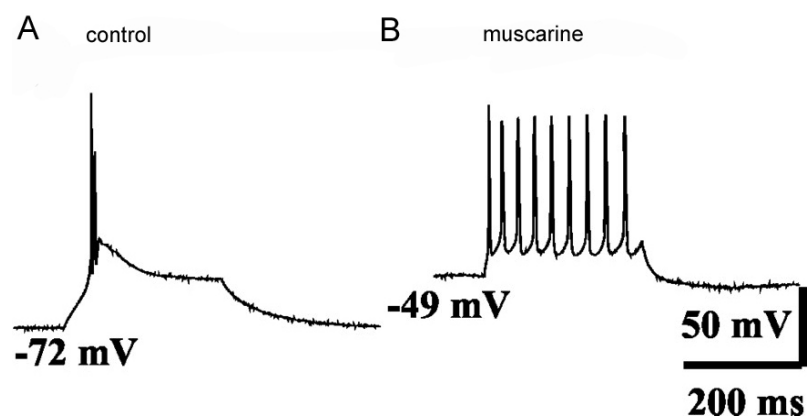


Figure 8. Effect of muscarine on the firing mode of thalamocortical relay neurons

**A**, Whole-cell current-clamp recording using a 100-200 pA depolarizing current (300 msec). From hyperpolarized potential (indicated near traces), depolarizing pulses induced burst firing; **B**, Application of muscarine (50  $\mu$ M) resulted in a depolarizing shift of the membrane potential and generation of tonic trains of action potentials in response to the same depolarizing current pulse (adapted from Meuth et al., 2003).

The thalamocortical relay neurons are hyperpolarized during natural sleep, firing rhythmic bursts of action potentials (Figure 8A), but depolarized during waking, firing sequences of action potentials (Figure 8B). The switch between the two states is thus accompanied by a depolarizing shift of the membrane potential of the thalamocortical relay neurons due to the decrease of the  $K^+$  leak conductance. This state transition of relay neurons seems to be mediated by the acetylcholine released from the thalamic terminals of the ascending brainstem system which acts on muscarinic receptors to promote the closure of TASK-1 and TASK-3 channels (Figure 8B) (Meuth et al., 2003). As it is believed that only tonically firing thalamic cells allow communication transfer between the neocortex and “outside world”, this acetylcholine-mediated inhibition of TASK channels would be crucial for promoting the awake state.

### 1.5.3 Second messenger systems for modulating TASK-1 and TASK-3 channels

The mechanisms for receptor modulation of TASK-1 and TASK-3 via G-proteins have been elusive. In cerebellar granule cells muscarinic activation, via M3 muscarinic receptors, promotes closure of TASK channels (Millar et al., 2000). Application of muscarine (10  $\mu$ M), acting on muscarinic acetylcholine receptors, produced a rapidly and fully reversible inhibition of TASK-1 currents. In *Xenopus* oocytes, which possess endogenous M3 subtype muscarinic receptors, application of carbachol (100  $\mu$ M) produced also a fully reversible inhibition of TASK-1 currents and an associated decrease in membrane conductance (Millar et al., 2000).

Thyrotropin-releasing hormone (TRH) modulation of TASK-1 and TASK-3 requires a channel region that does not contain any classical motifs that suggest a known signalling mechanism (Talley and Bayliss, 2002). A six amino acid region at the interface between the fourth transmembrane domain and the cytoplasmic C-terminus (VLRFMT motif in TASK-1 and a VLRFLT motif in TASK-3) is critical for channel inhibition by TRH (Figures 4 and 19). Moreover, this critical domain is necessary also for the activation of TASK channels by volatile anesthetics (see section 1.5.11 “K2P channels as targets for inhalational anesthetics”), indicating that a common molecular site is required for both increased or decreased activity of the channels (Talley and Bayliss, 2002).

A mechanism underlying the excitatory effects of group I metabotropic glutamate receptors via inhibition of K2P channels was proposed by Chemin et al., 2003 (Figure 9; see also Figure 11). By acting on group I Gq-coupled metabotropic receptors, glutamate strongly inhibits TASK channels via phosphatidyl-4,5-inositol-biphosphate (PIP<sub>2</sub>) depletion following phospholipase C (PLC) activation (Chemin et al., 2003). Activation of PLC leads to cleavage of PIP<sub>2</sub> (Figure 9)

into two second messengers: diacylglycerols (DAG), which activate protein kinase C (PKC), and inositol-1,4,5-triphosphate (IP<sub>3</sub>), which mobilizes Ca<sup>2+</sup> from intracellular stores via fixation to IP<sub>3</sub> receptors. Buffering intracellular Ca<sup>2+</sup> concentration or inhibiting/activating PKC did not significantly affect TASK currents or their inhibition by glutamate.

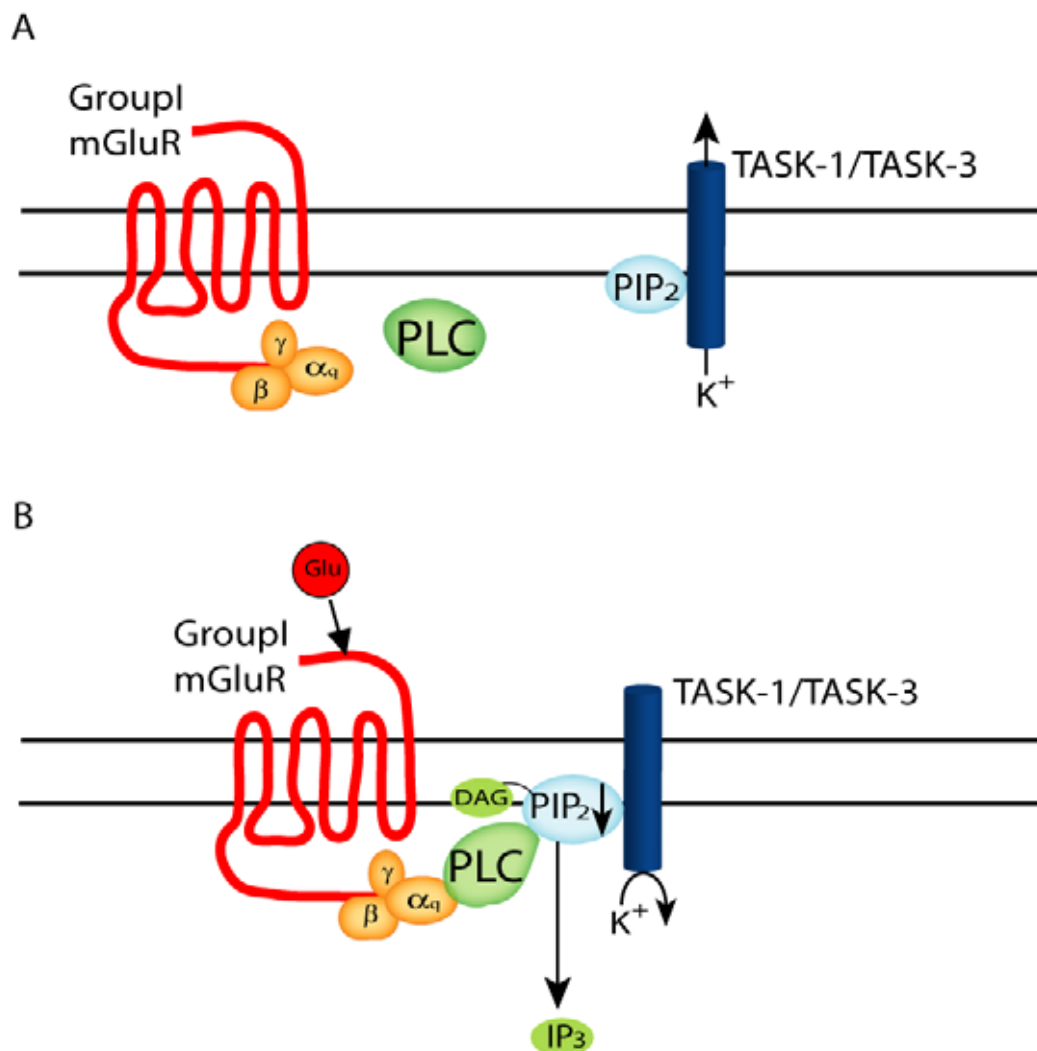


*Figure 9. A model of the of glutamate induced slow excitation mechanism via TASK channels*

A, PIP<sub>2</sub> binding to the TASK-1 and TASK-3 channels maintains them in the open state. B, Glutamate binding to group I Gq-coupled metabotropic receptors leads to the activation of PLC and PIP<sub>2</sub> hydrolysis into IP<sub>3</sub> and DAG. PIP<sub>2</sub> depletion promotes TASK channel closure and the depolarization of the membrane potential. The analogous mechanism for angiotensin II action at the AT<sub>1</sub>R is shown in Figure 11.

Investigating the possibility of direct roles of PIP2 and its downstream products, IP3 and DAG, revealed that PIP2 appears to be necessary to maintain the TASK channels active and its depletion and IP3 liberation involve glutamate-mediated inhibition of TASK currents, independently of IP3 receptors (Chemin et al., 2003).

A more recent study showed that PIP2 hydrolysis underlies muscarinic (M1) and angiotensin II (AT1a) receptor mediated inhibition of TASK-1 and TASK-3 channels (Lopes et al., 2005) (see Figure 11). C-terminus truncation of the TASK-3 channel, including the conserved VLR(F/M/L)T motif involved in TRH mediated inhibition of TASK channels (Talley and Bayliss, 2002), failed to disrupt the PIP2 activation of TASK-3 channel, suggesting that other molecular determinants are responsible for PIP2 interactions with TASK channels (Lopes et al., 2005).

#### **1.5.4 Endocannabinoids as agonists on TASK-1 and TASK-3**

Another proposed modulator of TASK channels is the endocannabinoid anandamide. This was reported to be an efficient blocker of human TASK-1 but not of TASK-3 (Maingret et al., 2001). The TASK-1 channel was directly blocked by submicromolar concentrations of the endocannabinoid anandamide, independently of the CB1 and CB2 receptors (Maingret et al., 2001). Thus it was suggested that anandamide is a selective blocker of the TASK-1 channel (Maingret et al., 2001).

However, it seems that TASK-1 selectivity for anandamide may be species dependent, because rat TASK-1 and TASK-3 clones are approximately equally sensitive to anandamide (Berg et al., 2004). Similar effects of anandamide were observed on the mouse TASK-1 and TASK-3 clones (Aller et al., 2005). Thus, it can be concluded that the original study (Maingret et al., 2001) was wrong or the rodent TASK-1 channels are much less sensitive to anandamide than the human TASK-1 channel.

#### **1.5.5 The pH sensitivity of TASK channels and their possible role in stimulating breathing during sleep**

TASK-1 and TASK-3 channels are very sensitive to small acidifications of the external media; they shut and so depolarise the cell. They are expressed and confer intrinsic pH sensitivity to somatic motor neurons, noradrenergic locus coeruleus neurons and serotonergic raphe neurons (Talley et al., 2000; Sirois et al., 2000; Washburn et al., 2002). One important neural reflex

evoked by the decrease of pH in the brain is behavioural arousal. pH-sensitive TASK-dependent regulation of arousal, mediated by noradrenergic locus coeruleus neurons and serotonergic raphe neurons, may be important when ventilation becomes excessively depressed during sleep. Activation of arousal mechanism is responsible, at least in part, for sleep disturbances associated with obstructive apneas. Also, the failure of this waking reflex in neonates might be a contributing factor to Sudden Infant Death Syndrome (SIDS) (reviewed in Bayliss et al., 2003).

### **1.5.6 The role of K2P channels in homeostatic plasticity: cerebellar granule cells**

Modulation of TASK channels by neurotransmitters is an important mechanism by which neuronal excitability may be altered in the short term. Interestingly, it was also shown that TASK channel modulation could occur over a longer time scale, participating in a long-term homeostatic regulation of neuronal excitability.

This mechanism was observed by Brickley et al., 2001, in a study on cerebellar granule cells from GABA<sub>A</sub> receptor  $\alpha 6$  subunit knockout mice ( $\alpha 6^{-/-}$ ). Genetic ablation of the  $\alpha 6$  subunit causes the complete loss of extrasynaptic GABA<sub>A</sub> receptors (composed of  $\alpha 6\beta 2/3\delta$  subunits) that are responsible for the tonic component of the GABA<sub>A</sub> receptor-mediated inhibition; the other subunits,  $\alpha 1\beta 2/3\gamma 2$ , persist at the synaptic location, being responsible for the phasic component of inhibition (Brickley et al., 2001). The loss of tonic inhibition was expected to result in a relatively depolarized membrane potential in cerebellar granule cells of  $\alpha 6^{-/-}$  mice. But  $\alpha 6^{-/-}$  cerebellar granule cells did not differ from wild-type granule cells in their excitability. The responses of these  $\alpha 6^{-/-}$  cerebellar granule cells to excitatory synaptic input remained unaltered, owing to an increase in a “leak” conductance (Brickley et al., 2001) (Figure 10).

Earlier studies showed that cerebellar granule cells express an outwardly rectifying K<sup>+</sup> current which does not inactivate and is responsible for the large negative resting membrane potential of these cells (Watkins and Mathie, 1996; Millar et al., 2000). This K<sup>+</sup> “leak” current was termed the “standing outward” current ( $I_{K(SO)}$ ) (Watkins and Mathie, 1996).  $I_{K(SO)}$  has no threshold for activation by voltage and blocking  $I_{K(SO)}$  leads to cell depolarization.  $I_{K(SO)}$  is inhibited by activation of G protein-coupled receptors such as the muscarinic receptor, by extracellular acidosis and by millimolar concentrations of Ba<sup>2+</sup> but is not inhibited by K<sup>+</sup> channel blockers such as tetraethylammonium (Watkins and Mathie, 1996; Boyd et al., 2000; Millar et al., 2000).

The characteristics of  $I_{K(SO)}$  are similar to those of TASK-1 and TASK-3 (Watkins and Mathie, 1996; Millar et al., 2000; Rajan et al., 2000; Kim et al., 2000). These studies, together with the finding that both TASK mRNAs are expressed in cerebellar granule cells (Brickley et al., 2001;

Aller et al., 2005) (Figure 5) have led to the hypothesis that in  $\alpha 6^{-/-}$  mice a compensatory upregulation of these TASK channels might be responsible for the long-term homeostatic regulation of cerebellar granule cell excitability (Brickley et al., 2001).

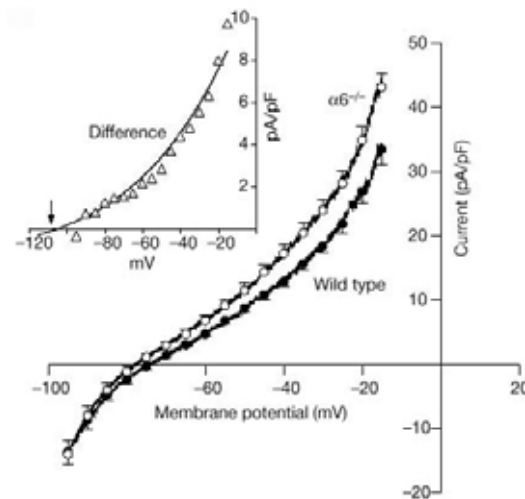


Figure 10. Increased  $K^+$  leak conductance in  $\alpha 6^{-/-}$  cerebellar granule cells

Averaged I–V relationships from wild-type and  $\alpha 6^{-/-}$  cerebellar granule cells (CGCs). In  $\alpha 6^{-/-}$  CGCs, the shape of the I/V curve is similar to that seen in wild-type CGCs, but the magnitude of the current was significantly increased. The difference current (inset) reversed at  $-104$  mV (arrow), close to the potential predicted for a pure  $K^+$  conductance (Brickley et al., 2001).

Northern blot analysis of whole cerebella showed a 20% increase in TASK-1 mRNA in  $\alpha 6^{-/-}$  mice (Brickley et al., 2001). Also, real-time PCR analysis showed that TASK-1 mRNA levels increased 2-fold and TASK-3 mRNA levels increased of about 1.7-fold in  $\alpha 6^{-/-}$  cerebella (Aller et al., 2005). Thus,  $I_{K(SO)}$  might be composed of several  $K^+$  channels, such as TASK-1 and TASK-3, but whether these channels really are responsible remains to be demonstrated.

### 1.5.7 Why are so many K2P channels expressed in the same neuronal cell?

Excitable cells express a high diversity of  $K^+$  channels. A major challenge is to relate the many different channel subunits to the functional  $K^+$  currents observed in native neurons.

A good example of a neuronal population expressing a large number of K<sup>+</sup> channels is cerebellar granule cells: at least 26 potassium channel subunit genes are moderately or strongly expressed in cerebellar granule cells (Mathie et al., 2003). Of these, five K2P channel genes, TWIK-1, TASK-1, TASK-3, TREK-2 and THIK-2 are expressed at high levels in cerebellar granule cells (Brickley et al., 2001; Duprat et al., 1997; Talley et al., 2001; Karschin et al., 2001; Rajan et al., 2001, 2005; Vega-Saenz et al., 2001; Aller et al., 2005) (see Figure 5). By single channel recording it was claimed that the TASK-like background K<sup>+</sup> current in cerebellar granule cells comprises at least four distinct K<sup>+</sup> channels, some of which show strong similarity with cloned TASK channels (Han et al., 2002). However, the absence of selective pharmacological agents has hindered the identification of the K2P channels responsible for I<sub>K(SO)</sub>.

In rat cerebellar granule cells, an approach based on single channel analysis was used to identify native heterodimeric channels among a mixed population of TASK homodimeric and heterodimeric channels (Kang et al., 2004b). In this study, it was noted that TASK-1/TASK-3 heterodimeric channels have a unitary conductance that is twice that of TASK-1 but indistinguishable from that of TASK-3. The demonstration that these TASK heterodimers are resistant to ruthenium red application provided evidence that the recorded channels represent native TASK heterodimers. Kang and collaborators (2004b) also estimated that 56% of native TASK channels are represented by TASK-3 homodimers and 44% of TASK-1/TASK-3 heterodimers. However, all of these conclusions are based on indirect evidence.

Thus, gene knockouts and expression of dominant negative K2P constructs offer a useful strategy for the identification of K2P subunit composition *in vivo* (Lauritzen et al., 2003; Berg et al., 2004; Heurteaux et al 2004; Warth et al., 2004; Aller et al., 2005).

### **1.5.8 K<sup>+</sup>-dependent neuronal apoptosis. A role for TASK-1 and TASK-3 channels?**

Neurons undergo apoptosis during normal development and in certain disease states. Programmed cell death is particularly evident in the developing cerebellum: during the first post-natal week, intense proliferation of the external granular layer gives rise to several millions of granule neurons that migrate across the molecular and Purkinje layers to reach the inner granular layer. Massive apoptosis contributes to numerically match granule cells with the post-synaptic Purkinje neurons. Both synapse-dependent and -independent events are involved in developmental granule cell apoptosis (Wood et al., 1993; Lossi et al., 2002). Mature rat granule cells undergo cell death if cultured in a medium with physiological 5mM K<sup>+</sup>; this process is prevented in a depolarising medium containing 25mM K<sup>+</sup> (Lauritzen et al., 2003). Young rat

neurons lack  $I_{K(SO)}$  and are resistant to low  $K^+$ -induced cell death. Also, acidification of extracellular pH, ruthenium red and muscarine inhibit  $I_{K(SO)}$ , preventing cell death of mature granule cells (Lauritzen et al., 2003). Furthermore, extracellular acidosis abolishes lactate dehydrogenase (LDH) release, DNA fragmentation and caspase activation, the hallmarks of apoptotic cell death (Lauritzen et al., 2003). Thus there is a strong correlation between  $I_{K(SO)}$  and  $K^+$ -dependent granule cell death in culture (Lauritzen et al., 2003).

The contribution of TASK-1 and TASK-3 channels to neuronal apoptosis was demonstrated by virally expressing them in hippocampal neurons that lack  $I_{K(SO)}$  (Lauritzen et al., 2003). Indeed, TASK-1 and TASK-3 overexpressing hippocampal neurons were protected by acidosis and by increasing extracellular  $K^+$  concentration. Moreover, the induction of cell death requires TASK channel activity: inactivating the endogenous TASK channels of granule cells with dominant-negative TASK-1<sup>G95E</sup> and TASK-3<sup>G95E</sup> mutants reduced cell death significantly in mature granule cells (Lauritzen et al., 2003) supporting earlier evidence that TASK subunits can assemble also as heterodimers (Czirjak and Enyedi, 2002a). Additional pharmacological results, based on ruthenium red sensitivity, suggest that TASK-3 homodimers play a dominant role in  $K^+$ -dependent granule cell death. However, TASK-1 and TASK-3 knockout mice will certainly be valuable to directly assay the role of these channels during *in vivo* granule cell developmental apoptosis.

### 1.5.9 TASK-3 gene amplified in some breast cancers

The link between  $K^+$  channels, apoptosis, survival and oncogenesis has become increasingly recognized over the recent years. For example, the enhancement of  $K^+$  current through HERG  $K^+$  potassium channel which is overexpressed in a variety of tumor cell lines, was shown to be directly involved in oncogenesis (Wang et al., 2002). By representational difference analysis (RDA) of human breast cancer it was discovered that the TASK-3 gene undergoes amplification within an amplicon located at chromosomal region 8q24.3 (Mu et al., 2003). TASK-3 gene is amplified from 3 to 10 fold in 10% of breast tumors and overexpressed up to 100 fold in 44% of breast cancers and 35% of lung cancers. Overexpression of TASK-3 channel in transfected, partially transformed mouse embryonic fibroblast cultured cell line (C8) cells strongly enhanced tumorigenicity; moreover, in cultured C8 cells, TASK-3 overexpression increased cell viability in low-serum conditions and hypoxic conditions (Mu et al., 2003). Expression of the dominant negative TASK-3<sup>G95E</sup> channel in C8 cells abolished oncogenic function, including proliferation in low serum, resistance to apoptosis, and promotion of tumor growth, establishing a direct link

between the potassium channel activity of TASK-3 and its oncogenic functions (Pei et al., 2003). Thus TASK-3 can be defined as a proto-oncogene.

#### **1.5.10 K2P channels and ischemia (stroke)**

One feature of hypoxic/ischemic episodes that occur during stroke is a rapid and transient depolarization of central neurons. The mechanisms underlying neuronal excitotoxicity during hypoxic/ischemic episodes are not fully understood. K2P channels significantly contribute in setting the resting membrane potential and thus providing input resistance to depolarizing influences.

This contribution was studied by Plant et al., 2002, on rat cerebellar granule cells exposed to acute hypoxia by using the whole-cell patch-clamp technique. A reversible and highly reproducible depolarisation was observed in this condition. Hypoxic depolarization and the hypoxic depression of  $I_{K(SO)}$  were abolished by decreasing extracellular pH suggesting that inhibition of TASK channels is responsible for hypoxic depolarisation of cerebellar granule cells (Plant et al., 2002). Opposite results were obtained by Liu et al., 2005. Initially, they studied the effects of recombinant K2P channels in transfected, partially transformed mouse embryonic fibroblast cultured cell line (C8) and determined that pH-sensitive K2P channels, TASK-1, TASK-2 and TASK-3 have effectively protected stressed cells by preventing activation of apoptotic pathways. Then, by infecting cultured hippocampal slices with Sindbis virus constructs containing the coding sequences of these channels they observed that overexpression of TASK-3 resulted in a significant cellular protection in CA1 and dentate gyrus neurons from an oxygen-glucose deprivation injury, especially in the presence of the volatile anesthetic isoflurane (Liu et al., 2005). Similar protective effects of TASK-3 were reported previously in a study on C8 cell line (Mu et al., 2003). TASK-3 overexpression, induced by retroviral infection, increased the viability of cultured C8 cells in low-serum conditions; moreover, TASK-3 overexpression allowed C8 cells to survive hypoxic conditions. TASK-3 contributes to tumorigenesis (Mu et al., 2003), possibly by promoting cancer cell survival in the poorly oxygenated areas of solid tumors. Based on this evidence, it could be hypothesized that TASK channels have a protective influence against ischemia.

### 1.5.11 K2P channels as targets for inhalational anesthetics

The mechanisms by which volatile anesthetics induce immobility and unconsciousness are only partly understood. According to older evidence the most widely recognized targets of these compounds are ligand-gated ion channels, and, in particular, enhanced GABA<sub>A</sub> receptor activity was believed to induce a general depression of neuronal activity that is a major component of the anesthetized state (Franks and Lieb, 1994). For example two anesthetics which are given intravenously (propofol and etomidate) selectively work on GABA<sub>A</sub> receptors with the  $\beta$ 2 and  $\beta$ 3 subunit (Rudolph and Antkowiak, 2004). Mice with a point mutation (N265M) in the  $\beta$ 3 subunit gene are resistant to propofol and etomidate-induced anesthesia, but volatile anesthetics potency is unchanged in these mice (Jurd et al., 2003).

One possibility that has long been considered is that volatile anesthetics reduce neuronal excitability by opening K<sup>+</sup> channels. Such an anesthetic-activated K<sup>+</sup> current was first characterized in molluscan pacemaker neurons (Franks and Lieb, 1994). Interestingly, the yeast K2P channel TOK1 (although it contains eight instead of four transmembrane domains) is similarly open by volatile anesthetics (Gray et al., 1998). The molecular basis of mammalian anesthetic-sensitive K<sup>+</sup> channels has been established recently: these channels belong to K2P family (Herteaux et al., 2004; Franks and Honoré, 2004).

The most commonly used inhalational anesthetics are halothane and the halogenated ethers isoflurane, sevoflurane and desflurane (Franks and Honoré, 2004). Opening of recombinant K2P channels by volatile anesthetics is summarized in Table 3.

Molecular dissection of TASK-1 and TASK-3 channels revealed that they contain an anesthetic-responsive sequence VLR(F/M/L)T in the proximal C-terminal domain (Talley and Bayliss, 2002) (Figures 4 and 19). This critical domain is the same region that is necessary for the inhibition of TASK channels by TRH. Thus, VLR(F/M/L)T site is required for both activation and inhibition of the channel (Talley and Bayliss, 2002). Cloned TASK-1 and TASK-3 are activated by clinically relevant concentrations of halothane (Patel et al., 1999; Meadows and Randall, 2001; Sirois et al., 2000; Talley and Bayliss, 2002). The effects of volatile anesthetics on TASK-1 and TASK-3 channels are sensitive to pH such that the extracellular acidification prevents anesthetic-induced channel activation or inhibits TASK-1 and TASK-3 channels preactivated by anesthetics (Sirois et al., 2000).

That volatile anesthetics exert some of their effects on K2P channels has been directly demonstrated using K2P knockout mice. The potency of anesthetic action on the whole animal is assessed by the loss of righting reflex (a mouse placed on its back automatically tries to roll over

onto its feet) and the insensitivity to pain in the tail flick/clamp assay. Using these criteria, TREK-1 knockout mice are more (although not totally) resistant to the effects of halothane and chloroform (Heurteaux et al., 2004). By contrast, although volatile anesthetics potently activate TASK-2 channels (Gray et al., 2000), TASK-2 knockout mice have unchanged sensitivities to volatile anesthetics (Gerstin et al., 2003), reflecting the fact that TASK-2 channel is not expressed in the brain. TASK-1 knockout mice have only mildly reduced sensitivity to isoflurane (Linden et al., 2004) even though TASK-1 is expressed in some neurons that could be relevant to the immobility aspects of anesthesia such as motor neurons. Thus it is clear that volatile anesthetics produce their profound effects on CNS function by targeting discreet populations of cells, and not by exerting a general action on the whole brain.

Family	Subunits	Volatile anesthetics		
		halothane	isoflurane	chloroform
TWIK	TWIK-1 TWIK-2 KCNK7	-		-
THIK	THIK-1 THIK-2	-		no
TREK	TREK-1 TREK-2 TRAAK	+ + no	+ + no	+ + no
TASK	TASK-1 TASK-3 TASK-1/TASK-3 TASK-5	+ + +	- <sup>1</sup> + <sup>1</sup> + <sup>1</sup>	no
TALK	TASK-2 TALK-1 TALK-2	+ - -	+ no +	+ - -
TRESK	TRESK			

Table 3. Anesthetic sensitivity of K2P channels

+, stimulated; -, inhibited; “no”, no effect

<sup>1</sup> Isoflurane has distinct effects on TASK-1 and TASK-3 channels. Thus, TASK-3 channels are activated by high concentrations of isoflurane, whereas TASK-1 channels are inhibited. The pH and isoflurane sensitivities were used to try to distinguish between native coexpressing TASK channels and to dissect their contribution to  $I_{K(SO)}$  in cerebellar granule cells. Based on this evidence TASK-1 and TASK-3 would assemble their subunits predominantly into heterodimeric channels in hypoglossal motor neurons (Berg et al., 2004) and facial motor neurons (Larkman and Perkins, 2005).

### **1.5.12 TASK-1 (and TASK-3?) channels could inhibit the spread of HIV in the brain**

TASK-1 interacts with Vpu-1 (Hsu et al., 2004), a HIV-1 accessory protein that enhances the release of progeny virions from infected cells. Vpu-1 is a single membrane-spanning peptide of 86 residues and has 56% identity from the N-terminus to the first transmembrane domain of TASK-1. This gave rise to the idea that during evolution molecular piracy was involved. Vpu-1, like TASK-1, has the ability to oligomerize. The high degree of Vpu-1-TASK-1 identity allows Vpu-1 and TASK-1 to form hetero-oligomers; they can physically interact in lymphoid tissues in patients with AIDS and diminish TASK-1 currents. In primary CD4<sup>+</sup> cells infected with HIV-1, this interaction results in degradation of the TASK-1 channel; conversely, overexpression of the TASK-1 channel leads to inhibition of Vpu-1 mediated virus release (Hsu et al., 2004). TASK-1 expression varies in different specialized cells; thus, in HIV infections, TASK-1 might be rapidly degraded by Vpu-1 in tissues expressing low levels of the channel and, reciprocally, TASK-1 might have an inhibitory effect on the spread of HIV when TASK-1 is highly expressed in tissues, such as brain (cerebellar granule cells, motor neurons) and kidney. The high identity between TASK-1 transmembrane domain involved in the interaction with Vpu-1 and the corresponding domain of TASK-3 suggests that TASK-3 might also interact with Vpu-1 and inhibit the release of virions (Hsu et al., 2004).

### **1.5.13 Contributions of TASK-1 and TASK-3 channels to the physiology of peripheral organs**

#### **Oxygen sensing**

Acute hypoxic inhibition of K<sup>+</sup> channels is a critical step in regulatory processes designed to link lowering of O<sub>2</sub> levels to cellular responses. Different types of cells respond to hypoxia via inhibition of specific K<sup>+</sup> channel subtypes leading to membrane depolarization. This phenomenon was initially described in type I carotid body cells (Lopez-Barneo et al., 1988). The carotid body (CB) is the main arterial chemoreceptor that senses the arterial levels of partial O<sub>2</sub> pressure (PO<sub>2</sub>), partial CO<sub>2</sub> pressure (PCO<sub>2</sub>) and pH, playing an important role in respiratory, cardiovascular and neurohumoral regulation. Arterial chemical stimuli (PO<sub>2</sub>, PCO<sub>2</sub>, pH) act on carotid body type I cells (primary sensory cells), through both membrane and mitochondrial transduction mechanisms. The transduction process(es) induces an intracellular [Ca<sup>2+</sup>] increase, mediated by Ca<sup>2+</sup> influx through voltage-dependent Ca<sup>2+</sup> channels and/ or Ca<sup>2+</sup> release from intracellular stores. This Ca<sup>2+</sup> increase mediates the exocytotic release of one or more

transmitters (such as excitatory transmitter catecholamines, acetylcholine, adenosine nucleotides and peptides) that activate receptors located on the sensory terminals of petrosal ganglion neurons. The resulting chemoafferent activity is conveyed through the carotid sinus nerve to the relay nucleus in the central nervous system, the nucleus tractus solitarius (Iturriaga and Alcayaga, 2004). The type I cells of carotid body respond to hypoxia and acidosis with a depolarisation initiating electrical activity,  $\text{Ca}^{2+}$  entry and neurosecretion.

A key ionic current involved in mediating these responses to hypoxia in rat type I cells is an oxygen- and acid-sensitive background  $\text{K}^+$  current (Buckler, 1997). In cell-attached patches of rat type I cells, hypoxia closes TASK-1 and TASK-3 like channels, but has no effect in the inside-out patch configuration (Buckler et al., 2000). Several studies have shown the expression of TASK-1, TASK-3, TASK-2 and TRAAK at the protein level in the type I cells (Yamamoto et al., 2002), although the specificity of the antibodies used is questionable (see section 4.3 in the Discussion chapter). Other examples of oxygen sensor cells are the neuroepithelial body cells and the lung carcinoma line H146 (an established model for neuroepithelial body cells) which sense the  $\text{O}_2$  levels via NADPH oxidase  $\text{H}_2\text{O}_2$ /free radical production; acute hypoxia promotes  $\text{K}^+$  channel closure and cell depolarisation. The identity of the  $\text{K}^+$  channel is still controversial. Again, the involvement of a member of the K2P family was proposed (O'Kelly et al., 1999; Hartness et al., 2001). RT-PCR screening demonstrated that all known K2P channels other than TWIK-1 and TRAAK are expressed in H146 cells (Hartness et al., 2001).

A more recent study (Williams and Buckler, 2004) gave more support to the idea that the oxygen-sensitive  $\text{K}^+$  channels in neonatal rat carotid body type 1 cells are the TASK-1 and TASK-3 channels. The biophysical properties of these channels do not, however, precisely conform to those of either TASK-1 or TASK-3, suggesting that these K2P channels are not simple homodimers of TASK-1 or TASK-3 (Williams and Buckler, 2004).

The NADPH oxidase NOX4 was proposed to modulate the oxygen-dependent activity of TASK-1 (Lee et al., 2005). By using NOX4 siRNA and NADPH oxidase inhibitors the oxygen sensitivity of TASK-1 was abolished suggesting that NOX4 functions as an oxygen-sensing partner of TASK-1 (Lee et al., 2005). It seems likely that NOX4 might bind as a  $\beta$  subunit to the TASK channels, analogous to the NADPH oxido-reductase  $\beta$  accessory protein bound to the  $\text{K}_v$  channels (Long et al., 2005).

TASK-3 overexpression in C8 cells confers resistance to hypoxia and enhances tumorigenicity (Mu et al., 2003) (see section 1.5.9 "TASK-3 gene amplifies in some breast cancers"). Thus, it seems like this protection from hypoxia is related to the ability of TASK-3 to respond to oxygen

levels. Does TASK-3 have a patho-physiological role for development of hypoxia tolerance in tumor cells?

### Regulation of aldosterone release from adrenal glomerulosa

The TASK-1 and TASK-3 channel genes strongly coexpress in glomerulosa cells of adrenal gland so TASK channels might contribute to the high resting negative membrane potential of these cells (Czirjak et al., 2000; Czirjak and Enyedi, 2002b; Talley et al., 2003). TASK-1 and TASK-3 channels are closed by the actions of the blood hormone/peptide angiotensin II (Figure 11) so controlling aldosterone secretion in these cells.

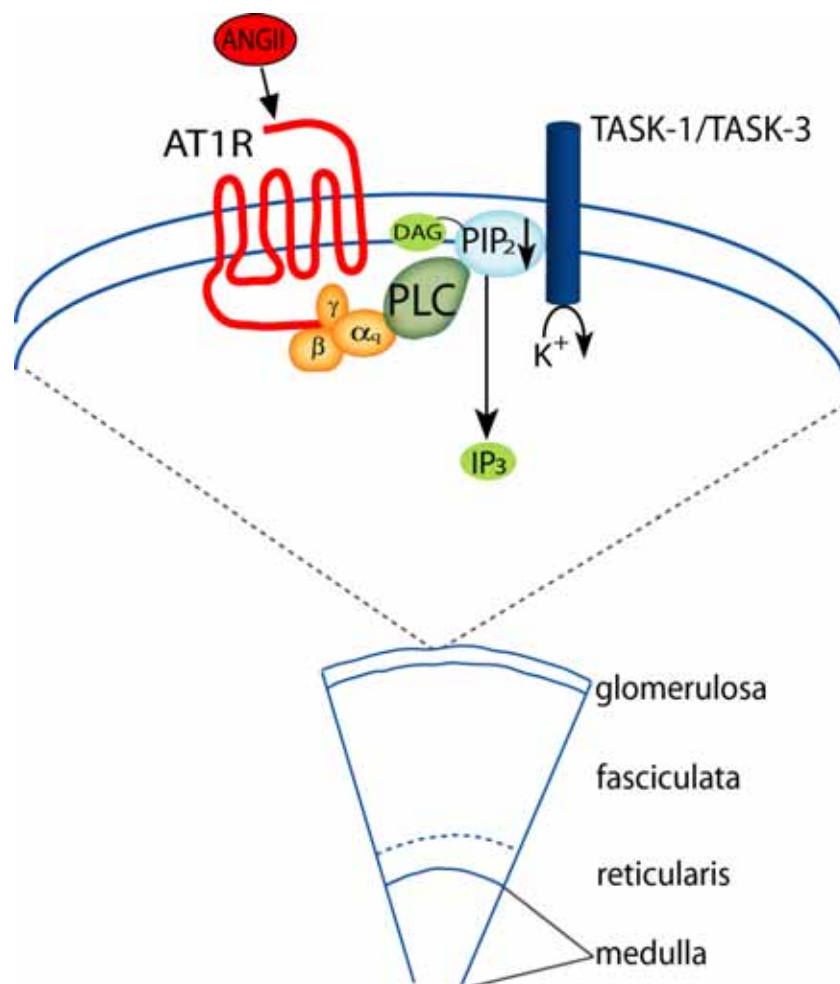


Figure 11. Inhibition of TASK channels by angiotensin II via angiotensin II type I receptor (AT1R) in glomerulosa cells of adrenal gland.

Angiotensin II binds a G-protein-coupled receptor (Angiotensin II type I receptor) stimulating phospholipase C and by hydrolyzing PIP<sub>2</sub> promotes TASK channel closure, thus depolarising the glomerulosa cells and inducing aldosterone secretion. Aldosterone is the most potent hormone regulating the body's electrolyte balance. Aldosterone acts directly on the kidney to decrease the rate of Na<sup>+</sup> excretion (with accompanying retention of water), and to increase the rate of K<sup>+</sup> excretion, maintaining a normal blood pressure. So double TASK-1 and TASK-3 knockouts might be hypotensive and have too much blood potassium.

### **1.6 Project aims with the TASK-3 knockout mice**

In this thesis I report the construction and preliminary analysis of TASK-3 knockout mice. The mutation of the TASK-3 gene, or a combined mutation of it together with loss of TASK-1, could give rise to a “multisystem disorder”, so making tissue-specific deletions of the genes a desirable feature. Nevertheless, a number of issues I would be interested in investigating with the “global” TASK-3 KO mice are outlined below:

1. Can we dissect the contribution of TASK-3 to the leak currents in particular neuronal types, with as a starting point, a primary focus on cerebellar granule cells and thalamic relay cells? As Aller et al. 2005 proposed, can we evaluate, by any changed electrophysiological properties of mutant neurons, if TASK-1 and TASK-3 assemble heteromerically *in vivo*?
2. It has been suggested that amines (e.g. serotonin) and acetylcholine, released by axons from the arousal systems in the brain stem, act to close TASK-1 and TASK-3 channels on thalamic relay cells, so making thalamic relay cells more excitable and so permitting communication between the neocortex and the “outside world” as part of the “waking up” process (Meuth et al., 2003). Are the TASK-3 channels expressed in the thalamic relay neurons involved as an endpoint in initiating arousal?
3. Recombinant TASK-3 channels are highly sensitive to physiologically active concentrations of the halogenated inhalational anesthetics (Talley and Bayliss, 2002). What contribution do TASK-3 channels make *in vivo* to the anesthesia produced by inhalational anesthetics?
4. One would predict that the pH sensitivity of the TASK-3 channel plays a protective role in brain ischemia? Do TASK-3 KO mice have increased ischemic damage after, for example, middle cerebral artery occlusion?

5. The Lazdunsky group suggested, from data obtained using infection of rat cerebellar granule cells with viruses that express dominant-negative TASK-1/TASK-3 channels, that  $K^+$  influx via TASK channels is critically involved in regulating the level of apoptosis in developing cerebellar granule cells (Lauritzen et al., 2003). What happens to postnatal brain development of TASK-3 knockouts?
6. With regard to the above five topics, is the phenotype of TASK-1 and TASK-3 double knockout mice more severe than the single knockouts?
7. Do TASK channels actually contribute to homeostatic plasticity in granule cells as proposed by Brickley et al., 2001? The evidence presented in that paper was indirect. What happens if we cross TASK-3/TASK-1 double knockouts with the GABA<sub>A</sub>  $\alpha 6$  knockout? This would be a rigorous test of the original proposal by Brickley et al.
8. What happens to blood pressure regulation in the TASK knockouts? It's predicted that on the adrenal glomerulosa, angiotensin II acts via TASK-1/TASK-3 channel closure to cause aldosterone release (Czirjak et al., 2000; Czirjak and Enyedi, 2002b). As aldosterone promotes  $Na^+$  reabsorption in the kidney, we would predict that TASK-1/TASK-3 knockouts (possibly double TASK-1 and TASK-3 knockouts) would have hypotension.
9. Sensing of blood oxygen concentration in arterial chemoreceptors is predicted to require TASK-1 and TASK-3 channels (Buckler, 1997; Buckler et al., 2000). Does it?

## 2 METHODS

### 2.1 Generation of TASK-3 knockout mice

Additional details are given in the Appendix chapter, where I also briefly review the background techniques

We initially obtained the mouse TASK-3 (KNCK9) gene sequence by aligning the rat TASK-3 cDNA sequence (accession No. AF192366) (Kim et al., 2000) with the Celera mouse genome database. Later we worked with the gene using the annotated “Ensembl mouse genome server” database ([http://www.ensembl.org/Mus\\_musculus/geneview?gene=ENSMUSG00000036760](http://www.ensembl.org/Mus_musculus/geneview?gene=ENSMUSG00000036760)).

The mouse TASK-3 gene (on chromosome 15, E1 region) consists of two exons (283 and 923 bp) with an intervening 38.5 Kb intron<sup>2</sup>. The intended targeting vector strategy consisted in flanking exon 1 of the mTASK-3 gene with loxP sites in the same orientation (Figure 21). A neomycin resistance gene cassette, flanked by *frt* sites, was inserted as a positive selection marker for embryonic stem (ES) cell culture (Appendix Figure 21B, 21C).

The mouse TASK-3 gene was obtained by screening a mouse 129 BAC library (BAC mouse ES release I, BAC-4921, Library Screening Services, Genome Systems Inc, USA) with a 1 Kb intronic probe (at the 5' end of intron 1) (see Figure 31). This probe was generated by PCR on C57Bl/6 mouse tail DNA using primers: 5'-CCA TCA CTG TCA TCA CAA CTA TCG-3' (sense) and 5'-CTC ACA GAT CCA AAG AGA TGG ACC-3' (antisense) (see also Appendix sections 5.6 “Hybridization probes” and 5.10 “List of primers”).

The targeting vector backbone was obtained by subcloning an 8 Kb *EcoRI* fragment of the TASK-3 gene (see Figure 31), containing exon 1, into the pLitmus38 vector (New England Biolabs) (see Appendix section 5.2.1 for details). After insertion of the 8 Kb fragment, the *Sall* site in the polylinker of the pLitmus38 plasmid was converted to *NotI* site (see Appendix section 5.2.2). This unique *NotI* site permitted later linearization of the targeting vector (Figure R4B).

An 5'-*EcoRV*-loxP site

---

<sup>2</sup> In the Ensembl database, exon 2 is split into predicted exons 2 and 3 by a small intron of 160 bp; however, this is most likely a misprediction or alternative splicing, as all TASK-3 cDNAs, including the one I cloned, incorporate this intron as part of the coding region.

(5'-GATATCccATAACTTCGTATAGCATAACATTATACGAAGTTAT-3', the EcoRV site is underlined) was inserted into the unique BclI site, 560 bp upstream of the initiator ATG codon of exon 1 (Appendix section 5.2.3). The loxP site includes a 5' EcoRV site to permit its detection in the genome (Figure 21B); the BclI site was first demethylated by transformation of the plasmid into the *E. coli* GM33 *dam*<sup>-</sup> strain (gift of Dr. Axel Meyer). The loxP site orientation was verified by sequencing. The final targeting vector was obtained by insertion of a 5'-XhoI-*frt*-neomycin resistance-*frt*-loxP-SalI-3' cassette (Cope et al., 2004), containing the transcriptionally-independent HSV thymidine kinase promoter driving the neo gene, into an engineered SalI site, 275 bp downstream of the 3' end of exon 1; the SalI site was introduced by ligation of SalI linkers into an unique AfeI site in intron 1 (Appendix section 5.2.4). The orientation of the *frt*-neomycin resistance-*frt*-loxP cassette was verified by complete sequencing; a plasmid was selected with both loxP sites in the same orientation. The functionality of the loxP sites and *frt* sites was confirmed by transforming the targeting vector into 294Flp and 294Cre *E. Coli* cells expressing the Flp and Cre recombinase respectively (Buchholz et al., 1996)

The targeting vector was linearized with NotI and 30 µg were electroporated into mouse embryonic stem (ES) cells (strain 129/Sv, RI). The cells were grown in G418 on top of feeder fibroblast cells (see section 5.7 "Mouse embryonic stem cell culture").

ES cell colonies were screened by Southern blotting (Appendix section 5.4); colony genomic DNA was digested with NcoI, and hybridized with a specific 5' external probe, giving a 5.8 Kb band for the wild-type allele and a 4.2 Kb band for the targeted allele (Figure 22D); the 5' external probe was generated by PCR on C57Bl/6 mouse tail genomic DNA using the primers: 5'-CCA TGG CTA GGG ACA GAG AAG ATA-3' (sense) and 5'-TCT CAT TTC CCC TCT CCA GCA GTA-3' (antisense). The presence of the 5' loxP site was confirmed by digestion with EcoRV and hybridising with the same 5' external probe, which gives a 15 Kb wild-type band and a 5,6 Kb targeted allele band (Figure 22D). Because of the high GC density in the intron 1 sequences flanking the 3' end of the targeting vector, I could not find a specific 3' external probe; all probes from this region gave smears on Southern blots (Figure 31C).

I undertook three consecutive electroporations and screenings of ES cell aliquots: in the first two screens (of 850 colonies in total screened), no correctly targeted colonies were identified (Figure 32); in a third attempt, of 700 colonies screened, one was positive with the 5' external probe (NcoI) digest and also contained the 5'loxP site (EcoRV digestion) (Figure 22D).

Cells from this targeted stem cell colony were injected (by Dr. F. Zimmermann at the Zentral Tier Labor Heidelberg) into mouse C57Bl/6 blastocysts; of 19 chimeras obtained, four high density male chimeras were bred with C57/Bl6 wild-type mice; germline transmission of the targeted TASK-3 allele was confirmed by Southern blots of mouse tail DNA digested with NcoI and EcoRV respectively, hybridised with the 5' external probe (Figure 22E). It turns out that the line has multiply integrated TASK-3 targeting vectors at the TASK-3 gene. We termed this line **mitv-TASK3** (see Results section 3.2 “Actual targeting of the TASK-3 gene: multiple targeting vector integration”) (mitv-TASK-3 mice are knockouts of TASK-3). This was shown on Southern blots by hybridizing with the entire neo gene probe (Figure 22C, 22F, 23).

The subsequent generations of mitv-TASK-3 have been maintained on a C57/BL6 background, and are genotyped using NcoI digestion with 5' external probe (Figure 33B) or by PCR with primers flanking the 5'loxP site (Figure 33A).

## 2.2 Breedings with deleter mice to remove neomycin gene insertions

To remove the multiply integrated TASK-3 targeting vector insertions (and thus their multiple loxP sites) from the TASK-3 locus we crossed the mitv-TASK3 mice with the Cre deleter mice (Williams-Simons and Westphal, 1999) (Figure 23). Offspring were genotyped with the 5' probe. One offspring had one remaining copy of the neo insertion (flanked by frt sites) and possibly an inversion of Exon 1 (Figure 23B). These mice were termed **neo-TASK3** and they were genotyped using the 5' external probe on NcoI digested tail DNA. We obtained a 2.5Kb band corresponding to the reversion of neo. This band is neo-positive (Figures 23C, 23D). To remove the neo gene from neo-TASK3 mice, they were crossed with a Flp-deleter strain (Figure 21E) (Rodriguez et al., 2000). By Southern blot analysis (EcoRV digestion), mice which were negative for neomycin hybridization but still contained a characteristic EcoRV band of 5.6 Kb, as assayed with the 5' external probe, were provisionally termed (heterozygote) “TASK3-KO” mice (but in fact it turned out the TASK-3 gene was reactivated - see Figure 35).

## 2.3 Recombinant expression of mouse TASK-1 and TASK-3 cDNAs in HEK cells

Total RNA from C57BL/6 mouse whole brain was obtained using the ULTRASPEC RNA isolation system (BIOTECHX Laboratories, Inc.). 5 µg of total RNA was reverse transcribed using SuperScript Double-Stranded cDNA Synthesis Kit (Invitrogen).

### 2.3.1 Cloning of mTASK-3 cDNA

The coding region of TASK-3 was amplified from mouse brain cDNA using *Pfu* turbo DNA polymerase (Stratagene). PCR primers were designed from the predicted mouse DNA sequence (Ensemble mouse server, ENSMUSG00000036760) and by alignment of the published rat TASK-3 sequence (Kim et al., 2000): forward primer 5'-tcc ttc ttc gcg gcc ATG AAG CGG-3' and reverse primer 5'-act tcc ctc cca cac TTA GAT GGA CTT-3' (25 cycles at 94°C for 45s, 54°C for 45s, 72°C for 1min20s, 1 µg of mouse brain cDNA). Lower case letters indicate the 5'UTR and 3'UTR sequences in the forward and reverse primers, respectively. The PCR fragment was gel-purified and subcloned into the pPCR-Script cloning vector (PCR-Script Amp Cloning Kit, Stratagene). The insert was then excised with BamHI and NotI, treated with Klenow enzyme (Roche) and subcloned into the pCS2+ eukaryotic expression vector (gift of Dr. Roberto Bruzzone) linearized with StuI (see <http://sitemaker.umich.edu/dlturner.vectors/home> for details of this vector). The final construct was verified by complete sequencing using the following primers: T3Seq1, T3Seq12, T3Seq3, 9AST3, 12AST3 (see Appendix section 5.10.2 “Sequencing primers used for mTASK-3 and mTASK-1 cDNA”).

### 2.3.2 Cloning of mTASK-1 cDNA

PCR primers were designed from the published mouse TASK-1 sequence (Kim et al., 1998) (accession No. AF065162): forward primer 5'-gga tcc ATG AAG CGG CAG AAT GTG-3' (lower case letters indicate BamHI site) and reverse primer 5'-gtc gac TCA CAC CGA GCT CCT GCG-3' (lower case letters indicate SallI site). PCR conditions with mouse brain cDNA were identical to those used to obtain the mTASK-3 cDNA. The PCR fragment was gel purified and subcloned into pPCR-Script. The insert was then excised with BamHI and SallI and subcloned into BamHI-XhoI cut pCS2+ vector. The final construct was verified by complete sequencing with the following primers: T1Seq1, T1Seq2, T1Seq3, T1Seq1AS, T1Seq2AS (see Appendix section 5.10.2 “Sequencing primers used for mTASK-3 and mTASK-1 cDNA”).

The mTASK-1 and mTASK-3 expression vectors were transfected into HEK cells and analysed with patch-clamp electrophysiology by E. Veale, L. Evans and A. Mathie (Biophysics Section, Imperial College London, UK) (Aller et al., 2005).

## 2.4 In situ hybridization

*In situ* hybridization with <sup>35</sup>S-labeled oligonucleotide probes was performed as described by Wisden and Morris (1994). Hybridization buffer contained 50% formamide, 4 x SSC (0.6 M NaCl, 0.06 M sodium citrate), 10% dextran sulphate, 5 x Denhardt's solution (0.1% BSA, 0.1% Ficoll-400, 0.1% PVP), 200 µg/ml acid-alkali cleaved salmon sperm DNA, 100 µg/ml long chain polyadenylic acid, 25 mM sodium phosphate pH 7.0, 1 mM sodium pyrophosphate; hybridization was performed at 42°C overnight and washing at 60°C with 1 x SSC. Two independent oligonucleotides for each gene were hybridized in parallel as a control for specificity. Probes within each pair gave identical results. Non-specific labelling of the sections was assessed by hybridizing labelled oligonucleotide in the presence of a 100-fold excess of unlabelled oligonucleotide. Images were generated by exposure to Biomax MR (Kodak) X-ray film, and then scanned and processed in Adobe Photoshop. Brain structures and nuclei were confirmed with the atlas of Franklin and Paxinos (1997). The oligonucleotide sequences used are included in the Appendix section 5.11 "*in situ* hybridization oligonucleotides". For cellular resolution, sections were dipped in Ilford K5 emulsion and exposed at 4°C for 3 months. After development with D19 developer, the brain slices were Nissl stained with 30% sodium thiosulphate, dehydrated in ethanol and xylene, and coverslipped (Wisden and Morris, 1994).

## 2.5 Real-Time quantitative RT-PCR

Total RNAs from cerebellum and forebrain were isolated from adult homozygous mitv-TASK-3 and wild-type mice using the ULTRASPEC RNA isolation system (BIOTECX Laboratories, Inc.). The RNA was treated for 15 min at room temperature with DNase I (Qiagen) and cleaned with the RNeasy Mini kit (Qiagen). 5 µg of total RNA was reverse transcribed using the SuperScript Double-Stranded cDNA Synthesis Kit (Invitrogen). Real-time PCR was performed using a SYBR<sup>®</sup> Green PCR Kit (PE Applied Biosystems). A gene Amp 5700 sequence detector (PE Biosystems, courtesy of Dr. M. Schwaninger, Dept. of Neurology, Heidelberg) was used for the real-time PCR analysis. The cycling conditions were: initial denaturation at 95°C for 10 min, followed by 40 cycles of 95°C for 15 s and 60°C for 1 min. Fluorescence measurements were recorded during each annealing step. For each PCR, 5 µl of cDNA template was added to 25 µl of the PCR master mixture. All amplification reactions were performed in triplicate. To control for the recovery of intact cellular RNA and for the uniform efficiency of each reverse transcription reaction, a cyclophilin fragment was amplified by real-time RT-PCR. The

efficiency of real-time amplification was determined by running a standard curve with serial dilutions of pooled samples. A linear concentration-amplification curve was established. Quantified results for individual cDNAs were normalized to cyclophylin and the purity of the amplified products was checked by the dissociation curve (Aller et al., 2005).

The TASK-1, TASK-3 and cyclophylin oligonucleotide sequences were as used by Lauritzen et al. (2003) and TWIK-1, THIK-2, TREK-1, TREK-2, TRAAK and GABA $\alpha$ 6 oligonucleotide sequences were as used by Heurteaux et al. (2004). The oligonucleotide sequences are included in the Appendix section 5.12 “Real-time quantitative-PCR oligonucleotides”.

## 2.6 Immunohistochemistry

Adult mice were perfused transcardially with PBS (0,13 M NaCl, 3 mM NaH<sub>2</sub>PO<sub>4</sub>, 7 mM Na<sub>2</sub>HPO<sub>4</sub>, pH 7.4) and then with ice-cold 4% PFA/PBS. The brains were removed, postfixed 2 hours in 4% PFA/PBS and preserved overnight at 4°C in PBS. Fixed brains were blocked in 4% agar/PBS and cut at 50  $\mu$ m on a vibratome. The sections were washed 3 times in TBS (50 mM Tris-HCl, 150 mM NaCl, pH 7.6) (each time 5 minutes) at RT, then incubated 15 minutes at RT in 1% H<sub>2</sub>O<sub>2</sub> in TBS and washed again 3 times in TBS at RT (each time 10 minutes). The sections were preblocked for 1 hour in 10% normal goat serum and 0,3% Triton X-100 and then incubated at 4°C for 48 hours with a affinity purified rabbit anti-TASK-3 antibody (1:1000–1:10000) produced in Douglas Bayliss’s laboratory (Berg et al., 2004). After 3 washings in TBS for 10 minutes at RT, sections were incubated with biotinylated goat anti-rabbit IgG (H+L) secondary antibody BA-1000 (Vector Laboratories) (1:500) for 2 hours at RT, washed again 3 times with TBS (10 minutes, RT) and incubated 1.5 hours at RT with an avidin-biotin complex (ABC Elite kit; Vector Laboratories). The immunoreactivity was detected with diaminobenzidine (0.4 mg/ml) (Sigma). Sections were air-dried, dehydrated in ethanol and xylene, and coverslipped.

## 2.7 Western blots

Mice were killed under anesthesia with isoflurane and subsequently their brains were removed, weighted and homogenized (on ice) in a 10:1 v/w ratio with extraction buffer (25 mM HEPES, 150mM NaCl, pH 7.4) containing protease inhibitor. The homogenate was centrifuged 5 minutes at 3000 rpm at 4°C and then the supernatant was recentrifugated for 1.5 hours at 13000rpm at 4°C. The obtained pellet was resuspended in 5v of extraction buffer containing protease

inhibitor. The protein concentration of the samples was determined using Bradford protein assay reagent. The extracted proteins were stored at  $-80^{\circ}\text{C}$ .

The protein samples (20 and 40  $\mu\text{g}$ ) were separated by SDS-PAGE in a discontinuous system (5% acrylamide containing stacking gel and 10% acrylamide containing resolving gel) as described by Sambrook and Russell (2000) and then transferred to nitrocellulose membranes (Sambrook and Russell, 2000). The membranes were incubated in 5% powder milk in PBST (0.1% Tween 20 in PBS) overnight at  $4^{\circ}\text{C}$  and then washed twice with 2.5% powder milk/PBST for 10 minutes at RT. The membranes were then incubated with the affinity-purified rabbit anti-TASK-3 antibody (1:2000–1:10000) produced in Douglas Bayliss laboratory (Berg et al., 2004) for 1 hour at RT and washed with PBST 3 times for 10 minutes at RT. The membranes were next incubated with anti-rabbit IgG, horseradish peroxidase linked whole antibody (Amersham, Biosciences) (1:8000) for 1 hour at RT and then washed twice with PBST and then twice with PBS, for 10 minutes at RT. All membranes were visualized using ECL plus Western Blotting Detection System (Amersham Biosciences) and exposure to ECL Hyperfilm (Amersham Biosciences).

## **2.8 Electrophysiology experiments**

Electrophysiology experiments were performed by Dr. S. Brickley (Division of Cell and Molecular Biology, Imperial College London, UK)

### **2.8.1 Acute slice preparation**

Two month old mice were killed by cervical dislocation and the brains rapidly removed and placed into an ice-cold artificial cerebrospinal fluid. A sucrose replacement technique adapted from Mann-Metzer and Yarom (1999) was employed for preparation of parasagittal cerebellar slices (250  $\mu\text{m}$  thick). The brain was rapidly dissected and submerged in cold slicing solution ( $\sim 4^{\circ}\text{C}$ ), which contained (in mM) 85 NaCl, 2.5 KCl, 1 CaCl<sub>2</sub>, 4 MgCl<sub>2</sub>, 25 NaHCO<sub>3</sub>, 1.25 NaH<sub>2</sub>PO<sub>4</sub>, 75 sucrose, 25 glucose. All extracellular solutions were bubbled with 95% O<sub>2</sub> and 5% CO<sub>2</sub> (pH 7.4). After cutting on a moving blade microtome (Desaka), slices were maintained in sucrose solution at  $34^{\circ}\text{C}$  for a further 30 minutes before the slicing solution was gradually replaced with a solution containing (in mM): 125 NaCl, 2.5 KCl, 1 CaCl<sub>2</sub>, 4 MgCl<sub>2</sub>, 26 NaHCO<sub>3</sub>, 1.25 NaH<sub>2</sub>PO<sub>4</sub>, 25 glucose. Slices were then transferred to a recording chamber and constantly perfused (2ml/min) with standard recording solution that contained (in mM): 125 NaCl, 2.5 KCl,

1 CaCl<sub>2</sub>, 2 MgCl<sub>2</sub>, 26 NaHCO<sub>3</sub>, 1.25 NaH<sub>2</sub>PO<sub>4</sub>, 25 glucose, pH=7.4 when bubbled with 95% O<sub>2</sub> and 5% CO<sub>2</sub>.

### 2.8.2 Patch-clamp recording from cerebellar granule cells

All experiments were performed at room temperature with 1 mM kynurenic acid and 30 μM picrotoxin added to the external solution to block glutamatergic and GABAergic synaptic transmission (all drugs were supplied by Sigma-Aldrich; UK). The pipette solution contained (in mM) 120 KCH<sub>3</sub>SO<sub>4</sub> 4 NaCl; 1 CaCl<sub>2</sub>; 1 MgCl<sub>2</sub>; 10 HEPES; 5 EGTA; 2 Mg-ATP (adjusted to pH 7.3 with KOH). Granule cells were visualized using a Zeiss Axioscop 2FS fitted with Normaski optics optimized for infra-red video microscopy. Whole -cell recordings were made using either an Axopatch 200A or 700B amplifier (Axon Instruments; Foster City, CA).

### 2.9 Behavioural studies

Behavioural studies were performed by A.M. Linden and E.R. Korpi (Institute of Biomedicine and Pharmacology, University of Helsinki, Finland).

TASK-3 knockout, heterozygous and littermate wild-type mice (3 month old weighting 27-36 g) were maintained at the standard animal facilities in polypropylene macrolon cages with food pellets and tap water available *ad libitum*. Lights were on from 6 a.m. to 6 p.m. Temperature and humidity were controlled at 20 ± 1°C and 50 ± 10%, respectively. All animal tests were approved by the Laboratory Animal Committee of the University of Helsinki. The person who observed and recorded the behavior was not aware of the genotype of the tested animals. Behavioral and physiological characterization of phenotypes was performed using a modified version (Vekovischeva et al., 2004) of the primary screen described in the SHIRPA protocol (SmithKline Beecham Pharmaceuticals; Harwell, MRC Mouse Genome Centre and Mammalian Genetics Unit; Imperial College School of Medicine at St Mary's; Royal London Hospital, St Bartholomew's and the Royal London School of Medicine; Phenotype Assessment; Rogers et al., 1997).

To investigate motor coordination and learning, the mice were trained for 6 days (3-6 trials a day) to stay walking on a rotating rod (Rotamex 4/8, Columbus Instruments, Ohio, USA) for 180 s while the rotation speed accelerated from 5 to 40 rpm (Korpi et al., 1998). The latency to fall from the rod in each trial was recorded. The mice were also trained to walk across a 100 cm long wooden beam (1.2 and 0.8 cm in diameter) to return to their home cage. The beam is placed 84

cm above the floor. The latency to reach the other end of the beam and the number of falls were recorded.

The sensory functions of TASK-3 KO mice were examined by studying the acoustic startle response and prepulse inhibition of the response, using a two-unit automated startle system (Med Associates Startle Reflex System, Med Associates Inc., Georgia, Vermont, USA). The test session began with a 5 min acclimation period (65 dB) followed by seven trials containing seven stimuli (40 ms) of different intensities (65, 71, 75, 85, 95, 10, and 120 dB). Intertrial interval varied between 9-21 s. The prepulse inhibition of the acoustic startle response was analysed one week later using a 71 dB prepulse stimulus (20 ms) combined with a startle-eliciting stimulus of 95 dB. The interval between prepulse and startle stimuli was 100ms and intertrial interval varied between 9-21 s.

The T-maze test was used to evaluate the memory and motivation of TASK-3 KO mice. A T-maze consists of three arms (length of start arm and goal arms 50 cm; width 10 cm; height 15 cm). The maze is equipped with three doors that can be operated using a remote controller. For spontaneous alternation test (10 min), the mouse was placed in the start box with the door closed for 5 s and then the door was opened: the mouse could choose one of the arms of the maze and the opposite arm was closed. Every time the mouse returned to start arm after entering either left or right arm, 1 trial was completed and the mouse is confined for 5 s and the doors were opened again. The number of trials and the number of alternations between arms during 10 min were recorded. For evaluating the forced trial time, the mouse was placed in the start box with the door closed for 5 s. The left arm of the maze was open (forced trial to the left). The door was opened and the latency to go to the left arm and to return to start box was recorded.

### 3 RESULTS

#### 3.1. Expression of the TASK-1 and TASK-3 genes in the adult mouse

The expression of the TASK-1 and TASK-3 channel genes in mouse tissues was initially described by northern blot analysis. As seen in Figure 12, in contrast to TASK-1, TASK-3 gene expression in the adult mouse is largely brain-specific. TASK-1 transcripts were found in heart, brain, lung, liver kidney and testis (Figure 12A); after stripping and rehybridizing the membrane, TASK-3 transcripts (predominantly 9.5 Kb) were only seen clearly in an RNA sample from whole brain (Figure 12B) (although this does not exclude gene expression in for example, the adrenal gland (Bayliss et al., 2003)).

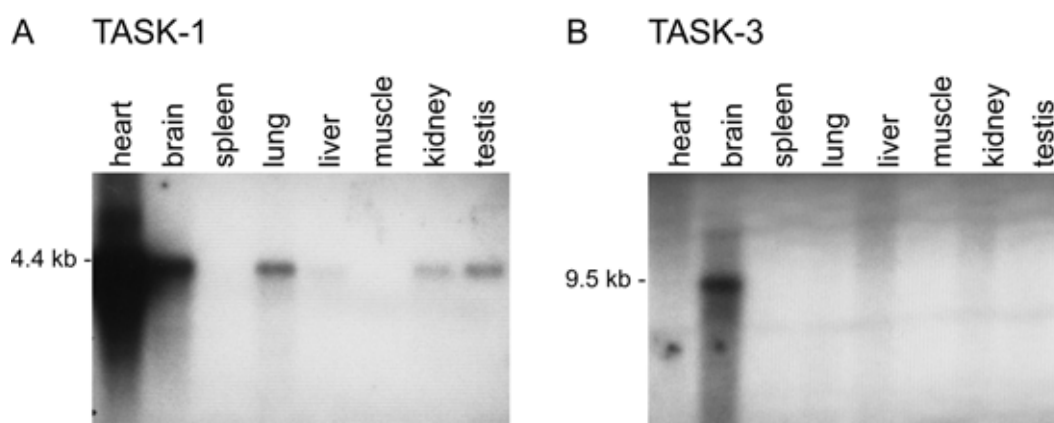


**Figure 12.** Expression of *TASK-1* (A) and *TASK-3* genes (B) in mouse tissues determined by northern blot analysis. A Clontech membrane was hybridized by Dr. Victoria Revilla when the Wisden laboratory was at the MRC, Cambridge, UK (the *TASK-1* and *TASK-3* probes, hybridized consecutively to the membrane, are described in Brickley et al., 2001)

The expression of the K2P gene family in the brain has been studied largely by *in situ* hybridization in the rat (e.g. Karschin et al., 2001; Talley et al., 2001). It is clear, however, that sometimes there can be differences in expression patterns of orthologous genes between rodent species or even between rodent subspecies, two examples being the 5-HT<sub>5B</sub> receptor gene that in the rat is expressed in CA1 hippocampal pyramidal cells and the medial habenula, but in the mouse is mainly expressed in the medial habenula (Wisden et al., 1993; Wisden and Morris, 1994), and the strong differences in vasopressin-1A receptor gene expression between brain nuclei of vole subspecies (Young et al., 1999). Thus as my project concerned investigating the

contributions of TASK-3 channels to *mouse* brain physiology using TASK-3 knockouts, I first described the distribution of the TASK-1 and TASK-3 channel mRNAs in the adult mouse brain by *in situ* hybridization to look at potential targets which could be affected by TASK-3 deletion. Using gene-specific <sup>35</sup>S-labelled TASK-1 and TASK-3 oligonucleotide probes, I hybridised a series of coronal (adult mouse brain) sections from the olfactory bulb through to the hindbrain (Figures 13 to 15). I examined both global (X-ray film autoradiographs) and, for TASK-3, nuclear emulsion (cellular resolution) images (Figures 16 to 18). The data are summarized in Table 4.

### 3.1.1 TASK-1 expression in the adult mouse brain

At the level of X-ray film analysis, the cell-type with the highest TASK-1 expression was cerebellar granule cells (Figure 15E), motor neurons (for example, motor nucleus VII, Figure 15E), followed by olfactory bulb granule cells (Figure 13A) (see also Aller et al., 2005). There was mild TASK-1 gene expression in the neocortex, some thalamic nuclei e.g. reticular thalamus (Figure 13G, 14A), reuniens thalamic nucleus (Figure 13G), parafascicular thalamic nucleus (Figure 14C) and medial geniculate nucleus (Fig. 15A). All of these nuclei had more TASK-1 hybridization signal than TASK-3 signal. Outside of the brain there are various tissues in the mouse, such as heart, where the TASK-1 gene is expressed but not TASK-3 (Fig. 12A). In the brain, can be found regions which express mainly the TASK-1 gene: reticular thalamus, reuniens thalamic nucleus (Figure 13G), parafascicular thalamic nucleus (Figure 14C), and possibly the medial geniculate nucleus (Figure 15A).

### 3.1.2 TASK-3 expression in the adult mouse brain

In contrast to TASK-1, the TASK-3 gene expresses more strongly, although variedly, throughout the neuroaxis. For example, expression is clear in olfactory bulb granule cells (Figure 13B), the external plexiform layer of the bulb (Figure 13B), piriform cortex (Figures 13D and 13F), and neocortex, with higher expression in layers 2 and 6 (Figures 16B and 16D). In the neocortex, it seems that most (but not all) neurons express TASK-3 (Figures 16B and 16D); Figure 18A shows a magnification of neocortical cells in layer VI. Large cells (putative pyramidal) have silver grains clustered over them, but there are also various small unlabelled cells. Other TASK-3 expressing areas are the septum (Figure 13F), amygdala (Figure 14B), many thalamic nuclei (Figures 13H, 17B and 18D), and rare large cells (putative cholinergic) in the caudate putamen

(Figures 16D and 18B), and many (but not all) cells in the inferior colliculi (Figures 17D and 18E).

### **3.1.3 Mainly TASK-3 expressing areas/cells**

There are many regions and cell types which only, or mainly, express the TASK-3 gene: hippocampal CA1 pyramidal cells (Figures 14B, 15B and 16F), dentate granule cells (Figures 14B, 15B and 16F), piriform cortex (Figures 13H), anterior dorsal thalamic nucleus (strongly, Figures 13H and 17B), dorsal lateral geniculate thalamic nucleus (Figure 14D), accumbens nucleus (Figure 13D), lateral septum, hypothalamic nuclei (for example, the suprachiasmatic nucleus that regulates the circadian rhythm has particularly strong expression (Figure 13H)) and the locus coeruleus (adrenergic projection neurons) (Figure 15F). In all of these areas, it is likely that channels in the TASK-1/-3 subfamily form only or largely from TASK-3 subunits.

### **3.1.4 Cell-types/areas expressing both TASK-1 and TASK-3**

The brain areas/cell types with both TASK-1 and TASK-3 transcripts include: cerebellar granule cells (Figures 15E, 15F and 17F), motor neurons (Figures 15E and 15F), dorsal raphe nucleus (Figure 15C and 15D) and the pontine nuclei (although higher TASK-1) (Figures 15A and 15B), possibly some cells in the neocortex (TASK-1 is uniformly weak in neocortex, TASK-3 expression is more prominent – see Figure 16B), medial habenula (Figures 14A and 14B), olfactory bulb granule cells and cells in the external plexiform layer (Figures 13A and 13B). In these areas and cell types it is likely that TASK-1/TASK-3 heterodimers exist.

### **3.1.5 Cell types with no detectable TASK-1 or TASK-3 expression**

There are some cell types that express neither the TASK-1 or TASK-3 genes: for example, cerebellar Purkinje cells (Figures 17E, 17F, and 18F illustrate this for TASK-3) and stellate/basket cells in the molecular layer of the cerebellum (Figure 18F). Another prominent cell type lacking both TASK-1 and TASK-3 expression is hippocampal CA3 pyramidal cells (Figures 14C and 14D). Glial cells in the white matter tracts (e.g. corpus callosum) also do not express the TASK-1 or TASK-3 genes (Figure 13).

<b>Brain region</b>	<b>TASK-1</b>	<b>TASK-3</b>
<b>Olfactory system</b>		
Olfactory bulb, glomerular layer (OBgl)	++	+++
Olfactory bulb, granule cell layer (Obgr)	++	+++
<b>Neocortex</b>		
Neocortex, layers II/III	+	++
Neocortex, layer IV	+	+
Neocortex, layers V	+	+
Neocortex, layers VI	+	++
Piriform cortex (Pir)	+	+++
<b>Basal forebrain</b>		
Accumbens (Acb)	-	+++
Caudate putamen –cholinergic cells (Cpu)	-	++
Lateral septal nucleus, intermediate (LSI)	-	+
<b>Amygdala</b>		
Medial amygdaloid nucleus (Me)	-	++
<b>Hippocampus</b>		
Pyramidal cell layer, CA1	-	+++
Pyramidal cell layer, CA3	-	-
Granule cell layer, dentate gyrus (DG)	-	+++
<b>Thalamus</b>		
Reticular thalamus (Rt)	++	+
Reuniens thalamic nucleus (Re)	++	-
Parafascicular thalamic nucleus (PF)	++	-
Dorsal lateral geniculate nucleus (DLG)	+	++
Medial geniculate nucleus (MG)	+	-
Medial habenular nucleus (MHb)	+	++
Anterodorsal thalamic nucleus (AD)	+	+++
<b>Hypothalamus</b>		
Suprachiasmatic nucleus (Sch)	-	+++
Ventromedial thalamic nucleus (VMT)	+	+
<b>Midbrain</b>		
Superior colliculus (SC)	+	++
Inferior colliculus (IC)	+	+++
Pontine nuclei (Pn)	++	+
Interpeduncular nucleus (IP)	+++	+
Interpeduncular nucleus, dorsomedial subnucleus (IPDM)	+++	+++
<b>Cerebellum</b>		
Granule cells (gr)	++++	+++
Purkinje cells (P)	-	-
Stellate/basket cells (S)	-	-
<b>Brainstem aminergic nuclei</b>		
Dorsal raphe nucleus (DR)	++	++
Median raphe nucleus (MnR)	-	++
Locus coeruleus (LC)	+	+++
Abducens nucleus (VI)	-	+
Facial nucleus (VII)	+++	++++

**Table 4.** Distribution of the TASK-1 and TASK-3 mRNA expression in the adult mouse brain

Expression ratings were pooled from the opinions of three independent observers (C. Sandu, W. Wisden and I. Aller): +++++, very strong signal; +++, strong signal; ++, medium signal; +, weak signal; -, no signal.

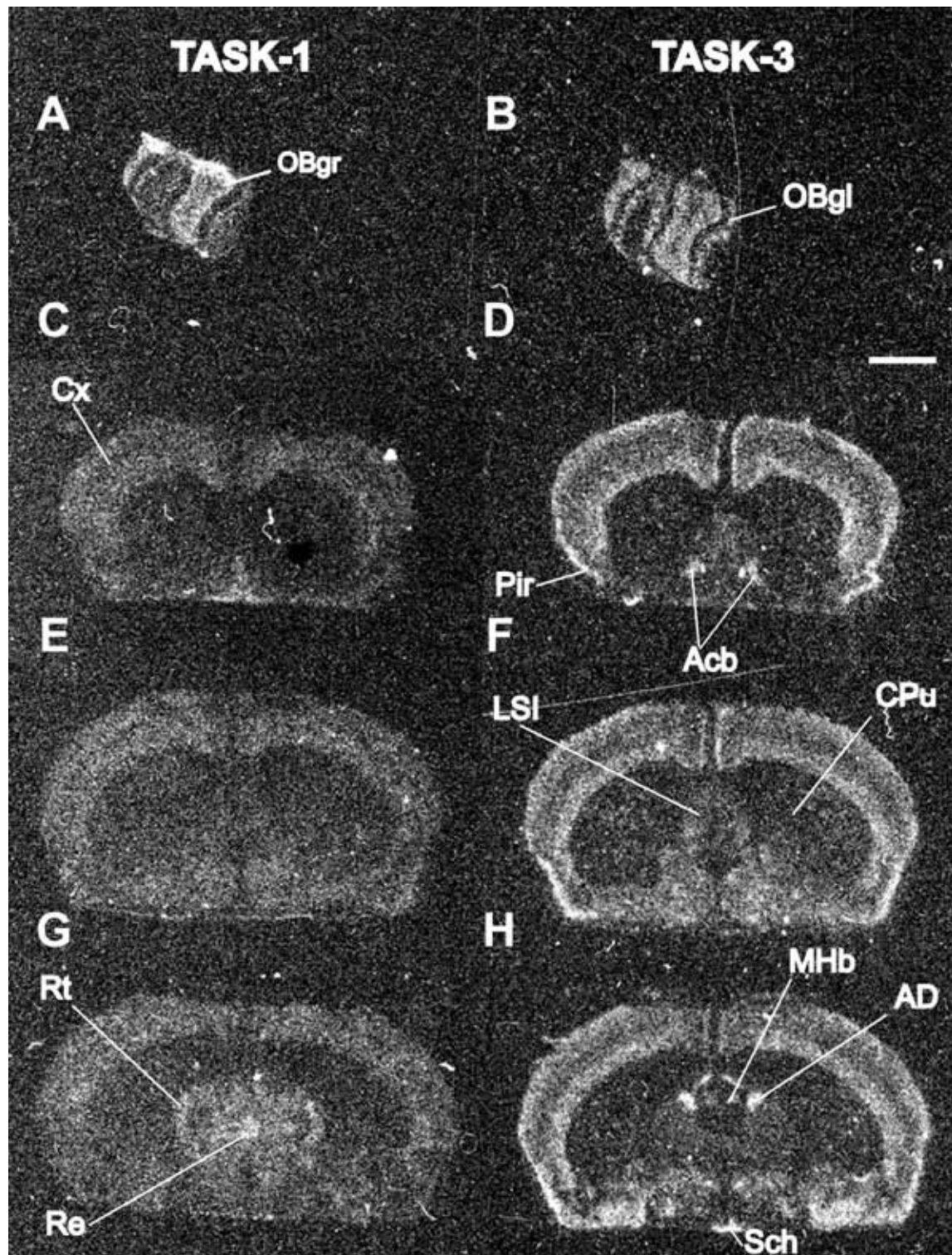


**Figure 13.** X-ray film autoradiographs indicating mRNA expression of TASK-1 and TASK-3 on coronal mouse brain sections (olfactory bulb to pre-hippocampus) by *in situ* hybridisation using  $^{35}\text{S}$ -labeled specific oligonucleotide probes

A, C, E, G, TASK-1 mRNA expression; B, D, F, H, TASK-3 mRNA expression. White areas indicate expression. Abbreviations given in Table 4. Scale bar 2mm.

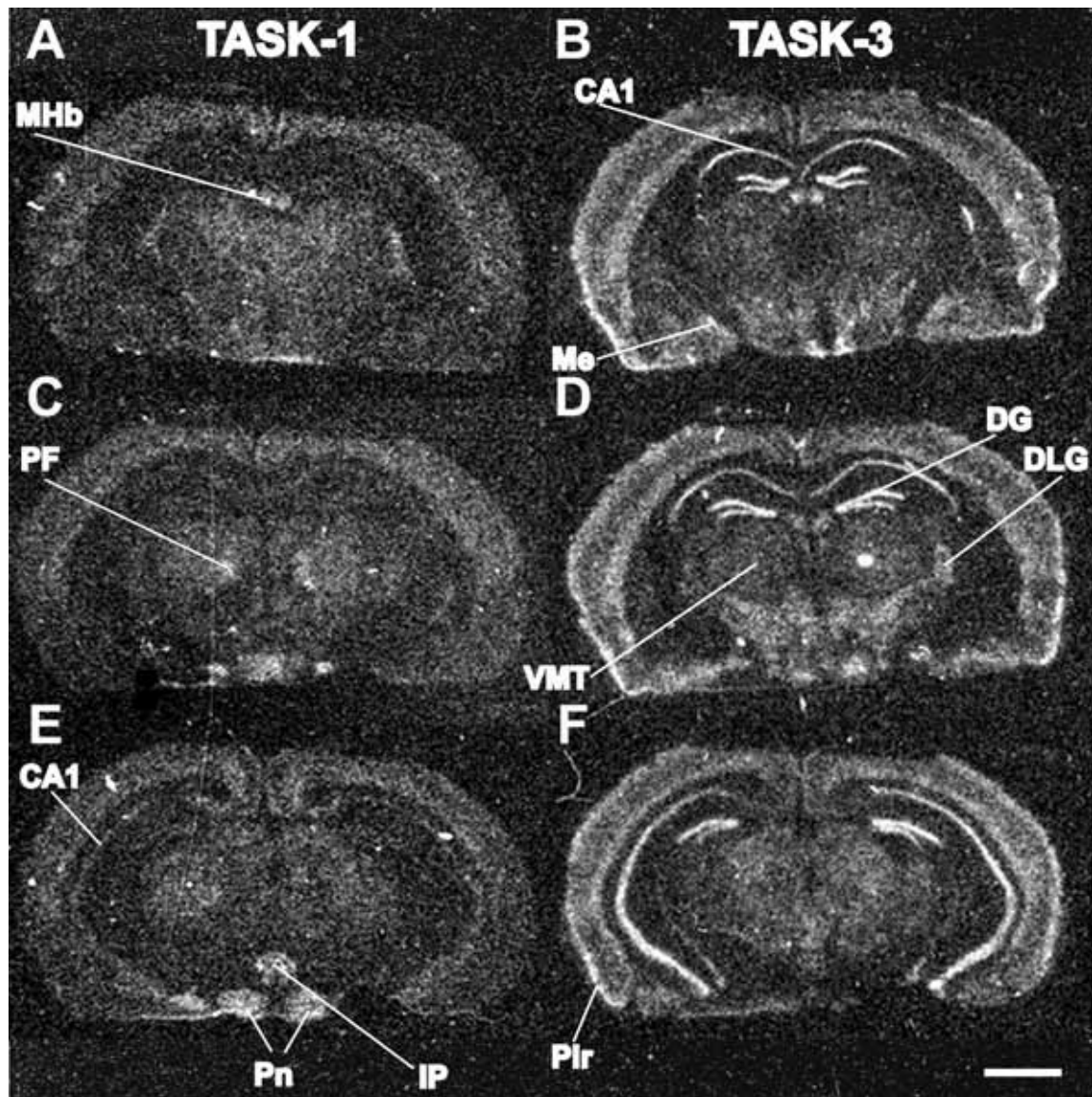


**Figure 14.** X-ray film autoradiographs indicating mRNA expression of TASK-1 and TASK-3 on coronal mouse brain sections (anterior to posterior hippocampus) by *in situ* hybridisation using  $^{35}\text{S}$ -labeled specific oligonucleotide probes

A, C, E, G, TASK-1 mRNA expression; B, D, F, H, TASK-3 mRNA expression. White areas indicate expression. Abbreviations given in Table 4. Scale bar 2 mm.

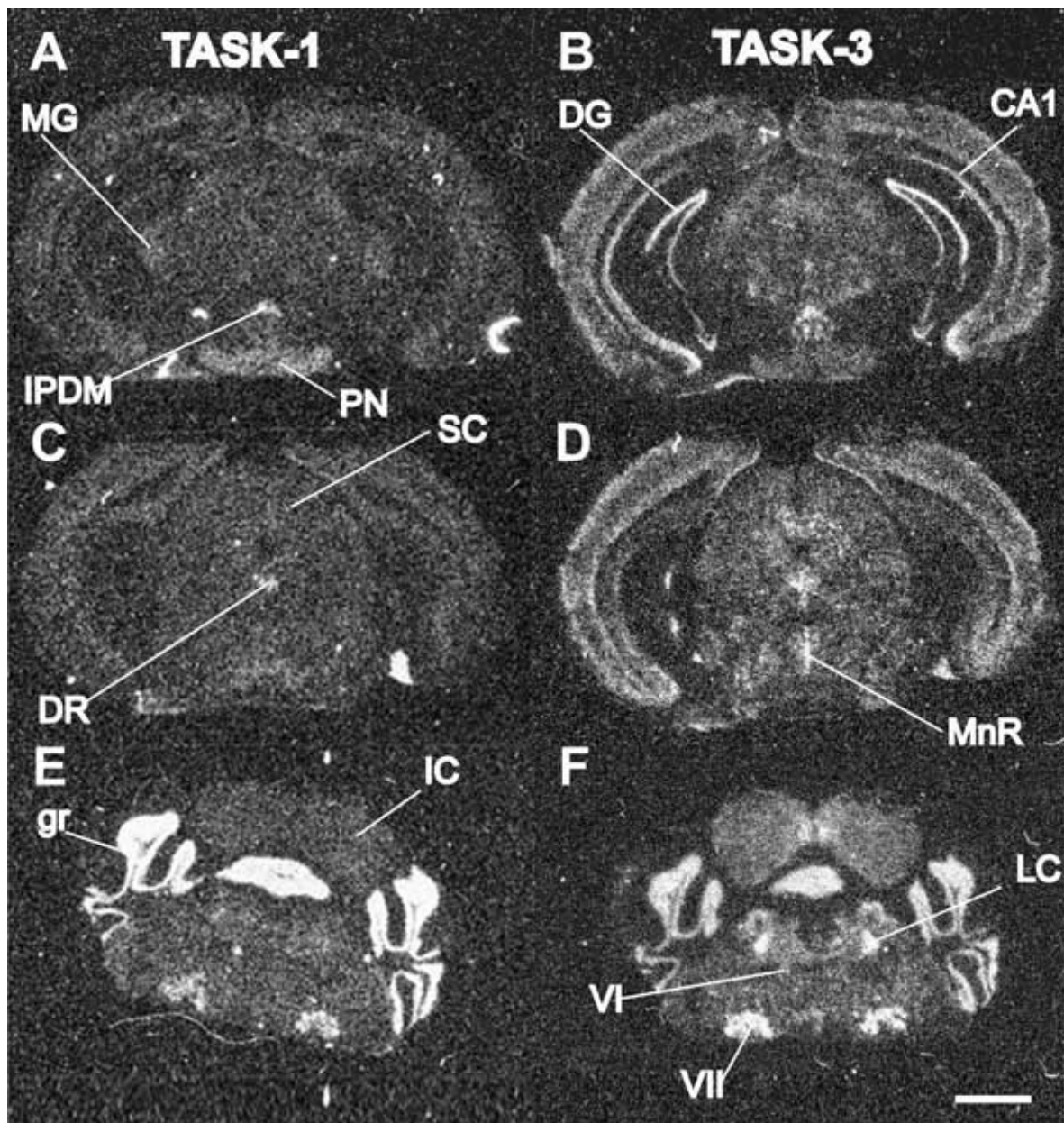


**Figure 15.** X-ray film autoradiographs indicating mRNA expression of TASK-1 and TASK-3 in coronal mouse brain sections (midbrain through to brainstem) by *in situ* hybridisation using  $^{35}\text{S}$ -labeled specific oligonucleotide probes. **A, C, E, G,** TASK-1 mRNA expression. **B, D, F, H,** TASK-3 mRNA expression. White areas indicate expression. Abbreviations given in Table 4. Scale bar, 2mm.

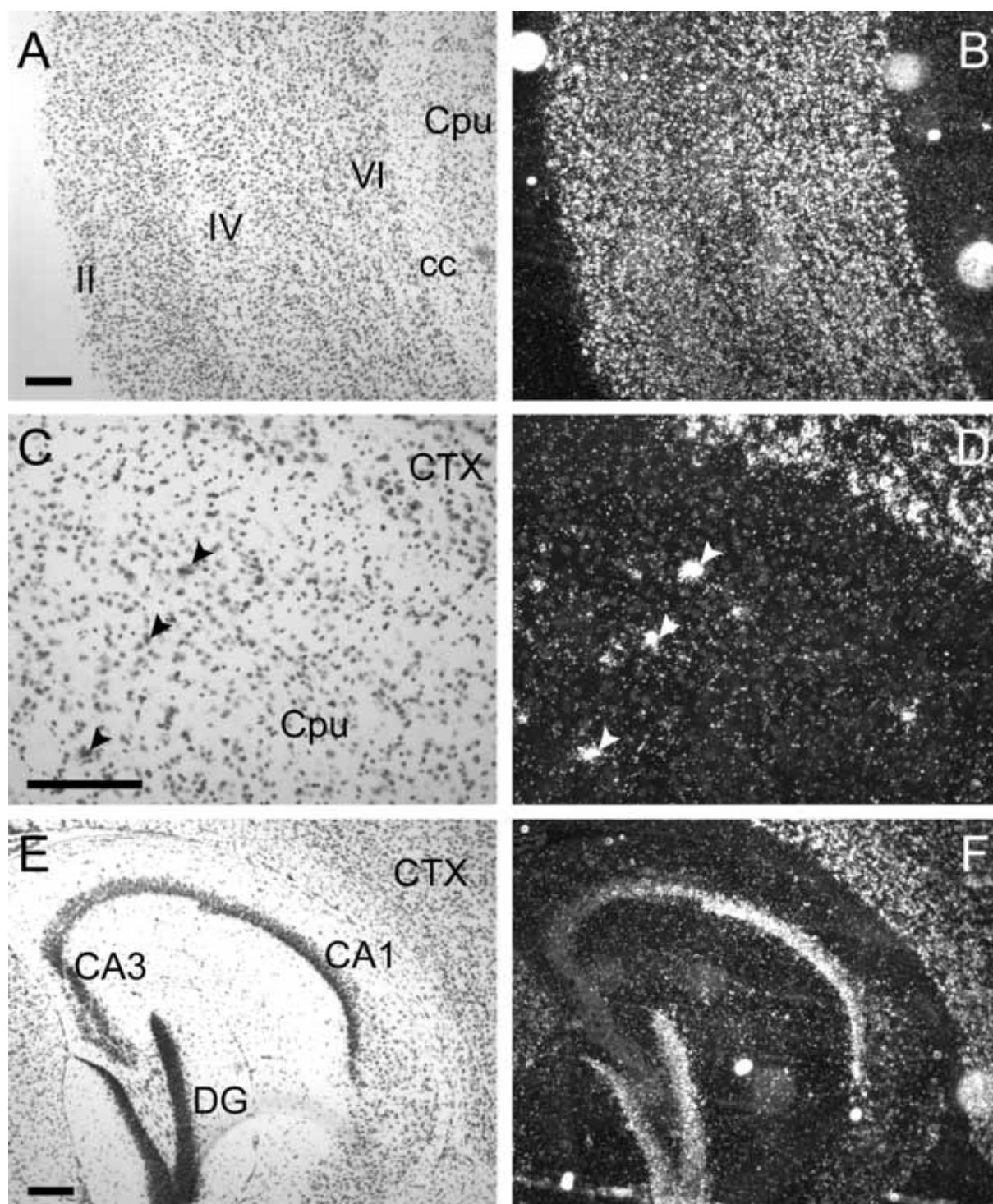


**Figure 16.** Expression of the mouse *TASK-3* gene in the neocortex (A-B), caudate putamen (C, D), and hippocampus (E, F) imaged with nuclear emulsion

The photographs in the left-hand column are the brain sections (Nissl-stained) viewed by bright-field optics; the left-hand images are the identical section placements viewed with dark-field optics to reveal the silver grains. The arrows in C indicate the large (putative cholinergic) cells with dense accumulations of silver grains over them. cc- corpus callosum, CA1- CA1 pyramidal cell layer, CA3- CA3 pyramidal cell layer, Cpu- caudate putamen, CTX- cortex, DG- dentate gyrus, II, IV, VI- neocortex layers. Scale bars, 200 $\mu$ m.

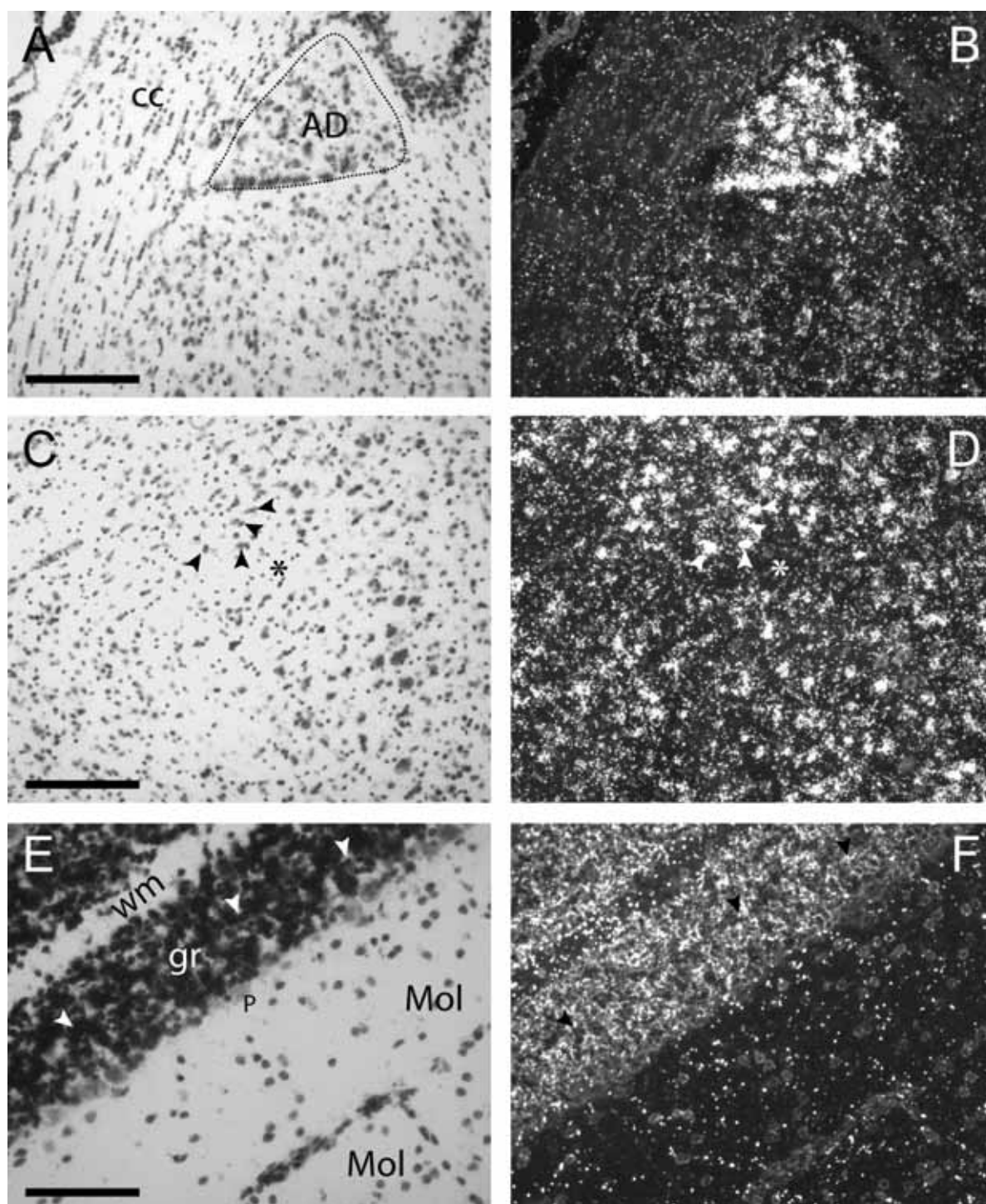


**Figure 17.** Expression of the mouse *TASK-3* gene in thalamic nuclei (anterodorsal thalamic nucleus) (A, B), inferior colliculus (C, D), and cerebellar granule cells (E, F) imaged with nuclear emulsion

The photographs in the left-hand column are the brain sections (Nissl-stained) viewed by bright-field optics; the left-hand images are the identical section placements viewed with dark-field optics to reveal the silver grains. Arrow heads in C indicate examples of labelled cells, whereas the \* indicates an example of a non-expressing cell. AD- anterodorsal thalamic nucleus cc- corpus callosum, gr- granule cell, Mol- molecular layer, P- Purkinje cell, wm- white matter; dashed line- marks the AD nucleus. Scale bars, 200 $\mu$ m.

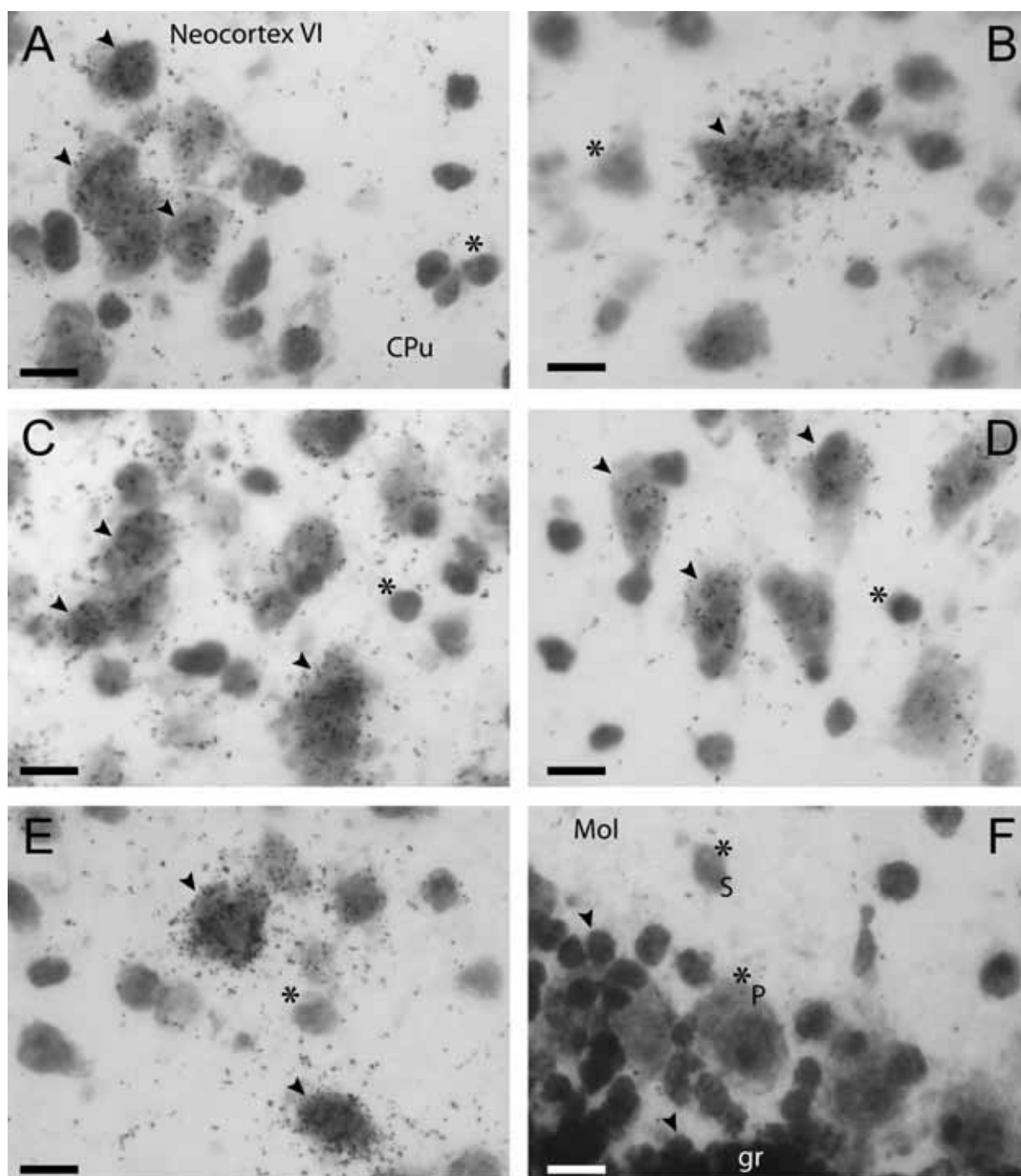


**Figure 18.** *Bright-field photomicrographs of emulsion autoradiographs illustrating cellular expression of the mouse TASK-3 gene in various brain areas*

**A**, neocortex, layer VI pyramidal cells positive for TASK-3 hybridization (arrows). **B**, putative large cholinergic interneuron in the caudate putamen (arrow) and one example of non-expressing cells (marked with \*). **C**, strongly expressing (putative relay) cells in the anteriodorsal thalamic nucleus (arrows). **D**, moderately expressing (putative relay) cells in the anteroventral thalamic nucleus. **E**, two strongly expressing cells in the inferior colliculus (arrows). **F**, cerebellar Purkinje cells (P) and stellate cells (S) do not express the TASK-3 gene. (note: the many silver grains over the granule cells are not visible in this image because of the dark Nissl stain, but they can be seen in dark-field, see Fig. 17F). Scale bars, 25  $\mu\text{m}$ .

### 3.2 Electrophysiological properties of recombinant mouse TASK-1 and TASK-3 channels

As further anticipation of characterizing the TASK-3 knockout mice, I contributed to studies characterizing the properties of the mouse TASK-3 and TASK-1 channels (Aller et al., 2005). It was necessary to establish diagnostic assays of TASK channel function that distinguish between the two subunit types.

By RT-PCR on brain cDNA, I isolated and sequenced the mouse TASK-1 and TASK-3 cDNAs and subcloned them into the eukaryotic expression vector pCS2+ (<http://sitemaker.umich.edu/dlturner.vectors/home>). The mouse TASK-3 cDNA sequence and the deduced topology of the mouse TASK-3 subunit are shown in Figure 19.

Electrophysiological properties of cloned mouse TASK-1 and mouse TASK-3 channels were analysed by patch-clamping on transfected HEK cells (Aller et al., 2005). The mouse TASK subunits form functional ion channels and generate pH-sensitive leak currents. By simply altering external pH it is possible to distinguish between TASK-1 and TASK-3 mediated currents (see Introduction section 1.4.1). As shown in Figure 20A, when mouse cDNA clones encoding TASK-1 channels were expressed the voltage-independent leak conductance present in these cells was sensitive to both external acidification and alkalization. Following a shift to pH 6.4, the leak conductance was inhibited by  $-75 \pm 4\%$  ( $n=5$ ) and at pH 8.4 the leak conductance was enhanced by  $96 \pm 8\%$  ( $n=5$ ). However, when TASK-3 channels were expressed the leak conductance was no longer sensitive to external alkalization ( $-2 \pm 1\%$ ,  $n=7$ ) though a clear block was still observed during external acidification ( $-41 \pm 4\%$ ,  $n=9$ ). Recent recombinant expression data on human TASK channels suggest that the blocking action of  $Zn^{2+}$  is also a useful diagnostic of TASK-3 channel function (Clarke et al., 2004). As shown in Figure 20B, at a concentration of 100  $\mu$ M,  $Zn^{2+}$  significantly blocks TASK-3-mediated currents ( $-86 \pm 3\%$   $n = 7$ ) with little effect on TASK-1 channels ( $-10 \pm 2\%$ ,  $n=4$ ). In a parallel series of experiments the blocking action of  $Zn^{2+}$  and the influence of external pH was compared between mouse and human clones. No significant difference in the blocking action of  $Zn^{2+}$  and the effect of external pH was observed between human and mouse clones (Figure 20C). Another signature of TASK-1 channel function should be the selective blocking action of cannabinoid agonists such as methanandamide or R-(+)-WIN 55,212-2 (Maingret et al., 2001). However, we found no practical difference in the potency of these drugs on TASK-1 and TASK-3 channels (data not shown).

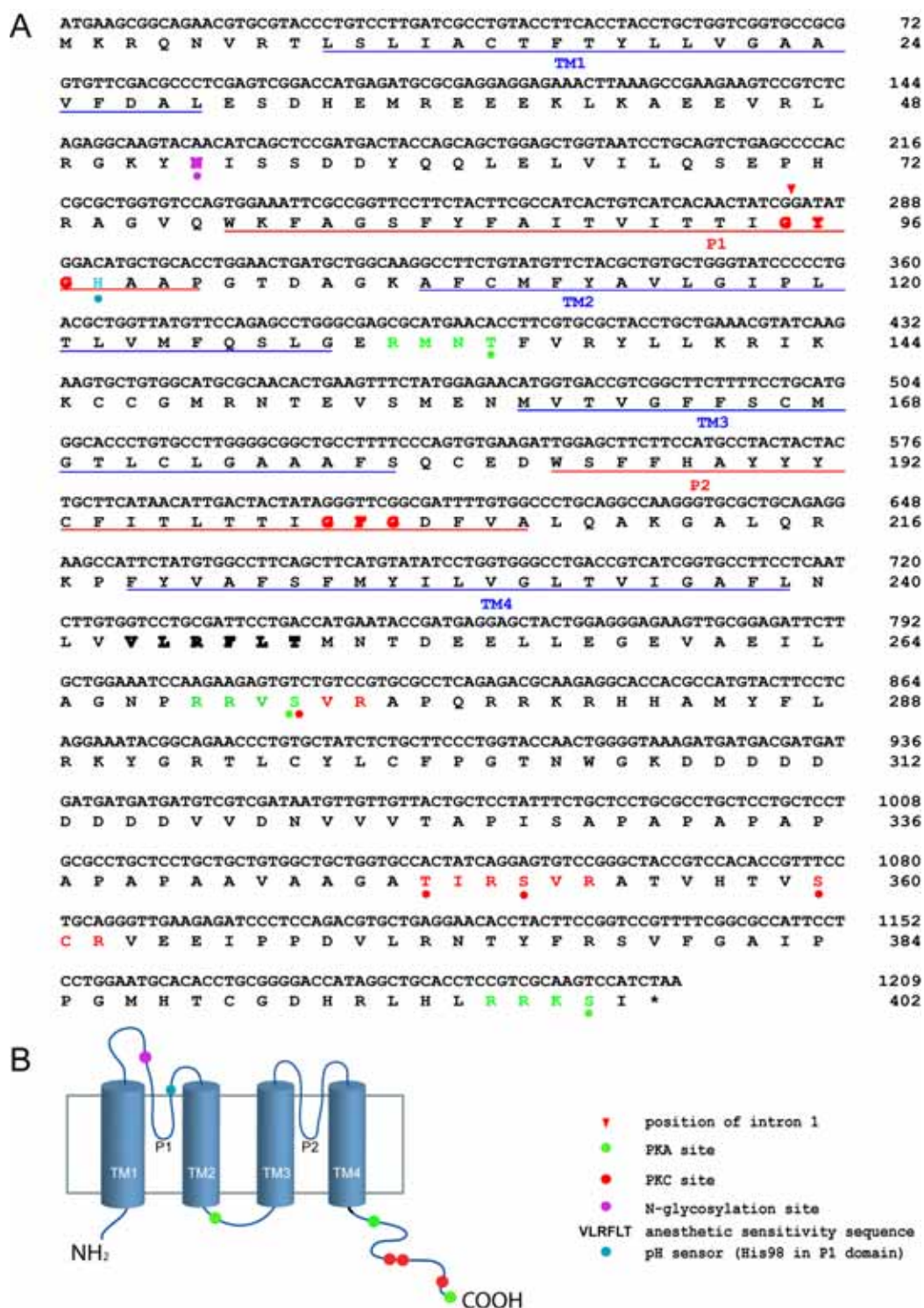


**Figure 19.** Sequence analysis of mouse TASK-3 subunit

**A**, Nucleotide and deduced amino acid sequence. The positions of the transmembrane domains (TM, blue lines) and pore domains (P, red lines) are indicated. Intracellular consensus phosphorylation sites for protein kinase A (green filled circles) and protein kinase C (red filled circles) are marked as well as the pH sensor histidine residue (blue filled circle) and a putative N-glycosylation site (purple filled circle). The inhalational anesthetic sensitivity sequence VLRFLT is indicated with bold letters. **B**, Deduced topology of mouse TASK-3. Symbols are the same as in **A**.

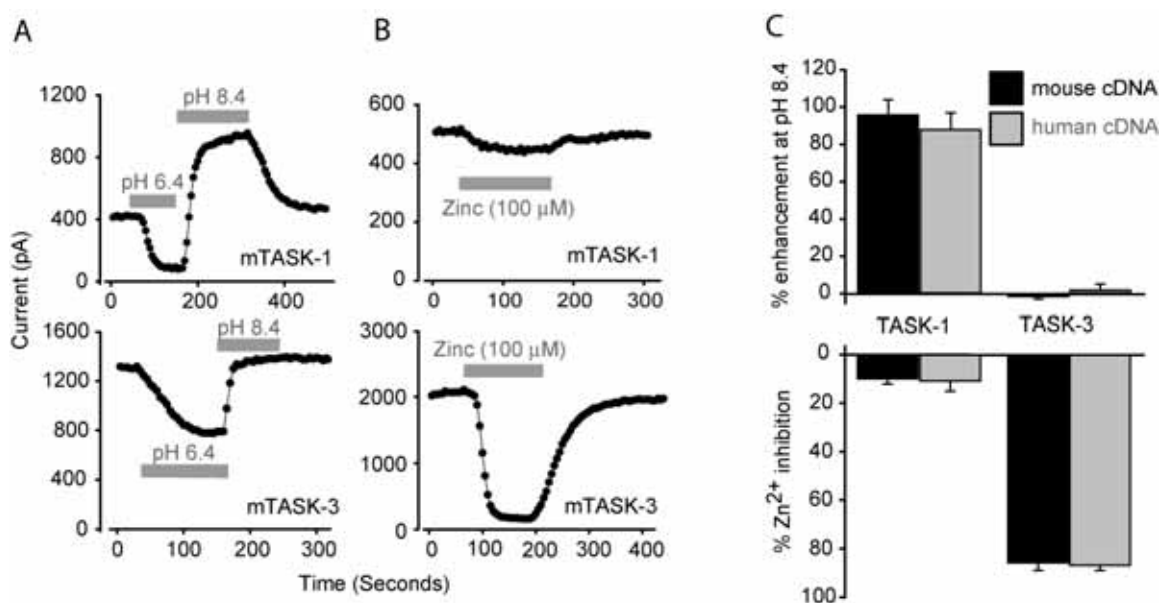


**Figure 20.** Discrimination between TASK-1 and TASK-3 mediated currents in HEK cells

**A**, Effect of altering external pH on the leak current recorded at  $-20\text{mV}$  following recombinant expression of mTASK-1 and mTASK-3 cDNA. In control conditions the external pH was maintained at pH 7.4 and during test periods the pH was shifted to 6.4 and 8.4. The upper plot illustrates the change in the mTASK-1-mediated current. External acidification blocks the current whereas alkalization enhances the leak current. In contrast, the lower plot illustrates how the mTASK-3-mediated current only responds to external acidification. **B**, Application of 100 mM  $\text{Zn}^{2+}$  to the external medium has little effect on mTASK-1-mediated currents (upper plot) but has a substantial blocking action on the mTASK-3-mediated leak current (lower plot). **C**, Comparing the effects of external alkalization and  $\text{Zn}^{2+}$  application when using either mouse (black fill) or human (grey fill) cDNA in the recombinant expression studies (Aller et al., 2005. Data provided by E.L. Veale and A. Mathie, Imperial College London, UK).

These recombinant expression studies demonstrate that extracellular alkalization and the addition of  $\text{Zn}^{2+}$  provide a useful diagnostic fingerprint for comparing TASK-1 and TASK-3 channel currents (Aller et al., 2005).

### 3.3 Generation of TASK-3 knockout mice

By homologous recombination in embryonic stem (ES) cells, I generated homozygous mice lacking a functional TASK-3 gene. However, as will become clear in the subsequent descriptions, the exact route of inactivation was not strictly conventional.

### 3.3.1 Planned TASK-3 gene targeting strategy

The TASK-3 gene has two exons: exon 1 encodes the first transmembrane domain through to the beginning of the first P1 loop. Inactivation of exon 1 will completely destroy protein function. My strategy was to make a conditional “floxed” allele of the TASK-3 gene (Figure 21D). I planned to flank exon 1 with loxP sites (red arrow heads in Figure 21, the substrate for Cre recombinase). This would permit either a cell-type-specific ablation of the gene, or if the mouse was crossed with a Cre-deletor strain, ablation of exon 1 from all cells and generation of a global knockout. The intended strategy is shown in Figure 21, which shows the wild-type TASK-3 allele (Fig 21A), the targeting vector I constructed (Figure 21B; see Appendix section 5.2 for details of its construction) and the expected recombined TASK-3 allele (Figure 21C). The neomycin gene was flanked by *frt* sites (blue diamonds in Figure 21, the recognition sites for F<sub>1</sub> recombinase). Crossing a mouse harbouring the floxed TASK-3 allele shown in Figure 21C with a F<sub>1</sub>-deletor mouse would remove the neomycin gene, leaving a floxed exon 1 and a single *frt* site (Figure 21D). The floxed allele should still be active. Subsequent introduction of Cre recombinase would then delete the exon (Figure 21E).

### 3.3.2 Actual targeting of the TASK-3 gene: multiple targeting vector integration

Using the targeting vector shown in Figures 21B, I tried three separate ES cell transfection and screening experiments before I obtained a fully targeted clone. In the first transfection I screened 350 clones using the 5' probe and all of them were negative. In the second transfection I screened 500 clones and I obtained two targeted clones (by *Nco*I digestion and using the 5' external probe) but lacking the 5'loxP site (by *Eco*RV digestion and using the 5' external probe) (see Appendix Figure 32). In the third and final try with this vector, I screened 700 clones and I obtained one targeted colony which included the 5'loxP site (as assayed with the 5' external probe, *Nco*I and *Eco*RV digests; *Nco*I marks the neomycin gene insertion, *Eco*RV marks the presence of the 5'loxP site) (Figure 22D). During my preliminary analysis of the TASK-3 gene before making the targeting vector, I had not been able to identify a reliable 3' external genomic probe, which could be used to verify the recombination event independently from the 5' probe. All attempts with putative 3' probes gave signals that were total smears on Southern blots of digested mouse tail DNA (see Appendix Figure 31C), probably because of the high repetitive DNA content of this area of intron 1. Thus the fidelity of the recombination event from the 3' end was hidden; I had only the 5' probe on which to assay for homologous recombination. Because of time pressure, we decided to use this one stem cell clone for blastocyst injections and not to do yet further stem cell transfections with the existing vector. The stem clone gave

excellent chimeras and germline transmission as assayed with the 5' probe (Figure 22E and Appendix Figure 33). When I got heterozygote animals, I examined in more detail the structure of the targeted locus. Specifically, I hybridised Southern blots of NcoI digested tail DNA with a neomycin (neo) gene-specific probe. As well as obtaining the two predicted neo-positive bands of 4.2 and 3.0 Kb (Figure 22F; NcoI cuts in the neo gene, thus hybridizing neo gene-containing NcoI-digested genomic DNA with an entire neo probe gives two bands), I actually got an unexpected additional 7.0 Kb band (possibly a doublet or triplet) (Figure 22F).

We considered it was possible that the extra neo-positive 7.0 Kb band(s) arose from a separate independent integration(s) of the targeting vector on another chromosome, and that this integration could be outbred from the targeted TASK-3 allele. Alternatively, the 7.0 Kb band(s) could arise by multiple insertions (or partial insertions) of the linearized targeting vector plasmid into the TASK-3 locus (see Figure 22C); in this case, the 7.0 Kb NcoI band(s) might represent the distance between the multiple neo genes; if the targeting vector was multiply integrated, there would also be multiple copies of loxP sites, which would reduce in number after the action of Cre recombinase. The loxP sites could be either in the same or opposite orientations. Confirmation that the neo genes were at the same locus was provided by pulse-field gel electrophoresis (see Appendix section 5.4.1 "Pulse-field gel electrophoresis"). As shown in Figure 22G, PacI digest of tail DNA hybridized with the neo probe gave one band of 10 Kb. The neo-positive PacI band indicates that most likely all neo genes are at one place; digestions with PmeI and NotI (Figure 22G) gave single neo-positive bands of approximately 40 Kb, again indicating one locus for all the neomycin genes.

The TASK-3-targeted mice were crossed with a CRE-deletor strain (Williams-Simons and Westphal, 1999) (Figure 21). Tail DNA from heterozygotes offspring were genotyped by NcoI digestion and hybridized with the 5' probe: a 2.5 Kb band was produced (together with the 5.8 Kb wild-type allele). In mice whose tail DNAs were Cre-positive by PCR (see Appendix Figure 34A), the ~7.0 Kb neo-positive band was now absent. We never found the 7.0 Kb neo band independently from the other neo bands, further suggesting that they were linked at the same locus. The absence of the 7.0 Kb band suggested that multiple neo-containing targeting vectors were removed from the TASK-3 locus (one of various possible configurations is shown in Figure 23B). Furthermore, when the neo cassette was entirely removed, the TASK-3 gene was reactivated (see Appendix Figure 35). The status of this line is unclear and I am not sure if the loxP sites flanking exon 1 are in the same or opposite orientations.

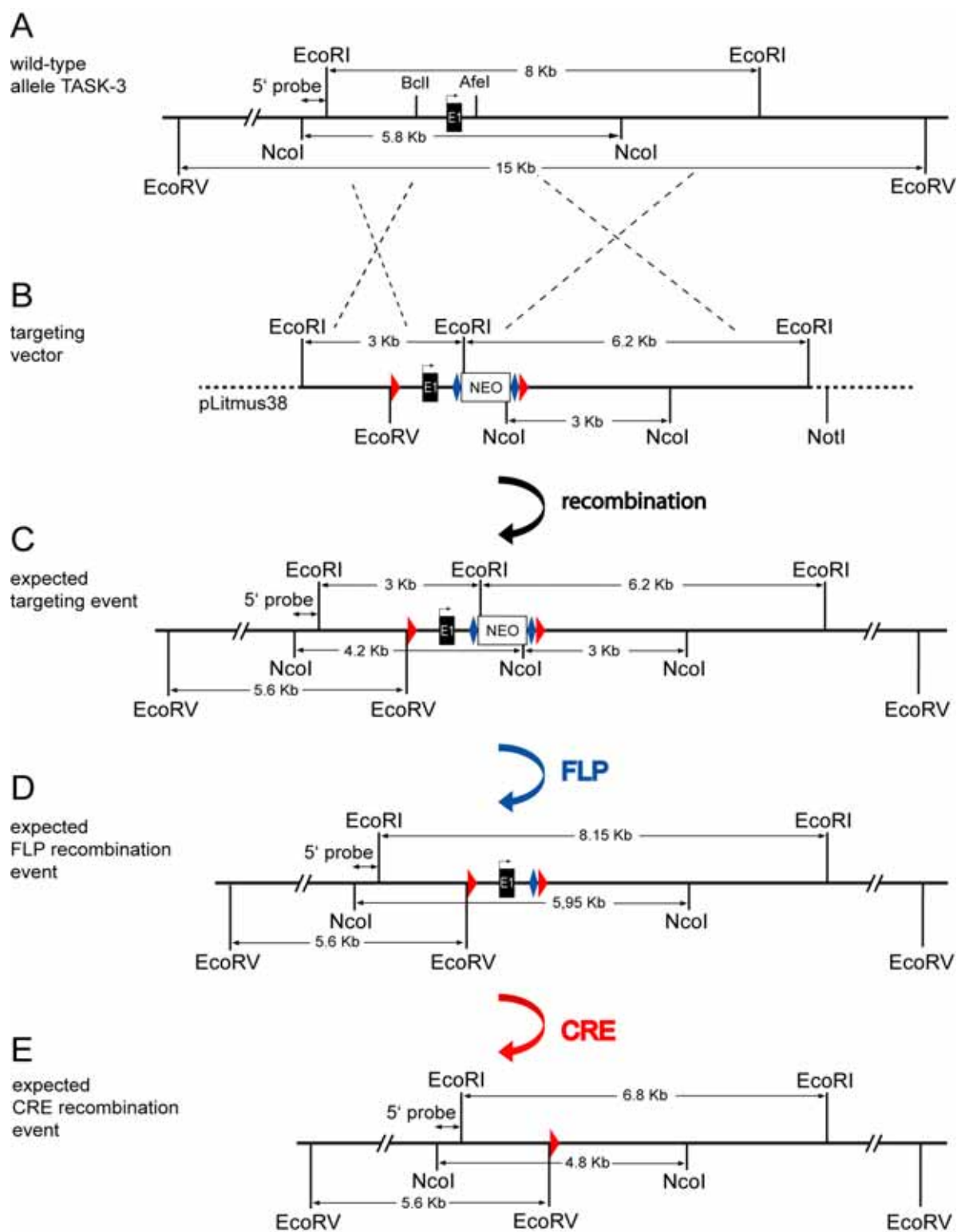


**Figure 21.** Strategy to flox the first coding exon of *TASK-3* gene

**A, B, C,** homologous recombination strategy for exon 1 of mouse *TASK-3* gene. **A,** native *TASK-3* gene. **B,** targeting vector. **C,** expected homologous recombination event. **D,** predicted structure of *TASK-3* allele after removal of the neomycin cassette by crossing with Flp deleter mouse. **E,** predicted structure of the *TASK-3* allele after crossing with the Cre deleter mouse. Exon 1, shaded box; loxP sites, red arrow heads, fit sites, blue diamonds. Double-headed arrows indicate the expected size of restriction fragments for Southern analysis.

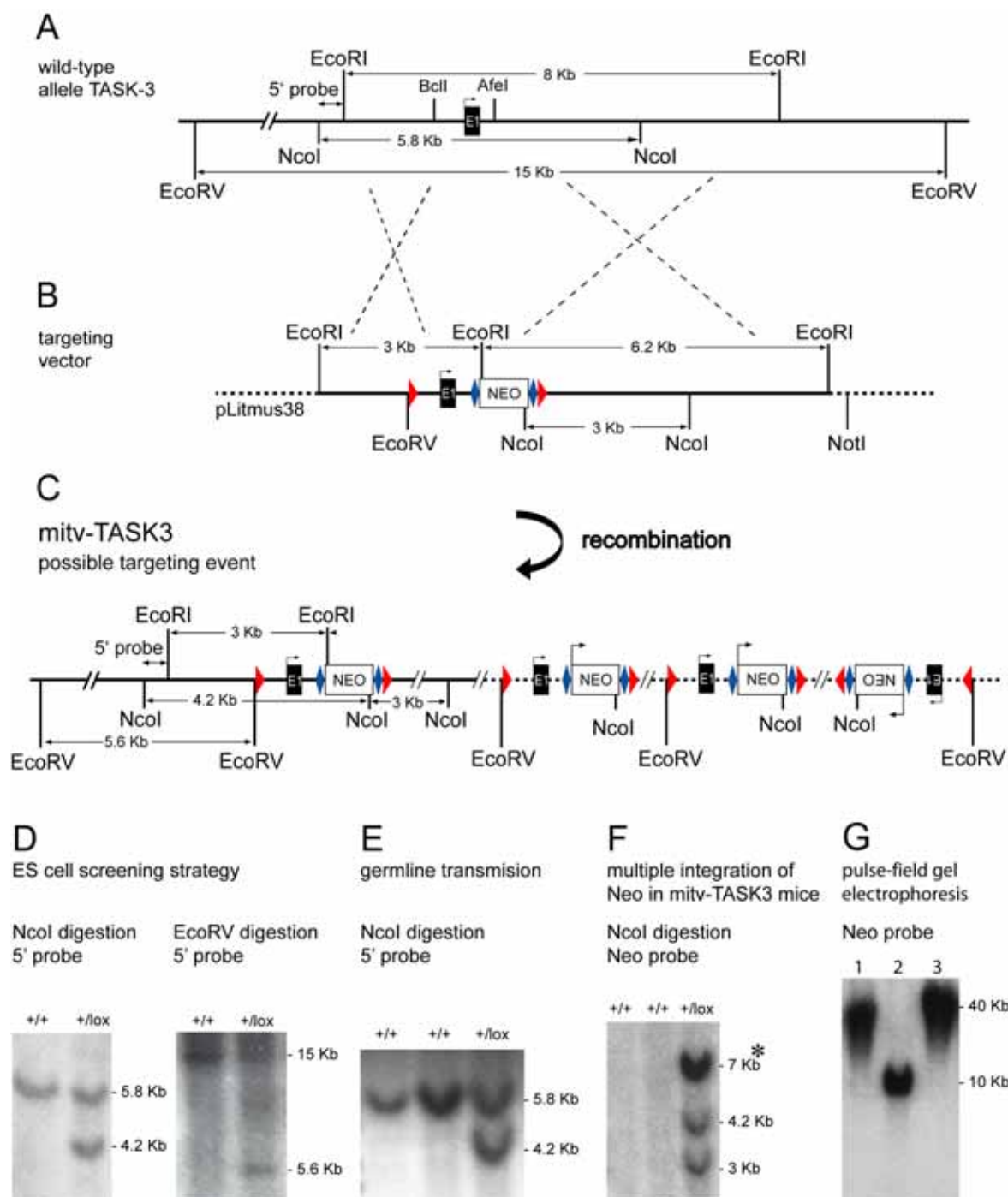


**Figure 22.** The possible mouse TASK-3 gene targeting

**A** and **B**, same as figure 21A and figure 21B. **C**, Schematic representation of the possible targeting event. Additional to the homologous locus, the targeting vector was multiply integrated, probably into the intron 1 of TASK-3 gene (the mitv-TASK3 allele). **D**, ES cell screening strategy by Southern blot using the 5' external probe on ES cell genomic DNA. **E**, Southern blot confirming the germline transmission of the targeted TASK-3 allele (mouse tail DNA). **F**, Southern blot showing a 7 Kb band (marked with star) corresponding to the multiple integration of the targeting vector in mitv-TASK3 mice. **G**, pulsed-field gel Southern blot analysis of mitv-TASK3 tail DNA digested with PmeI (lane 1), PacI (lane 2) and Not I (lane 3) and hybridized with the neomycin probe confirming that the multiple neomycin genes were integrated at the same locus.

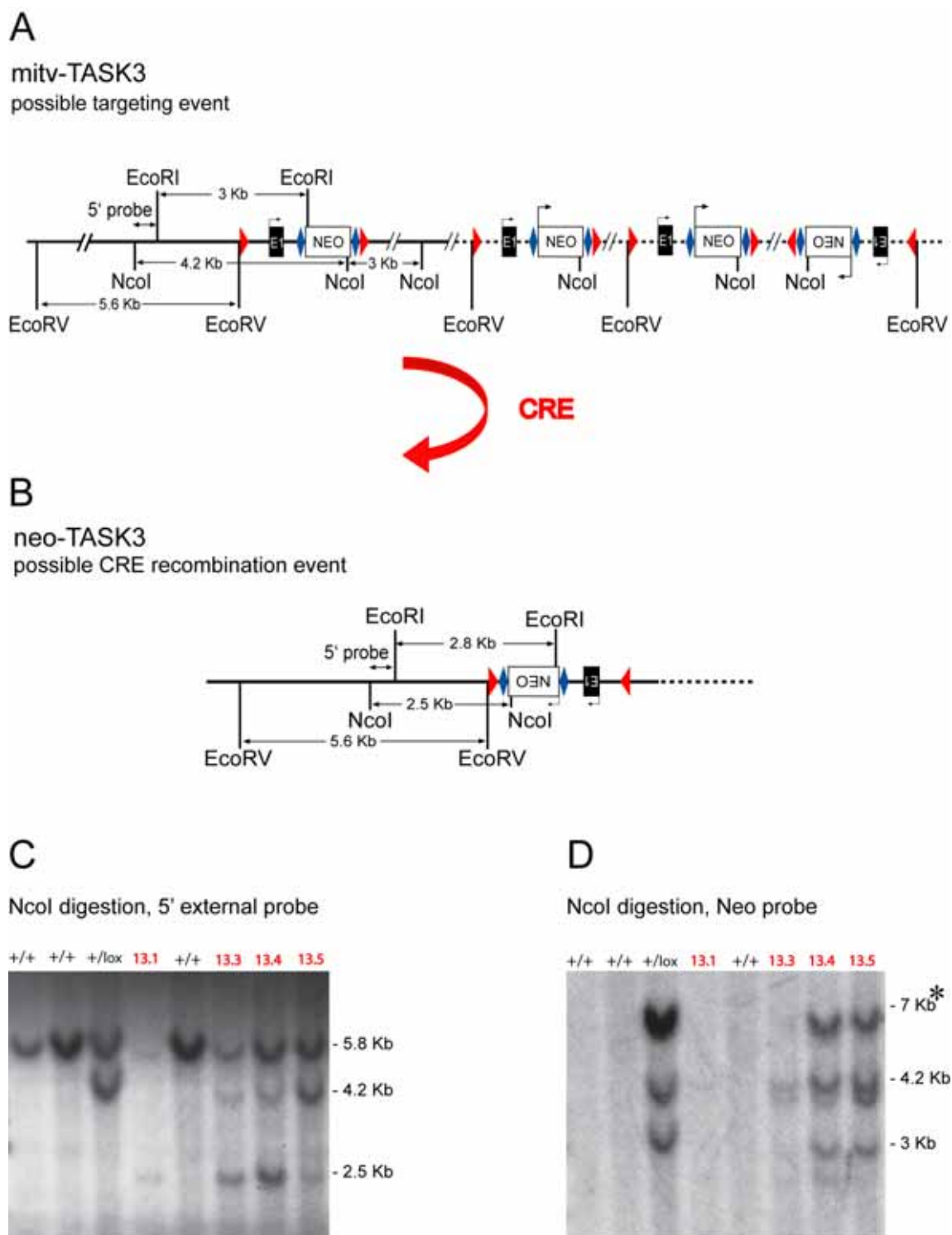


**Figure 23.** *Cre* recombination in heterozygote offspring after crossing of *mitv TASK-3* mice with *Cre* deleter.

**A**, probable targeting event in the *mitv-TASK3* mice. **B**, schematic representation of a probable *Cre* recombination event in *mitv-TASK-3* mice. **C**, Southern blot analysis of offsprings with 5' external probe reveal the 2.5 kb band (corresponding to the recombination event) and also, in lines 13.3, 13.4, 13.5 the presence of the targeted allele (4.2 kb), indicating a partial recombination. **D**, Neo probing on same blot as **C** shows the multiple integrated targeting vector of 7 kb (marked with star).

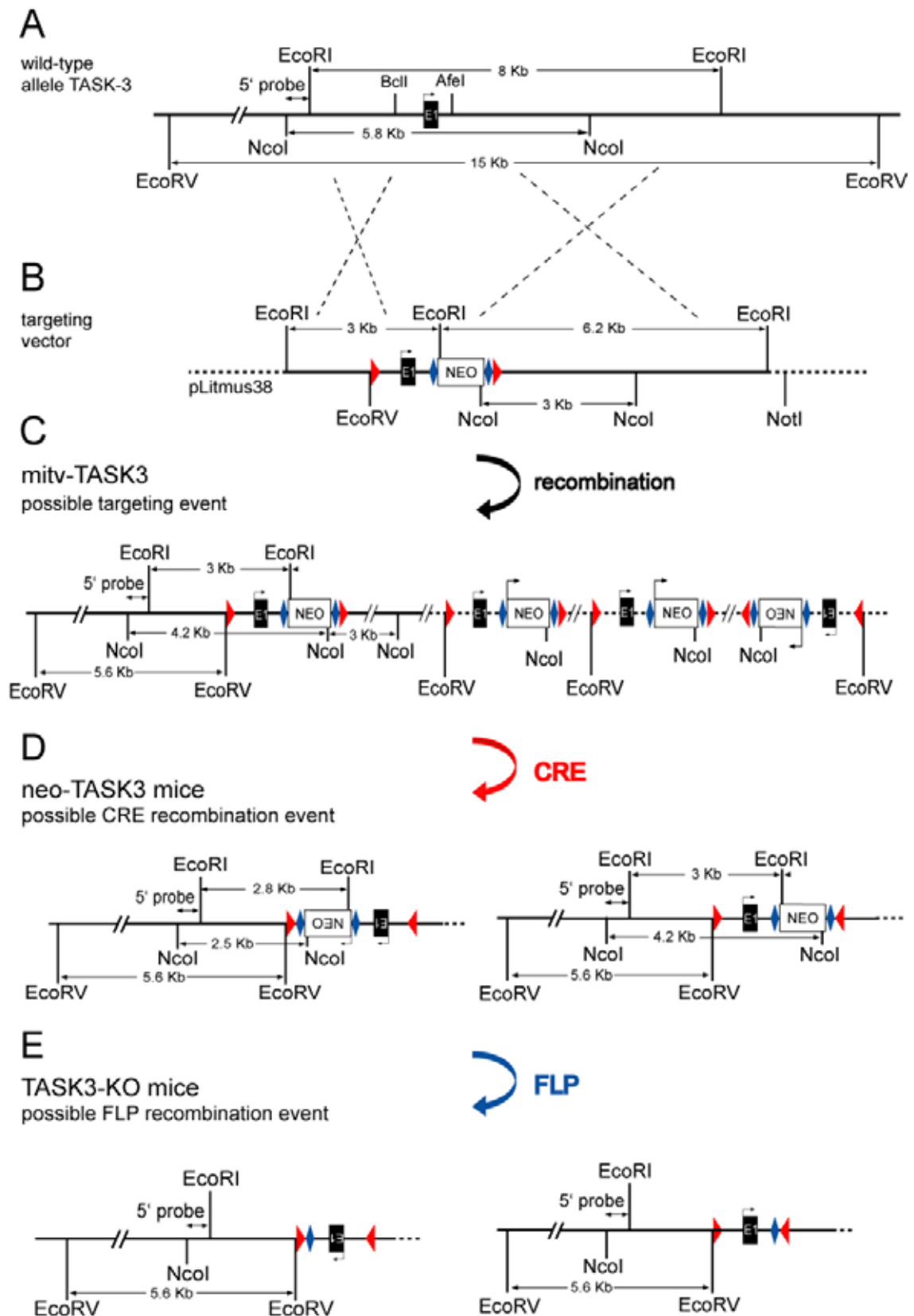


**Figure 24.** Removal of multiple integrated targeted vector in *mitv-TASK-3* mice.

**A, B, C,** similar with Figure 22. **D,** two possible Cre recombination event lead to the generation of neo-TASK3 mice, carrying only one copy of neo. **E,** two possible FLP recombination event, leading to an inversion of exon 1.

### 3.4 Analysis of TASK-3 physiological functions using mitv-TASK3 mice

We termed the TASK-3 allele with multiply integrated TASK3 targeting vectors, the mitv-TASK3 allele. Because of competition with other research groups generating TASK-1 and TASK-3 knockout mice, we decided to proceed with preliminary phenotype analysis of mitv-TASK3 mice, whilst at the same time carrying out breedings to simplify the inactivated TASK-3 locus down to an (inverted) exon 1 with no neo insertions (Figure 24E; see Appendix section 5.9 “Removal of the neomycin insertions from the mitv-TASK3 mice reactivates the TASK-3 gene”).

#### 3.4.1 The mitv-TASK3 allele is not expressed: *in situ* hybridisation and real-time PCR

Although slightly unorthodox, the mitv-TASK3 mice are knockouts of TASK-3. The multiple integrated targeting vector (mitv) in the homozygous floxed TASK-3 line has destroyed the expression of the TASK-3 gene. I confirmed this by both *in situ* hybridization with TASK-3 specific oligonucleotides (Figure 25) and real-time PCR with TASK-3-selective primers (Figure 26). Figure 25 shows horizontal sections of wild-type littermate and homozygous mitv-TASK3 brains. In the wild-type brain, TASK-3 mRNA is found in many brain regions: cerebellar granule cells, colliculi, dorsal raphe nucleus, hippocampus, ventral lateral geniculate (thalamic) nucleus, large cells in the caudate nucleus, cortex and olfactory bulb (Figure 25A; see also Figures 13-18). By contrast, the mitv-TASK3 brain has no specific TASK-3 signal (Figure 25B). By *in situ* hybridization, TASK-1 mRNA expression is unaltered between wild-type and mitv-TASK3 brains (Figure 25C and D).

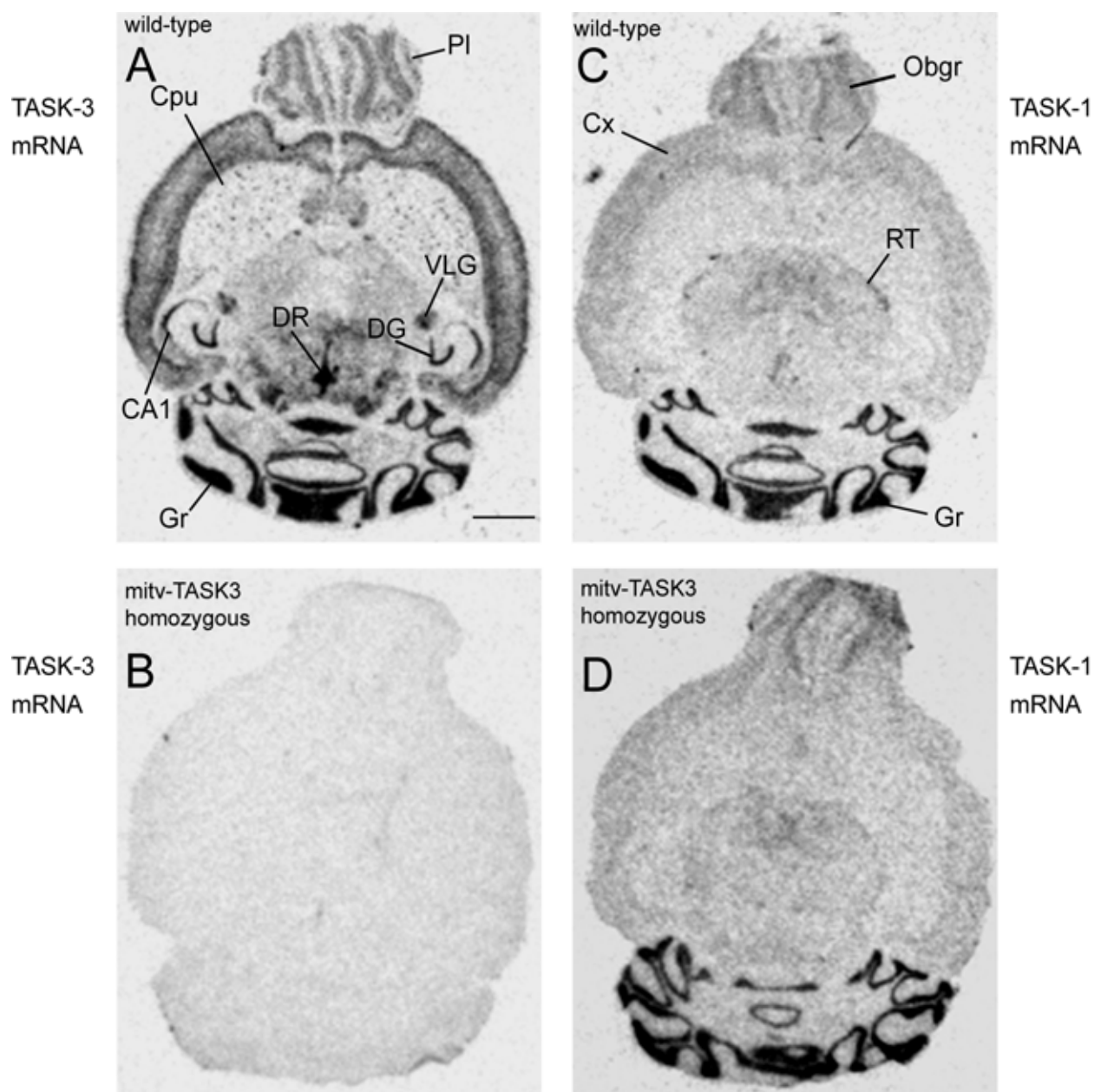


**Figure 25.** *In situ* hybridization showing absence of TASK-3 mRNA and normal expression of TASK-1 mRNA in adult mitv-TASK3 mouse brains.

*In situ* hybridization autoradiographs (X-ray film) with  $^{35}\text{S}$ -labelled antisense exon 1 oligonucleotide of TASK-3 (A, B) and, respectively, TASK-1 (C, D). Cpu, caudate putamen; Cx2-3, layers II and III of neocortex; DG, hippocampal dentate granule cells; Gr, cerebellar granule cells; Obgr, olfactory bulb granule cells; PI, olfactory bulb periglomerular cells; R, raphe nuclei; DR, dorsal raphe nuclei; RT, reticular thalamus; VLG, ventral lateral geniculate nucleus. Scale bar, 2 mm.

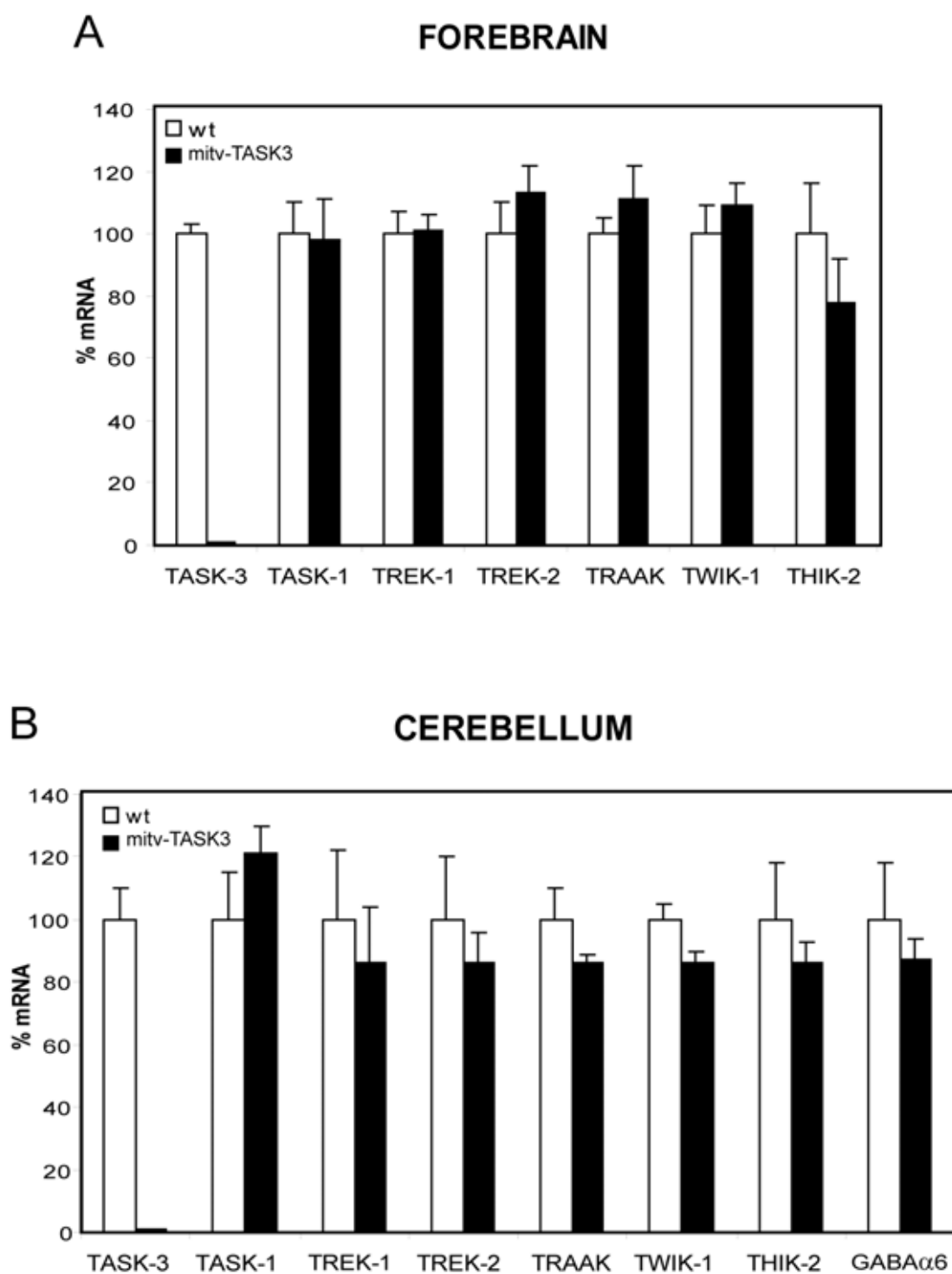


**Figure 26.** Real-time PCR analysis of mRNA levels of K2P family members *TASK-3*, *TASK-1*, *TREK-1*, *TREK-2*, *TRAAK*, *TWIK-1*, *THIK-2* and *GABA $\alpha$ 6* in wild-type and homozygous *mitv-TASK3* mice.

*TASK-3* mRNA expression is abolished in *mitv-TASK3* mice both in forebrain (**A**) and cerebellum (**B**). No significant changes could be detected in the expression of any other K2P family member or the *GABA $\alpha$ 6* subunit in either forebrain (**A**) or cerebellum (**B**).

### 3.4.2 Attempts to confirm the absence of TASK-3 protein by western blotting and immunocytochemistry

The *in situ* hybridisation and real-time PCR data indicated that TASK3 transcripts were absent in homozygous mitv-TASK3 brains, but additionally I tried to confirm the absence of TASK-3 protein by western blotting and immunocytochemistry. I tried different antibodies. The first was the polyclonal “Anti-K<sub>2p</sub>9.1 antibody” from the Alomone company. However, this antibody still stained mitv-TASK3 brains by immunocytochemistry and western blot (data not shown). (A TASK-1 selective antibody from the same company also stained TASK-1 KO brains, Aller et al., 2005). Recently Berg et al., 2004 developed a new antibody against the TASK-3 protein termed T<sub>3</sub><sub>2</sub> (obtained from serum from rabbits immunized with the rat C-terminus peptide CRVEEIPPDVLRNTY), which seemed to have promising specificity. In particular, the immunocytochemical pattern obtained with this antibody on rat brain sections somewhat resembled the TASK-3 mRNA distribution (Berg et al., 2004). Prof. Bayliss kindly sent us some of this antibody to try on the mitv-TASK3 tissues. I tried both western blots (Figure 27A and B) and immunocytochemistry (Figure 27C-F). Unfortunately, in my hands, I could detect no differences in signal between homozygous mitv-TASK3 mice and wild-type mice with the T<sub>3</sub><sub>2</sub> antibody. For the western blot, a 45 Kda band was expected (Berg et al., 2004), but I obtained an 80 KDa band in all samples (Figure 27A and B); changing the antibody incubation conditions on the membrane made little difference, except that a wider range of bands was produced (Figure 27A, B). I tried various conditions (e.g. antibody dilutions) but have so far been unable to get convincing results.

For the immunocytochemistry, although the antibody gave defined patterns of immunoreactivity in all brain regions (e.g. cerebellum, facial nuclei), the patterns did not markedly differ between genotypes (e.g. Figure 27C and D). For example, the facial motor nucleus (known to be a site of strong TASK-3 expression – see Figure 15F), are nicely stained by the antibody in both wild-type (Figure 27E) and mitv-TASK3 sections (Figure 27F); similarly, the granule cells (another key TASK-3 expressing area- Figure 15F) have clear immunoreactivity in both phenotypes (Figure 27C and D).

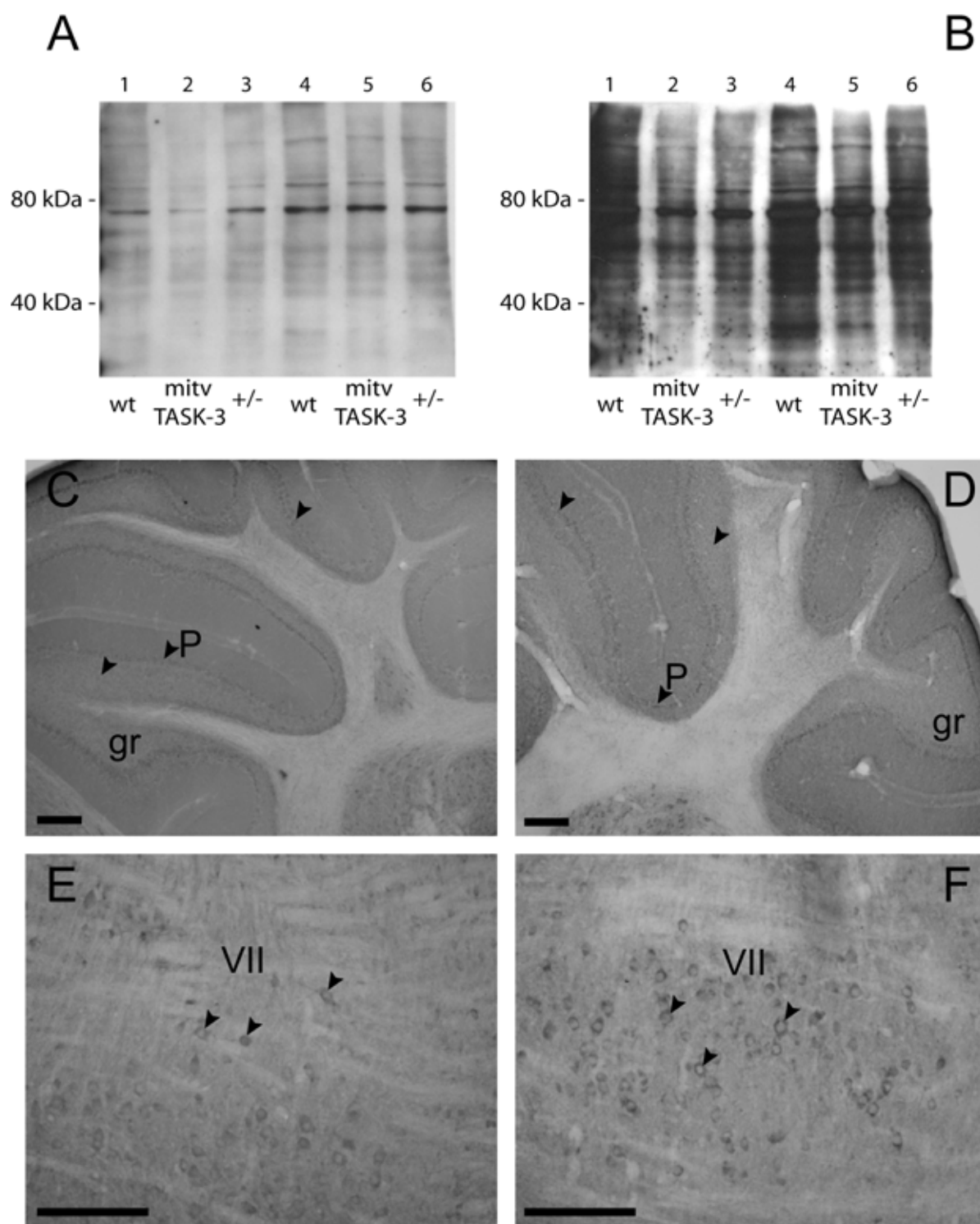


**Figure 27.** Protein analysis using the T3<sub>2</sub> antibody (Berg et al., 2004)

**A** and **B**, Western blots on membranes incubated with T3<sub>2</sub> antibody (1:1000, **A**; 1:200, **B**), overnight at 4°C. On lanes 1, 2, 3 and 4, 5, 6 were loaded 20 µg and, respectively, 40 µg protein. The corresponding genotype of the mice used for whole brain protein extraction is indicated under the lanes. **C**, **D**, **E**, **F**, Immunostaining using the same T3<sub>2</sub> antibody. **C**, **D**, staining on cerebellum slices (1:1000); incubation was performed for 48 hours at 4°C (CG, granule cell; P, Purkinje cell), **E**, **F**, Facial nucleus (VII) motoneurons. Similar staining was obtained in both wild-type (left hand panels) and mitv-TASK-3 (right hand panels) slices. Scale bar, 200 µm.

### 3.4.3 No compensation at level of gene expression by other K2P family members for loss of TASK-3

Real-time PCR analysis was used to evaluate possible changes in steady state transcript levels of other K2P family members (TASK-1, TREK-1, TREK-2, TRAAK, TWIK-1, THIK-2) as a result of loss of TASK3 expression (Figure 26). No significant changes could be detected in the expression of any K2P family member in either forebrain (Figure 26A) or cerebellum (Figure 26B).

### 3.4.4 Expression analysis of genes flanking the mitv-TASK3 locus.

We showed no change in expression of other K2P family members, at least at the RNA level. However, neomycin gene insertions could affect expression levels of neighboring genes (Olsen et al., 1996; Pham et al., 1996, Uusi-Oukari et al., 2000). Consulting the Ensembl server shows that no obvious gene candidates lie 3' of the TASK-3 gene; the nearest clear gene 3' of TASK-3, predicted to encode a protein of the collagen alpha1 chain family, is the 2310067L16Rik gene ([http://www.ensembl.org/Mus\\_musculus/geneview?gene=ENSMUSG00000045567](http://www.ensembl.org/Mus_musculus/geneview?gene=ENSMUSG00000045567)), 561 Kb downstream, an unlikely gene to influence brain function. However a large (466 Kb) gene, ortholog of the human Tularik gene 1 (T1) ([http://www.ensembl.org/Homo\\_sapiens/geneview?gene=ENSG00000167632](http://www.ensembl.org/Homo_sapiens/geneview?gene=ENSG00000167632)) predicted to encode a protein with cytochrome c-like activity, is approx 43 Kb upstream of the TASK-3 allele ([http://www.ensembl.org/Mus\\_musculus/geneview?gene=ENSMUSG00000047921](http://www.ensembl.org/Mus_musculus/geneview?gene=ENSMUSG00000047921)) (Figure 28A). According to the web annotation, a T1 cDNA was originally isolated from human cerebellum, and so the gene is expressed in an overlapping region with the TASK-3 gene. Thus any alterations in T1 expression would be a potential cause for concern for its effects on brain function, complicating phenotypic interpretations of the mitv-TASK3 knockouts. I looked at brain expression of the T1 gene by *in situ* hybridization in wild-type littermates and homozygous mitv-TASK3 brains (Figure 28B). The T1 gene has a pan-cellular distribution in wild-type brain, with the highest expression in cerebellum, hippocampus and olfactory bulb; expression is also likely in glial cells of white matter tracts. No change in expression of the T1 gene was observed in homozygous mitv-TASK3 brains compared with wild-type littermates.

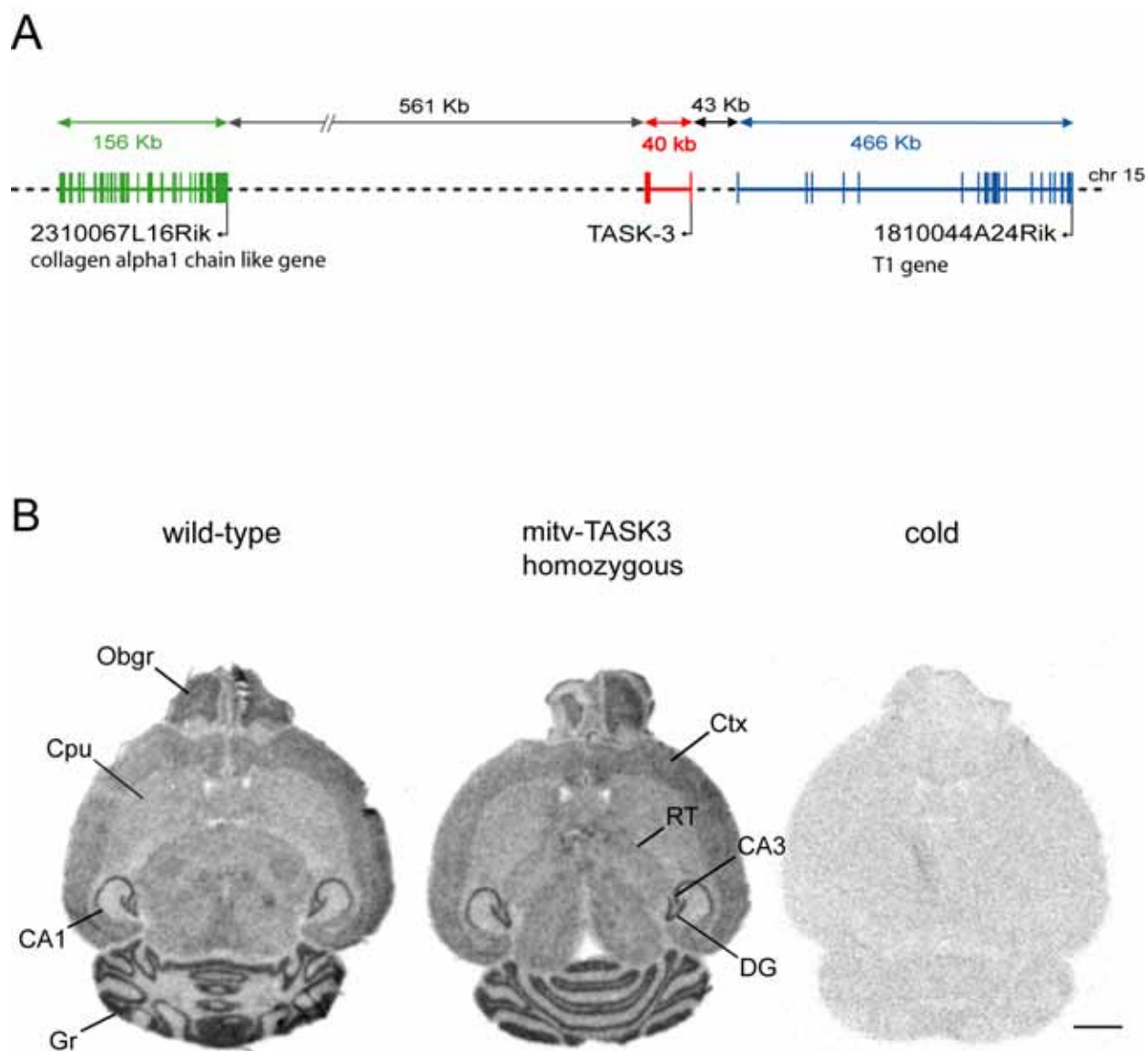


**Figure 28.** *TASK-3* neighbouring genes

**A**, diagram of the genes flanking the mitv-*TASK-3* locus. **B**, mRNA expression of the T1 gene in mouse brain. The expression level of T1 mRNA is not altered in mitv-*TASK3* brain. Scale bar, 2mm.

### 3.5 Behavioural studies of mitv-*TASK3* mice

The homozygote mitv-*TASK-3* mice are healthy, and breed normally; mutants are obtained in the expected Mendelian ratio. SHIRPA analysis (see Methods section 2.9) showed that the mitv-*TASK3* mice have normal weight, normal body posture, respiration rate and spontaneous activity. During my histological experiments (*in situ* hybridization, immunocytochemistry) I did

not observe any difference between mitv-TASK-3 and wild-type brains: their morphology and size were identical. Thus TASK-3 expression is not essential for any gross developmental aspects of nervous system function.

In the ideal case, behavioural studies on mice require at least thirteen to fifteen same sex mice (male) (Crawley, 2000); this is because of the inherent variability of animal performance in these tests, so to increase the statistical power a large “n” is needed. Breedings are still ongoing, and I have not yet obtained enough male mice. For a pilot study, however, I sent a small number of young adult mice to Prof. Esa Korpi’s laboratory in Helsinki. The preliminary behaviour experiments, using three homozygote mitv-TASK3, three heterozygote, three wild-type littermates of mitv-TASK3 together with four pure C57/Bl6 mice (as a control for strain) showed no significant difference between phenotypes.

### **3.5.1 mitv-TASK3 mouse behaviour: motor skills**

There were no gross motor abnormalities comparing homozygous mitv-TASK3, heterozygote mitv-TASK3, wild-type littermates or C57/Bl6 controls (Figure 29A). In the beam walking test (where mice have to cross a narrow diameter suspended beam) (Figure 29A) and rotarod test (where mice have to learn to stay on an accelerating rotating rod, a good indicator of cerebellar function (reviewed Crawley, 2000) (Figure 29B), the mitv-TASK3 mice perform slightly less well compared with their wild-type littermates. No ataxia or any overt motor deficit was observed during the tests.

### **3.5.2 mitv-TASK3 mouse behaviour: acoustic startle reflex and prepulse inhibition**

The acoustic startle reflex (how quickly a mouse respond to a tone, measured by whole body twitch) is one parameter to assess the health of a nervous system and gross hearing ability (Crawley, 2000). The mouse is placed in a small cylinder; brief tones varying from 65 to 120 dB are randomly delivered through a small speaker in the chamber’s wall. Normal mice of many strains respond to tones of 100 dB and louder by a whole body twitch; the equipment measures flinch amplitude through an electrostatic sensor located immediately under the chamber in which the mouse is resting (Crawley, 2000). mitv-TASK3 mice do not have increased (or decreased) startle reactions compared with wild-type littermates and C7/Bl6 controls (Figure 29C, left

panel); we can conclude that homozygous mitv-TASK3 mice have normal hearing and correctly functioning auditory reflex circuitry.

The prepulse inhibition of the acoustic startle response test is a neurophysiological and behavioural measure of sensorimotor gating (Crawley, 2000). In a healthy animal, a weak startle stimulus, the 95 dB tone, inhibits the subsequent response to a strong startle stimulus, a very loud 120 dB tone, if presented within 100 msec (Crawley, 2000). The “subconscious” processing of the first stimulus and subsequent reduction in response to the second stimulus indicates how well the brain integrates and responds to sensory stimuli – the so called “sensorimotor gating”. If undertaken with a range of other tests, a deficit in the prepulse inhibition performance is one index for “schizophrenic-like” symptoms (Crawley, 2000). The homozygous mitv-TASK3 mice showed no clear difference in the % prepulse inhibition they exhibited compared with heterozygotes and wild-types (littermates and C57/Bl6) (Figure 29D).

### **3.5.3 Mitv-TASK3 mouse behaviour: memory and motivation**

The T-maze is a simple way of evaluating memory and motivation. In the T-maze mice initially have access to explore only one particular alley of the T (an arm of a “T”). Another arm of the “T” is then opened up and the old one is also kept open; healthy mice, in the ideal case, then show a preference for exploring the newly opened arm and make more entries to this new space – hence the name of the test “alternating T maze”. The alternation percentage, however, was similar for homozygous mitv-TASK3 mice (left panel) compared with wild-type littermates, although the forced trial time was significantly reduced (middle panel); it seems that mitv-TASK-3 mice do more trials during 10 minutes of testing time than wild-type littermates (right panel), although the “n” numbers are probably too small to make this a robust result.

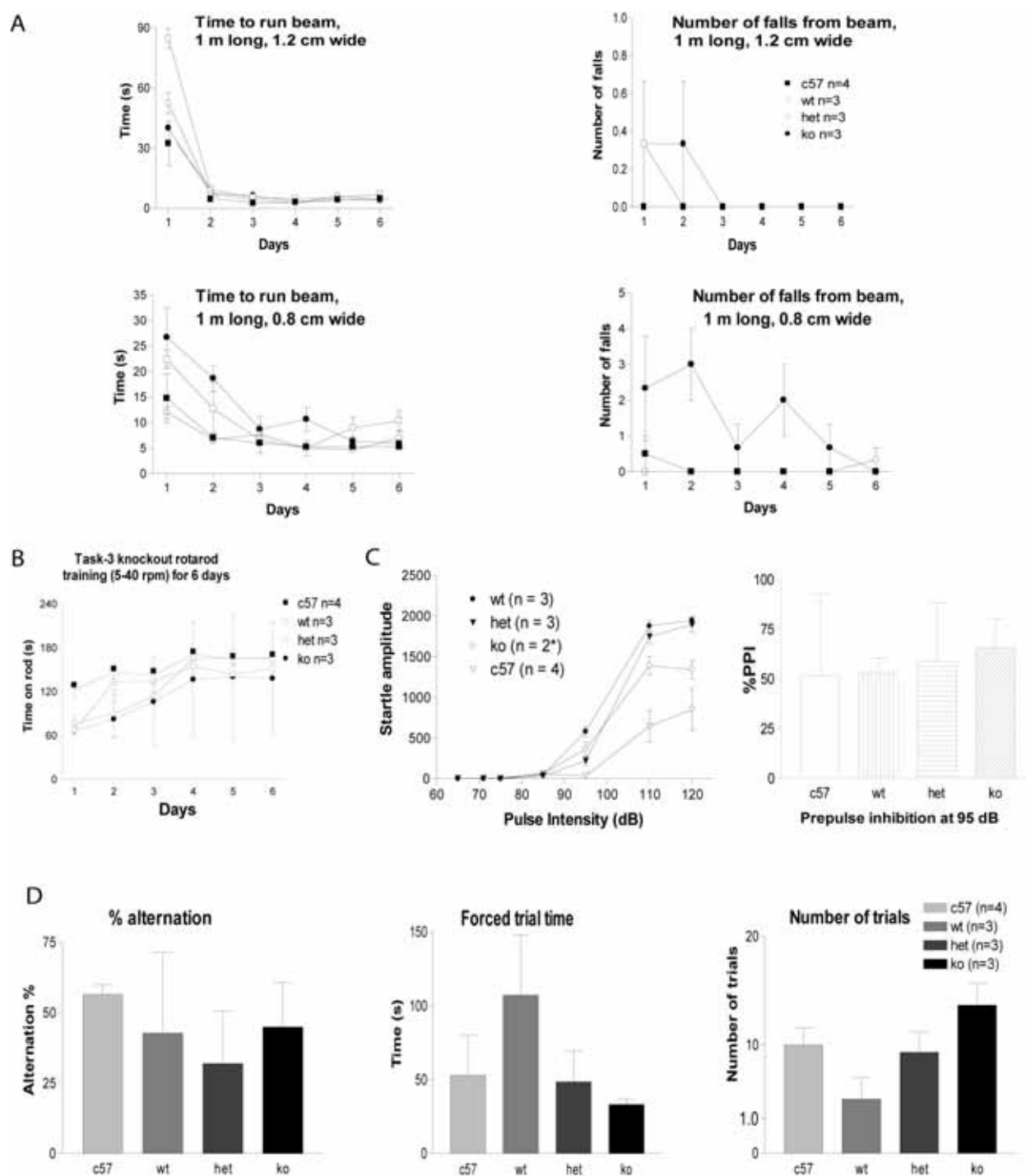


**Figure 29.** Behaviour tests on *mitv-TASK-3* mice and their heterozygote and wild-type littermates.

**A**, beam walking test; **B**, rotarod test; **C**, acoustic startle test; **D**, T-maze test. KO, *mitv-TASK3* homozygotes; het, heterozygous *mitv-TASK3*; wt, wild-type littermates from *mitv-TASK3*<sup>+/+</sup> x *mitv-TASK3*<sup>+/+</sup> crossings. (Data provided by A. M. Linden and E. R. Korpi, University of Helsinki)

### 3.6 Electrophysiological analysis of adult cerebellar granule cells lacking TASK-3 expression

Electrophysiology studies were performed on homozygous mitv-TASK3 granule cells in acute cerebellar (adult) slices to examine the significance of the changes in TASK-3 channel expression for granule cell function. So far we have only collected preliminary data, but already there are some clear differences. By blocking the glutamatergic and GABAergic synaptic transmission with kynurenic acid and picrotoxin, a standing outward conductance ( $I_{K(SO)}$ ) was present in cerebellar granule cells (Figure 30), as shown in the previous studies of Brickley et al., 2001 and Aller et al., 2005.

Figure 30A shows two individual patch clamp records on wild-type and homozygous mitv-TASK3 cerebellar granule cells (CGS); the holding potential was ramped from  $-20\text{mV}$  to  $-140\text{mV}$ . A difference in the magnitude of the standing outward current was detected between genotypes. As shown in the top panel of figure 30B, the shape of the  $I$ - $V$  relationship was similar between the two genotypes, but the magnitude of the current was strongly reduced, to about half, in the homozygous mitv-TASK3 mice (also Figure 30C). Thus, when cerebellar granule cells were held at  $-20\text{mV}$ , the standing outward conductance was larger in the wild-type mice. Also, a slow inactivating current component was observed in the wild-type granule cells, when the holding potential was maintained at  $-20\text{mV}$  for 60 seconds. This slow inactivating component is gone in the mitv-TASK-3 mice compared with wild-type mice (Figure 30B, lower panel). (This inactivation property was mimicked by recombinantly expressed mouse TASK3 channels in HEK cells – A. Mathie, personal communication).

A second novel result concerns the action potential frequency in the homozygous mitv-TASK3 cerebellar granule cells. As shown in Figure 30D, the firing pattern is different between wild-type and mitv-TASK3 granule cells in acute slices when the granule cells are injected with current and their responses recorded at room temperature in the presence of the GABA<sub>A</sub> receptor blocker picrotoxin. The mitv-TASK-3 granule cells fire fewer action potentials after  $+32\text{ pA}$  injected current compared with wild-type granule cells (Figure 30D).

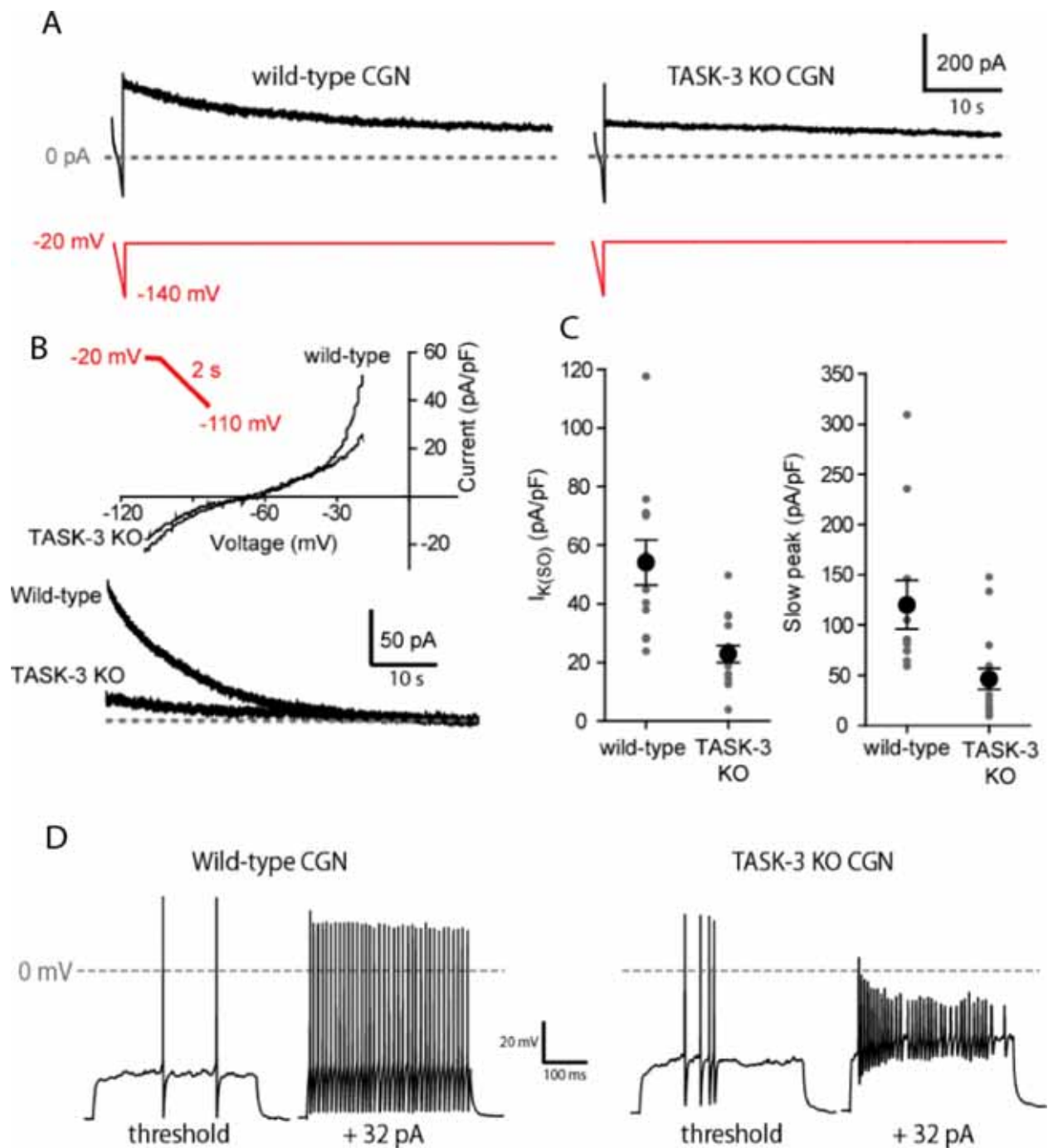


**Figure 30.** Acute slice preparation recordings show modifications of  $I_{K(SO)}$  in *mitv-TASK3* mice.

**A**, Individual current traces taken from one wild-type (left panel) and one *mitv-TASK-3* (right panel) granule cell. The holding potential was ramped from  $-20$  mV to  $-140$  mV and maintained at  $-20$  mV for 60 seconds; **B**, Averaged  $I$ - $V$  relationships from wild-type ( $n=12$ ) and *mitv-TASK3* ( $n=16$ ) granule cells (upper panel); **C**, Measurement of  $I_{K(SO)}$  at  $-20$  mV from wild-type and homozygous *mitv-TASK-3* granule cells. **D**, Action potential firing pattern at  $+32$  pA in a wild-type and a *mitv-TASK3* cerebellar granule cells. (Data courtesy of Dr. Stephen Brickley, Imperial College London).

## 4 DISCUSSION

K2P channels are able to drive the membrane potential towards the  $K^+$  equilibrium, starting from all potentials. Some of these channels are constitutively open and behave as selective “holes” for potassium, thus constituting the so called “leak conductance”. Thus these channels strongly hyperpolarise the cell membrane. Indeed targeted overexpression of K2P channels to particular neuronal types (in *Drosophila*) can be used to selectively silence these cell types, so aiding attempts to dissect the roles of particular cells types in neural circuits (White et al., 2001). Because a polarized membrane potential is fundamental for electrical signalling, one might suspect that K2P channels perform functions that are purely static and unchanging. Instead, it turns out that regulation of the resting conductance is a primary mechanism for the control of cellular excitability. Thus, far from being “housekeeping channels” with static roles in cellular function, these channels are important loci for dynamic modulation of membrane properties. Such modulation occurs via different endogenous and clinical compounds such as neurotransmitters (peptides and amines) and inhalational anesthetics and also by changes in parameters such as pH, oxygen tension, osmolarity and temperature, all being important agents which alter neuronal excitability in short times. The aim of my PhD project was the generation and analysis of TASK-3 knockout mice so that the contributions of TASK-3 channels to brain physiology could be revealed.

Fifteen members of the K2P channel family (including TASK-1 and TASK-3) have been identified and characterized, mainly in recombinant or *in vitro* systems. The expression of the K2P gene family in the rat and mouse brain was largely described by *in situ* hybridisation (Talley et al., 2001; Karshin et al, 2001) showing that only the TASK-1, TASK-3, TREK-1, TREK-2, TWIK-1, THIK-1, THIK-2 and TRAAK genes are expressed in CNS neurons, all with different patterns (Talley et al., 2001; Aller et al., 2005) (Figure 5), a situation typical also for many other gene families encoding ion channels (e.g. GABA<sub>A</sub> receptors or glutamate receptors). Since K2P channels assemble as dimers, it is possible that different K2P subunits can assemble as heterodimers when co-expressed in neurons, thus making it more difficult to reveal their contribution to the leak  $K^+$  background current and modulation of membrane properties.

#### 4.1 Generation of TASK-3 knockout mice: technical considerations

Initially, I planned to make both a conditional “floxed” allele of the TASK-3 gene in order to generate conditional TASK-3 mutant mice by cell-type-specific ablation of the gene with cell type-selective Cre expression, and a global TASK-3 knockout mouse, by crossing with a Cre-deletor line. The intended strategy consisted in flanking the exon 1 of TASK-3 gene with loxP sites. Also, a neomycin cassette, flanked by frt sites was inserted as a positive selection marker for embryonic stem cell culture. Crossing the mice harbouring the “floxed” TASK-3 allele with a Cre deletor should generate the global TASK-3 knockout mouse whereas the crossing with a Flp deletor should remove only the neo cassette and generate the conditional knockout mouse, in which the floxed allele should still be active. However, after three trials of targeting stem cells, I obtained only one ES cell clone fully targeted at the TASK-3 locus. Afterwards it turned out that the generated mouse line has multiply integrated TASK-3 targeting vectors, apparently in intron 1 at the TASK-3 gene locus: the mitv-TASK3 line. TASK-3 gene expression is clearly inactivated in the mitv-TASK3 line, possibly because of the multiple integrations of the neomycin resistance gene, which has been reported to have an inhibitory effect on some of the genes into which it integrates (e.g. Single et al., 2000), although this is not always the case (e.g. Jones et al., 1997); alternatively the multiple repetitive insertions of the targeting vector into intron 1 could have produced aberrant splicing, such that the primary TASK-3 transcript cannot splice to mRNA.

How could the multiple insertion have happened? This is unclear. The targeting vector was the standard replacement vector type, designed to “swap sequences” at the homologous locus (Cappechi, 2005; Smithies, 2005). The gene targeting mechanism in ES cells probably hijacks the homologous recombination enzymes that normally carry out homologous DNA repair (repairing a lesion on one chromosome by copying/recombining the sequence from the sister chromosome). There could have been a “correct” homologous recombination event followed by some kind of aberrant copying and ligation of the vector which was then inserted at the neighbouring position by non-homologous recombination (analogous to what happens with transgene integration when DNA is injected into a mouse egg nucleus). Alternatively, some of the electroporated targeting vector may have been damaged and unintentionally internally cut/sheared, as opposed to being linearized outside the region of homology. A cut within the homology domain promotes a duplication event and not a replacement event; cutting the vector *within* the region of homology has been used to deliberately introduce multiple copies of a sequence at a defined location (Smithies, 2005).

In any case, regardless of its mechanism, given the unorthodox nature of the TASK-3 gene inactivation, the mitv-TASK3 mouse line requires careful assessment for two reasons: (i) we must establish that the neo genes and the targeting vector insertions are in fact only in TASK-3 intron 1 and not integrated in another locus, so potentially damaging other (unknown) genes; (ii) neomycin gene insertions can, but do not always, influence neighbouring gene expression (Olsen et al., 1996; Pham et al., 1996, Uusi-Oukari et al., 2000), so we must evaluate if the expression of neighbouring genes has altered in the mitv-TASK3 mice (the inhibitory effect of the neo gene insertions is thought to be related to promoter quenching; some of the promoters used to drive neo in ES cells are powerful landing platforms for key transcription factors, and so “squench” neighbouring promoters<sup>3</sup>). I showed that the expression of the neighbouring gene T1 encoding a cytochrome c-like activity (located approximately 43 Kb upstream of the TASK-3 allele) is not altered compared with wild-type mouse brain (Figure 28). The nearest clear (450 Kb) downstream gene from TASK-3 allele is a member of the collagen gene family: it is, in principle, possible that a collagen defect could produce a neuronal phenotype (e.g. deafness, as found for e.g. the collagen type IX gene; various of the collagen genes express in the inner ear e.g. tectorial membrane and basement membrane and so affect cochlear function (Asamura et al., 2005)). However, based on the auditory startle reflex data (Figure 29D), the mitv-TASK3 mice have no hearing impairments.

#### 4.2 Phenotype analysis of mitv-TASK3 knockout mice

Having established reasonably securely that the multiple neomycin gene insertions were confined to the TASK-3 locus and that there were no consequences other than TASK-3 gene inactivation, we decided to use these mitv-TASK3 mice for phenotypic analysis. By *in situ* hybridisation analysis on wild-type mouse coronal and horizontal sections we showed that TASK-3 mRNA has a wide distribution in the wild-type brain with a clear expression in olfactory bulb granule cells, the external plexiform layer of the bulb, piriform cortex, neocortex (many cells in all layers except I), putative cholinergic neurons in the caudate-putamen, CA1 pyramidal cells, dentate granule cells, certain thalamic nuclei (e.g. anterior-dorsal the highest, but also many other thalamic nuclei), many cells in the inferior colliculi, cerebellar granule cells, motor neurons (Figures 5, 13-18). In parallel, we checked also for mRNA expression of TASK-1 channel in the mouse brain, showing that it has a more restricted expression pattern, colocalizing

---

<sup>3</sup> By pulse-field gel electrophoresis I demonstrated that neomycin genes were inserted at the same locus. Hybridization with neo probe revealed a 10 Kb band on PacI digested mitv-TASK3 tail DNA.

with TASK-3 in some cell types (e.g. cerebellar granule cells, motor neurons, dorsal raphe cells). Thus loss of TASK-3 will potentially affect many neural systems and circuits.

#### **4.3 Antibodies as immunohistochemical tools: knockouts as tests for antibody specificity**

I was interested in TASK-3 protein localization in neurons, since there is nothing known about the subcellular distribution of TASK channels. For example, are the channels enriched on dendrites or are they uniformly distributed on the cell? There have now been many papers published by different groups using commercially available TASK-1 and TASK-3 antibodies and other antibodies against e.g. TASK-2 (e.g. Yamamoto et al., 2002; Kanjhan et al., 2004). In one example, TASK-3 immunoreactivity was detected in subsets of neocortical cells, the pattern looked nothing like the *in situ* hybridization pattern, so the authors of that paper suggested translational control of TASK-3 mRNA (Callahan et al., 2004). However, TASK-3-like immunoreactivity was detected convincingly in one study (Berg et al., 2004) in a distribution pattern that was strikingly similar to TASK-3 *in situ* hybridization reports (Brickley et al 2001; Karschin et al., 2001; Talley et al., 2001; Aller et al., 2005). I used both the commercially available Alomone TASK-3 antibody (APC-044, Alomone Labs) and a TASK-3 antibody generated in the Bayliss lab (Berg et al., 2004) on fixed mouse brain slices from wild-type and TASK-3 KO mice and western blots. Thus, with both assays I obtained immunoreactivity on wild-type and mitv-TASK3 tissues which suggests that the specificity of these antibodies is questionable. Dr. Isabel Aller found similar results with TASK-1 antibodies on the TASK-1 KO mice (Aller et al., 2005). Thus various wrong papers have been published based with these dubious antibodies, in particular with the Alomone and Sigma antibodies.

Saper and Sawchenko (2003) have written an informed critique on the misuse of antibodies in immunocytochemistry to help, as they put it, “aspiring authors through the rocky shoals of immunolocalization in the nervous system”. They point out that the most important thing to understand is that antibodies are biological agents, not standard chemical reagents: antibodies may bind to a wide variety of antigens other than the one that they were raised to recognize, and there is no way to be sure that the pattern they stain really represents that antigen. Clearly, if one is investigating localization in the mouse nervous system, a knockout mouse for the particular antigen is the best control of antibody specificity (Saper and Sawchenko, 2003). Indeed, the use of TASK-3 KO mice is a good control for the specificity of the above mentioned antibodies. A very interesting commentary was recently made by Jones and Wonnacott (2005) on the specificity of the commercially available and commonly used anti-nicotinic receptor (AChR)-

subunit antibodies, which were previously reported as specific and on which many papers are based. For example, the antibody anti- $\alpha 7$  nAChR subunit still displayed exquisite interneuron-specific immunoreactivity on  $\alpha 7^{-/-}$  mouse brain tissue (Jones and Wonnacott, 2005). This suggests the necessity of re-examination of the published data concerning the reported distribution of nACh receptors by immunoreactivity and perhaps other proteins by using the relevant antibodies on specific knockout mice. It is probably the tip of the iceberg.

#### **4.4 Dissecting the contribution of K2P channels to leak currents in vivo: cerebellar granule cells as an example**

To dissect the contribution of the various K2P subunits to the background  $K^+$  currents that set the resting membrane potential in native neurons is a challenge. There are no ideal pharmacological agents that will selectively block the channel subtypes and allow us to say definitively that, for example, “that current must be TWIK-1 because it is blocked by agent x”. Given the absence of selective pharmacological agents, specific ablation of K2P genes or expression of dominant-negative versions (Lauritzen et al., 2003) may reveal the significance of K2P channels *in vivo*. As an example, I consider cerebellar granule cells. In mouse and rat adult cerebellar granule cells five K2P genes, TWIK-1, TASK-1, TASK-3, TREK-2 and THIK-2 are expressed at significant levels (Aller et al., 2005). An additional complicating feature is that some of these channels (TWIK-1 and THIK-2) are not active in recombinant expression systems (Rajan et al., 2001), but under certain circumstances they may become active. For example, recombinant TWIK-1 is inactive when a small ubiquitin-like protein SUMO is covalently attached to an internal lysine of the channel subunit; however, activation of a specific SUMO ligase cleaves SUMO, and activates TWIK-1 (Rajan et al., 2005). The resulting channel resembles the TASK-1 and -3 channels in its properties. The particular physiological stimuli that would trigger sumoylation (or de-sumoylation) of TWIK-1 *in vivo* are not known. Such events make it hard to accurately assess the contributions of the subunits to the macroscopic current seen in granule cells.

To study the problem of K2P diversity, various investigators have adopted cultured cerebellar granule cells, probably because these cells are easy to culture and give large numbers of homogeneous cells (Han et al., 2002, Lauritzen et al., 2003, Clarke et al., 2004). In primary cultures of cerebellar granule cells, at least four K2P channels (TASK-1, TASK-3 and TREK-2 and probable TASK-2) were *suggested* to contribute to the leak conductance  $I_{K(SO)}$  (Han et al., 2002). This analysis was based on the fingerprints of single channel conductances. In particular, one of these channels, TASK-2, identified by Han and collaborators in cultured granule cells by

indirect electrophysiological identification is not expressed at significant levels in developing or adult granule cells *in vivo* (Aller et al., 2005). It could be that in culture granule cells do not express the normal repertoire of channel genes: indeed, these cells are typically cultured in 25 mM K<sup>+</sup> in order to promote the survival of these cells; however, this concentration of K<sup>+</sup> profoundly forces the cells to adopt untypical patterns of gene expression, a good example being the GABA<sub>A</sub> receptor  $\alpha$ 6 subunit gene, which *in vivo* is strongly expressed in this cell type (Mellor et al., 1998); in 25 mM K<sup>+</sup>, the  $\alpha$ 6 gene is not transcribed, whereas in 5 mM K<sup>+</sup> it is (Mellor et al., 1998). Thus interpreting the results from granule cell cultures can be problematic or even misleading. Thus I would argue that it is better to study the electrophysiological properties of granule cells (or other types of neurons) in intact acute brain slices; at the moment the problem is best approached with genetics.

#### **4.5 Electrophysiological properties of recombinant mouse TASK-1 and TASK-3 channels: Zn<sup>2+</sup> and ruthenium red as diagnostic agents to distinguish them**

Previously, the electrophysiological properties of human and rat TASK-3 channels were described (Lesage et al., 1996b; Rajan et al., 2000; Kim et al., 2000; Clarke et al., 2004), revealing their ability to generate pH-sensitive whole-cell K<sup>+</sup> currents with little time-dependence and weak rectification, Zn<sup>2+</sup> sensitivity, ruthenium red inhibition and modulation by neurotransmitters and volatile anesthetics. It was necessary to first define the electrophysiological properties of mouse TASK-1 and TASK-3 channels as further anticipation of characterizing the TASK knockout mice. The mouse TASK-1 channel voltage-independent leak conductance was sensitive to both external acidification and alkalinisation, whereas the TASK-3 channel leak conductance was not sensitive to external alkalization. Also, the concentration of 100  $\mu$ M Zn<sup>2+</sup> significantly blocks only TASK-3-mediated currents. These recombinant expression studies demonstrate that ruthenium red, and the addition of Zn<sup>2+</sup> provide useful diagnostic fingerprints for dissecting TASK-1 and TASK-3 channel currents: ruthenium red and Zn<sup>2+</sup> block homomeric TASK-3 channels, but not heteromeric TASK-1/TASK-3 or homomeric TASK-1 channels (the mechanism of ruthenium red block of homodimeric TASK-3 channels is described in the Introduction, Figure 7). Unfortunately, neither Zn<sup>2+</sup> nor ruthenium red are “clean”, in the sense that they both block or activate many other ion channel types (Dray et al., 1990; Hirano et al., 1998; Cibulsky and Sather, 1999; Wu et al., 1999).

#### 4.6 Comment on preliminary behaviour and electrophysiology data on mitv-TASK3 mice

Our electrophysiology data on mitv-TASK3 mice prove that TASK-3-containing channels strongly contribute to the standing outward conductance  $I_{K(SO)}$  of cerebellar granule cells (contributing to about half of this current) and also show a novel aspect, the contribution of TASK-3 channels to a slowly inactivating component of the  $I_{K(SO)}$ . Usually, the leak conductance is *defined* as non-inactivating. However, the mouse recombinant TASK-3 channel also shows this inactivating property (Alistair Mathie, personal communication). The reduced magnitude of the standing outward conductance and the absence of the slow-decay component were not observed in TASK-1 KO cerebellar granule cells generated by our group (Aller et al., 2005) and it was concluded that inactivation of the TASK-1 gene did not alter the intrinsic excitability of the cerebellar granule cells (Aller et al., 2005). However, TASK-1 subunits can associate with TASK-3 subunits to form functional heterodimers which are  $Zn^{2+}$ -insensitive in recombinant systems (Czirjak and Enyedi, 2002; Clarke et al., 2004; Aller et al., 2005). The  $I_{K(SO)}$  of wild-type granule cells is not sensitive to application of  $100 \mu M Zn^{2+}$ , but the  $I_{K(SO)}$  of the TASK-1 KO granule cells is, suggesting that normally cerebellar granule cells have a heteromeric TASK-1/TASK-3 population, which becomes replaced by a homomeric TASK-3 population in the TASK-1 KO granule cells (Aller et al., 2005). We suggested that a possible role of TASK-1, by dimerizing with TASK-3, was to confer  $Zn^{2+}$ -insensitivity on the leak currents of granule cells. In most places in the brain, TASK-3 is expressed without TASK-1, and so these channels would be  $Zn^{2+}$ -sensitive.  $Zn^{2+}$  has been suggested to be an important neuromodulator, being co-released with GABA or glutamate at various locations in the brain (Assaf and Chung, 1984; Frederickson, 1989). In this view, at least for the brain, TASK-1 could be regarded as an accessory subunit for TASK-3, modifying TASK-3's properties in the cells in which they are co-expressed (e.g. cerebellar granule cells, dorsal raphe cells, motor neurons). Why can TASK-3 channels apparently compensate for the loss of TASK-1, but not vice versa? One explanation is that the single channel conductance for TASK-1 is about half that for TASK-3 (see Table 2, Introduction). Consistent with the “accessory function” of TASK-1, granule cells lacking TASK-1 have an unchanged  $I_{K(SO)}$ , whereas those lacking TASK-3 have a halved  $I_{K(SO)}$ . Double TASK-1/TASK-3 deletions may give further information. The remaining  $I_{K(SO)}$  in the mitv-TASK3 cells might come from the TWIK-1, TREK-2 or THIK-2 channels.

The mitv-TASK3 cerebellar granule cells fire fewer action potentials with injected current compared with wild-type granule cells (Figure 30D). This is a surprising feature of these granule cells, since we expected mitv-TASK3 granule cells to be hyperexcitable compared with the wild-

type granule cells, due to the approximately halved leak conductance (standing outward current). One hypothesis would be that the regulation of the voltage-gated Na<sup>+</sup> channels has changed in mitv-TASK3 granule cells, but the patch-clamp experiments show that mitv-TASK3 granule cells have normal voltage-gated Na<sup>+</sup> channel densities and kinetics (Stephen Brickley, personal communication). Rather, Na<sup>+</sup> channels seem to inactivate and lose the ability to support high frequency action potential firing. One possibility is that the membrane time constant is altered contributing to the inactivation of the Na<sup>+</sup> channels (Stephen Brickley, personal communication). In spite of these electrophysiological differences, the preliminary behaviour studies showed no ataxia or any clear motor deficit in mitv-TASK3 mice.

#### **4.7 Future plans**

As outlined in the Introduction, TASK-1 and TASK-3 channels are expected to impact on a variety of physiological functions, including some important ones (such as oxygen sensing and aldosterone secretion) in the periphery. My plans for these mice are outlined in the last section (1.6) of the Introduction.

## 5 APPENDIX

The Appendix contains supplementary material on methods and probes relating to gene targeting/homologous recombination.

Homologous recombination as a technique was invented/discovered by Capecchi and Smithies independently. Both have recently published retrospective reviews on how they developed this method (Capecchi, 2005; Smithies, 2005). The basic protocol is still the same as originally developed. The targeting technology was then married with the embryonic stem cell biology discovered by Martin Evans (Evans and Kaufman, 1981), paving the way for the first application of gene targeting in the 1990s. Making a knockout mouse requires a full application of molecular biology skills. The total technology concerns making the targeting vector by, first, screening a genomic library (section 5.1), subcloning a relevant fragment (section 5.2.1), inserting a removable neomycin resistance cassette (section 5.2.4) and characterizing hybridization probes to detect homologous gene targeting (section 5.6) by Southern blotting (section 5.4). Once finished, the targeting vector is transfected into embryonic stem cells (section 5.7) and screening undertaken for homologous events.

### 5.1 “Fingerprinting” the TASK-3 BAC clones

After screening of the BAC (bacterial artificial chromosome) library with the TASK-3 intronic 1 Kb probe (Library Screening Services of Incyte Genomics Inc.) we obtained three BAC clones: 27891, 27892 and 27893. These clones were fingerprinted with BamHI, EcoRI and MscI (not shown) and blotted by a standard alkaline Southern procedure (Figure 31A). The membrane was hybridized with the intronic 1Kb probe (see section 5.6.1 “1 Kb intronic TASK-3 probe”) to confirm the presence of the predicted 8 Kb EcoRI TASK-3 gene fragment. Hybridization showed that two out of three BAC clones (BAC 27892 and BAC 27893) contained the DNA fragment we were interested in. Moreover, the TASK-3 BAC gave identical restriction fragments with those obtained on mouse genomic Southern when probing with the same 1 Kb intronic probe (Figure A1B), confirming that the BAC clones contained no rearrangements, at least in the local region we were interested in. The sizes of the experimental bands also matched the virtual bands predicted from the genome sequence data.

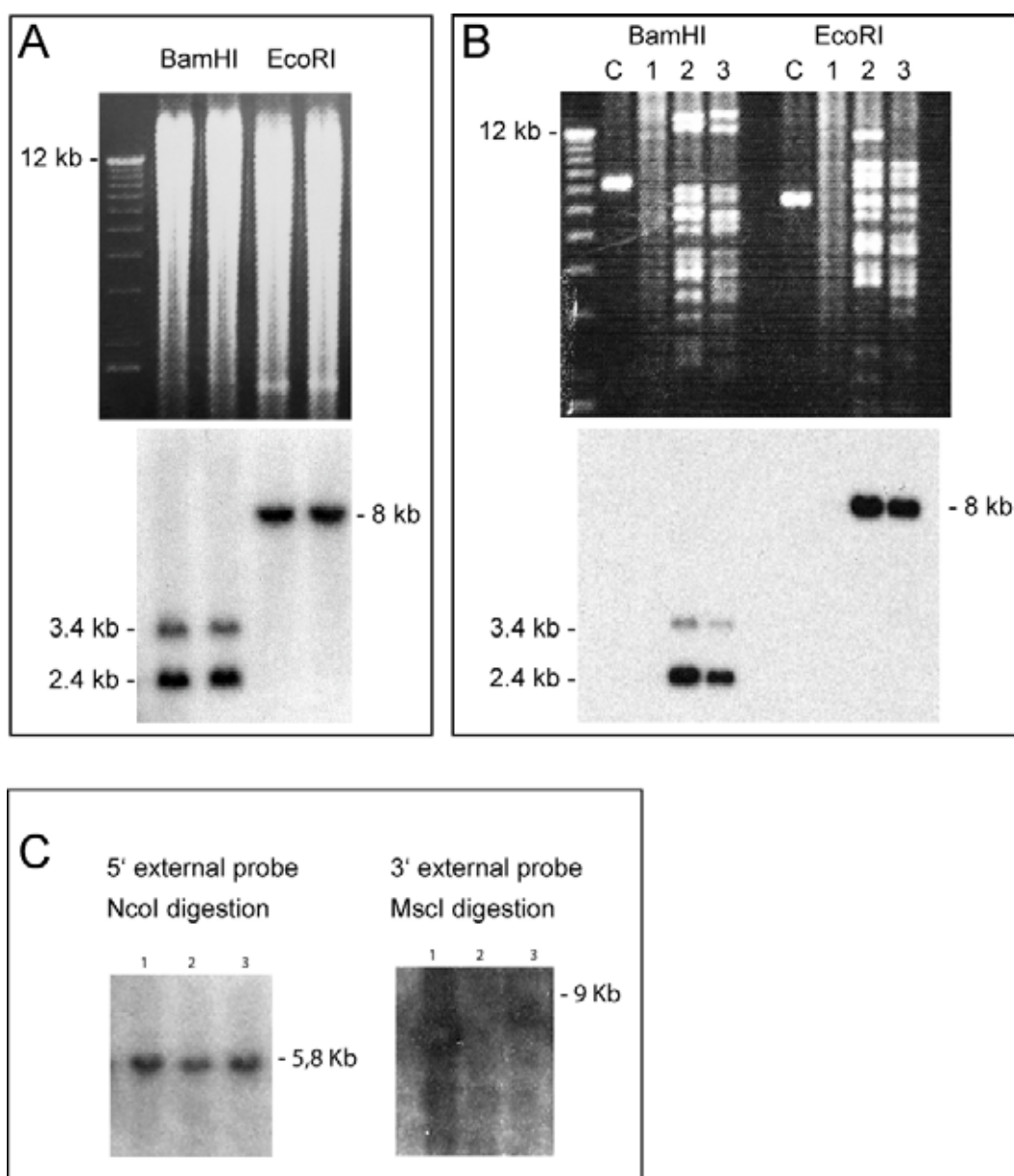


**Figure 31.** Characterization of the native mouse *TASK-3* gene and *TASK-3* BACs by hybridization with 1 Kb intronic probe.

**A**, genomic Southern blot of mouse tail DNA showing the specificity of the library screening probe. **B**, BAC fingerprinting using the same probe. Lane C, control BAC clone. Lanes 1, 2, 3 correspond to 27891, 27892, 27893 BAC clones. BAC clones 2 and 3 show the same pattern as on a genomic blot. **C**, test of designed external probes for screening of the targeted ES cells. The left picture shows the specificity of the 5' external probe on a wild-type tail DNA genomic Southern blot. A predicted NcoI 5.8 Kb band was obtained. The right-hand picture shows an example of the nonspecific hybridization result given by one of the designed 3' external probes on a wild-type genomic Southern blot. A MscI 9 Kb band was expected.

## 5.2 Further details on construction of TASK-3 targeting vector

### 5.2.1. Shotgunning the 8Kb EcoRI exon-1 containing TASK-3 gene fragment from the BAC into pLitmus 38

To subclone the targeting vector backbone, 3-5 µg the BAC 27892 plasmid (containing the 8 Kb fragment of TASK-3 gene) and pLitmus38 (100 ng) were digested with EcoRI and precipitated together with 3M NaOAc and 100% ethanol, washed in 70% ethanol, and redissolved in 8 µl water. The precipitated DNA was then ligated with T4 DNA ligase (1U/µl) in 10 µl final volume, overnight at 16°C. For colony screening, the ligation mixture was transformed into DH5α *E. coli* cells and plated on agar plates containing ampicillin. Filters of colony lifts were screened with the <sup>32</sup>P-labelled (random primed) TASK-3 intron 1 probe (see section 5.3 “Colony screening protocol for ligations”). Six positive clones carrying the TASK-3 gene fragment were found, three of them containing only the 8 Kb insert (pTASK3-EcoRI-8Kb) when digested with EcoRI. The sequence of this fragment was partially confirmed by sequencing pTASK3-EcoRI-8Kb with the Lac, Lac reverse, pL7S1, pL7S2, pL7AS1, pL7AS2 primers (see section 5.10.1 “Sequencing primers used for targeting vector construction”)

### 5.2.2 Changing the Sall site to a NotI site in pTASK-3EcoRI-8Kb

1 µg of pTASK3-EcoRI-8Kb was linearized with Sall in 20 µl reaction mixture for 1 h at 37°C and then blunted using Klenow enzyme (Roche) (10 µl pTASK3-EcoRI-8Kb digestion, 1 mM each dNTP, 2 µl 10X filling buffer, 1 U Klenow enzyme and H<sub>2</sub>O up to 20 µl) for 15 min at room temperature. Klenow was heat inactivated at 70°C for 20 min. 10 µl of blunted DNA was used in a 20 µl ligation reaction with 2.4 µg NotI phosphorylated linkers (NEB), overnight at 16°C. Ligated DNA was then diluted and digested with NotI in 100 µl reaction mixture, for 4 h at 37°C, and afterwards spun through a Chroma Spin TE-1000 column (Clontech) at 3000 rpm for 3 min (this removed the digested excess linkers). The vector was then recircularized: to 8 µl of column eluate, I added ligation buffer, ATP and T4 ligase; after 4 h at room temperature the ligation was transformed into DH5α *E. coli* cells. Randomly picked colonies were minicultured and the isolated plasmid DNA was restricted with NotI. A NotI-positive clone (pTASK3-EcoRI-8Kb-NotI) was used for the next cloning step.

### 5.2.3 Insertion of loxP oligo into BclI site of pTASK-3EcoRI-8Kb-NotI

Before insertion of loxP site, the BclI site was demethylated by retransformation of pTASK3-EcoRI-8Kb-NotI into the *E. coli* GM33 *dam*<sup>-</sup> strain, cut (1h/50°C) and blunted with Klenow enzyme (see previous section for blunting procedure).

The 5'EcoRVloxP fragment was obtained using two oligos: RVloxP1 5'-gatatcCCATAACTTCGTATAGCATACATTATACGAAGTTAT-3' and RVloxP2 5'-ATAACTTCGTATAATGTATGCTATACGAAGTTATGGgatatc-3' of 42 bp each which were mixed together, denatured for 5 min at 95°C and annealed by decreasing slowly the temperature. 2.4 µg of the double stranded 5'EcoRVloxP was ligated to 250 ng of blunt BclI digested pTASK3-EcoRI-8Kb-NotI in 20 µl ligation reaction and transformed into DH5α *E. coli* cells. Randomly picked colonies were tested for EcoRV digestion. The clones that were positive for EcoRV digestion (pTASK3-EcoRI-8Kb-loxP) were sequenced with two primers flanking the loxP insertion, pL7S1 and P4TV2 (see section 5.10.1 "Sequencing primers used for targeting vector construction") in order to determine the orientation of the loxP site and its unique insertion.

### 5.2.4 Insertion of lox-neo-lox-frt cassette into pTASK3-EcoRI-8Kb-loxP

The 5'-XhoI-frt-neomycin resistance-frt-loxP-Sall-3' cassette (Cope et al., 2004) was inserted into a Sall site which was generated by ligation of Sall linkers into an unique AfeI site of pTASK3-EcoRI-8Kb-loxP. 1 µg of pTASK3-EcoRI-8Kb-loxP plasmid was digested with AfeI for 1 h at 37°C (AfeI generates blunt ends). 10 µl of digested DNA was used in a 20 µl ligation reaction with 2.4 µg Sall phosphorylated linkers (NEB), overnight at 16°C. Diluted ligation was then digested in 100 µl reaction mixture with Sall for 4 h at 37°C and then spun down on Chroma Spin TE-1000 column. 8 µl of eluate was religated and transformed into DH5α *E. coli* cells. The 5'-XhoI-frt-neomycin resistance-frt-loxP-Sall-3' cassette was ligated into the Sall digested pTASK3-EcoRI-8Kb-loxP-Sall positive clone and the ligation was transformed into DH5α *E. coli* cells. For colony screening (see section 5.3 "Colony screening protocol for ligations"), I used as a probe the (random primed) neo cassette labeled with α<sup>32</sup>P-dCTP. The direction of cassette insertion was determined with sequencing primers P5TV2, P6TV2, P7TV2 and P8TV2 (see section 5.10.1 "Sequencing primers used for targeting vector construction").

### 5.3 Colony screening protocol for ligations

Agar plates containing transformed colonies were kept 1 h at 4°C before colony lifting. Afterwards, the colonies were lifted on Hybond N+ (Amersham) membranes (after the membranes and plates had been co-marked with pinholes) and the membranes were transferred (colony side up) for 5 min on Whatmann paper soaked in 2 x SSC/5% SDS solution for cell lysis (Buluwela et al., 1989). The filters were then microwaved at high power for 2.5 minutes, so crosslinking DNA with the membrane (Buluwela et al., 1989). Colony lifted agar plates were kept 24 hours at room temperature allowing the regrowth of the colonies for later picking. The membranes were hybridized overnight at 42°C with either <sup>32</sup>P-labeled (random-primed) probes (hybridization buffer contained 50% formamide/5 x SSC), or oligonucleotides labelled (kinased) at their 5' end with T4 polynucleotide kinase and <sup>32</sup>P-ATP (hybridisation with 50% formamide/5 x SSC for 30-45 mers, or lower % formamide/5 x SSC for shorter oligonucleotides). After hybridization, filters were washed once with 2 x SSC solution at room temperature for 5 min and twice with 0.1 x SSC at 65°C (for restriction fragment probes) and 1 x SSC at 60°C for oligonucleotides (30 to 45 mers); filters hybridized with shorter oligonucleotides were washed with 1 x SSC at 42°C. Hybridized filters were exposed 2 h to autoradiographic film at -70°C in cassettes with scintillation screens. Positive colonies were picked and minicultured.

### 5.4 Southern blotting

“Southern blots” were developed by Edwin Southern in the early 1970s. The anniversary of this technique and its development was recently reviewed by Eisenstein, 2004.

Digested genomic DNA fragments were separated by electrophoresis on 0.7% agarose gel (containing 0,5 µg/ml ethidium bromide) in 1 x TAE buffer (800mM Tris-HCl, 400mM NaOAc, 40mM EDTA, pH 8.3 adjusted with acetic acid). After electrophoresis, the gel was exposed for 5 min at 254 nm UV light to nick the DNA fragments (or 10 min for a pulse-field gel) and then incubated 20 min in 0.4 M NaOH solution to denature the DNA. Blotting was performed by a standard alkaline Southern transfer set up (using 0.4 M NaOH as transfer solution) onto a positively charged nylon Zetabond N<sup>+</sup> (Bio-Rad) membrane (the denatured DNA binds covalently to the membrane). After 6 h of transfer the membrane was neutralized with 4 x SSC solution and air dried.

### 5.4.1 Pulse-field gel electrophoresis

Pulse-field gel electrophoresis was used for separation of large DNA fragments and it was performed using a CHEF-DR III pulse field gel electrophoresis system (Bio-Rad) in 1 x TBE buffer (89 mM Tris, 89 mM boric acid, 2 mM EDTA, pH 8.0) for 15 h at 14°C.

### 5.5 Southern blot membrane hybridization

The Southern blots were hybridized with specific DNA probes labelled with  $\alpha^{32}\text{P}$ -dCTP (Amersham) by using a Random Prime DNA Labelling Kit (Amersham) (the technique for radiolabeling DNA restriction endonuclease fragments was introduced by Feinberg and Vogelstein, 1983). Hybridization was performed 1-2 h at 68°C in Quick-Hybridization buffer (Amersham) (the QuickHyb buffer composition is a “trade secret”, the buffer is probably 5 x SSC mixed with a rate enhancer such as PEG), After hybridization, the membrane was washed twice in 5 x SSC/0.1% SDS at room temperature for 15 min and twice with 1 x SSC/0.1% SDS at 68°C for 20 min. The membrane was then exposed to an X-ray film at -70°C in cassette with scintillation screens.

### 5.6 Hybridization probes

Double stranded probes were obtained by PCR amplification from C57Bl/6 mouse tail DNA using Taq DNA Polymerase (Invitrogen).

#### 5.6.1. 1 Kb intronic TASK-3 probe

A 1 Kb DNA fragment was amplified on 5' end of TASK-3 gene intron 1 using specific primers 32510mTA3S and 33510mTA3AS (see section 5.10.3 “Probe primers”). The PCR product was gel extracted using QIAquick Gel Extraction Kit (QIAGEN), ligated into pBluescript II SK (+) (Stratagene) which was previously digested with EcoRV and transformed into DH5 $\alpha$  *E. coli* cells. Positive colonies (pBS-1KbI1P) were identified by colony screening with a  $\gamma^{32}\text{P}$ -kinased oligonucleotide (45mT3I1 5'- GCA GCA GGT GAC CTG CAA TGC GGT CCT GGT GGG TTG GAT GTG GCA-3') (see section 5.3 “Colony screening protocol for ligations”) and checked by complete sequencing using T3 and T7 primers (see section 5.10.3 “Probe primers”). As a probe for Southern blot hybridisation I used a Sall-1KbI1P-NotI fragment obtained by double digestion of pBS-1KbI1P and gel extraction.

### 5.6.2. 5' external TASK-3 genomic probe

The 5' external probe is a 420 bp fragment located immediately upstream of the 5' end of the 8 Kb EcoRI-EcoRI fragment used for the construction of the TASK-3 targeting vector. This fragment was obtained by PCR using specific primers PB/S and PB/AS (see section 5.10.3, "Probe primers"). After gel extraction, the PCR fragment was ligated into EcoRV digested pBluescript II SK (+) and transformed into DH5 $\alpha$  *E. coli* cells. For colony screening, I used a  $\gamma^{32}$ P-kinased oligonucleotide (45mT35'P 5'-TTC CTT AAA CTC AAA GGC TAG TAG CTC CCT GGC CAG ATC CTC CTG-3') (see section 5.3 "Colony screening protocol for ligations"). Positive clones pBS-5'P were checked by complete sequencing using T3 and T7 primers (see section 5.10.3 "Probe primers"). As a probe for Southern blot hybridisation (Figures 32 and 33B), I used a Sall-5'P-NotI fragment obtained by double digestion of pBS-1Kb11P and gel extraction.

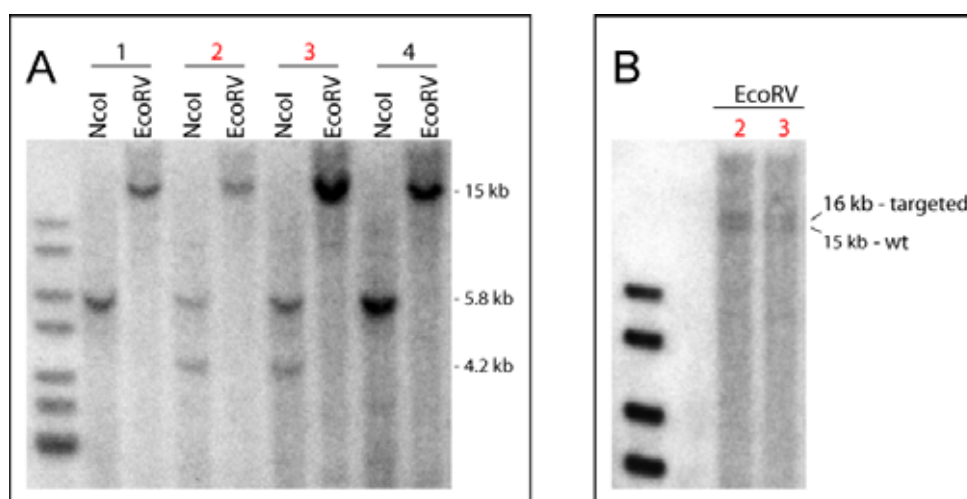


**Figure 32.** Southern blots of ES cell clones missing the 5' loxP site obtained after the second electroporation of ES cells.

**A**, lanes 1 and 4 show the wild-type pattern when probing with the 5' external probe. Lanes 2 and 3 show the integration of the targeting vector at the homologous locus, giving a 4.2 Kb NcoI band, but only a wild-type 15 Kb EcoRV band, demonstrating absence of the 5' loxP site. **B**, long running gel of EcoRV digested DNA of clones 2 and 3 from panel A revealed a 16 Kb band when probing with the 5' external probe indicating that the 5' loxP site of the targeting vector was not integrated during homologous recombination.

### **5.6.3. Neo probe**

The neo probe consists of a 1.3 Kb 5'-XhoI-frt-neomycin resistance-frt-loxP-Sall-3' fragment cassette obtained by double digestion with XhoI and Sall of a p-frtNeofrtlox plasmid (Cope et al., 2004) and purified by gel extraction.

### **5.7. Mouse embryonic stem cell culture**

Electroporated cells (129/SV RI, gift from G. Schuetz lab, DFFZ, Heidelberg) were cultured on mouse fibroblasts inactivated with mitomycin C (Sigma) in ES cell Medium containing Dulbecco's modified Eagle high glucose Medium supplemented with 2 mM L-glutamine (Gibco), 0.1mM non essential amino acids (Gibco), 1 mM sodium pyruvate (Gibco),  $10^{-4}$  M  $\beta$ -mercaptoethanol (Sigma), 20% foetal bovine serum (PAN Biotech GmbH), 50  $\mu$ g/ml penicillin/streptomycin (Gibco), 1000U/ml leukaemia inhibitory factor (Gibco). Electroporated cells were grown in ES cell medium supplemented with G418 (250 mg/ml, Stratagene) for selection. Individual resistant colonies were picked up 6-8 days after electroporation and split into 96 well feeder plates and 24 well plates (coated with 0.1% gelatine) for expansion. After 2-3 days, the clones cultured in 96 well feeder plates were slowly frozen in ES cell medium containing 10% DMSO and 25% FCS and stored at  $-70^{\circ}\text{C}$ . The clones cultured on gelatine plates were expanded for genomic DNA isolation.

### **5.8. Genotyping of mice**

#### **5.8.1. Preparation of mouse tail DNA**

Tail biopsies were digested with proteinase K (500  $\mu$ g/ml) (Roche) overnight at  $55^{\circ}\text{C}$  in 500  $\mu$ l HIRT buffer (10mM Tris pH 8, 100mM EDTA, 0.5% SDS). Afterwards, the proteins were precipitated with 167  $\mu$ l Protein Precipitation Solution (Puregene) and spun down 5 min at 13000 rpm. The DNA from the supernatant was precipitated with 500  $\mu$ l 100% isopropanol, washed with 70% ethanol, air dried and dissolved in 50  $\mu$ l TE.

#### **5.8.2. Mouse tail DNA digestion for Southern blotting**

The tail biopsy DNA was digested overnight at the appropriate temperature in 25  $\mu$ l reaction mixture containing 10  $\mu$ l DNA, 2.5  $\mu$ l 10X restriction endonuclease buffer, 2.5  $\mu$ l 10X

spermidine (40mM), 8  $\mu$ l H<sub>2</sub>O and 2  $\mu$ l restriction endonuclease (10U/ $\mu$ l). All the digestion volume was loaded for electrophoresis.

### **5.8.3. PCR genotyping of mice**

The tail DNA was diluted 1:10 prior to the PCR reaction.

For genotyping the mitv-TASK3 mice, two primers flanking the 5' loxP site were used: pL7S1 and P4TV2 (see section 5.10.1 "Sequencing primers used for targeting vector construction"), giving a 350 bp wild type band and a 400 bp loxP band (Figure 33, 34A, 34B). PCR reactions were done for 35 cycles at 94°C for 45s, 70°C for 45s, 72°C for 30s.

During crossing of mitv-TASK-3 mice with the Cre deleter mice, we detected the Cre-positive mice by PCR using primers CRE/S and CRE/AS (see section 5.10.4 "Primers for genotyping") that give a 300 bp amplicon (Figure 34A). PCR conditions were 35 cycles at 95°C for 30s, 55°C for 30s and 72° for 30s.

During crossing of the neo-TASK3 mice with Flp deleter mice, we detected the Flp-positive mice by PCR using primers FLP/S and FLP/AS (see section 5.10.4 "Primers for genotyping") that give an amplicon of 700 bp (Figure 34B). PCR conditions were similar as for Cre PCR: 34 cycles at 95°C for 30s, 55°C for 30s and 72° for 30s.

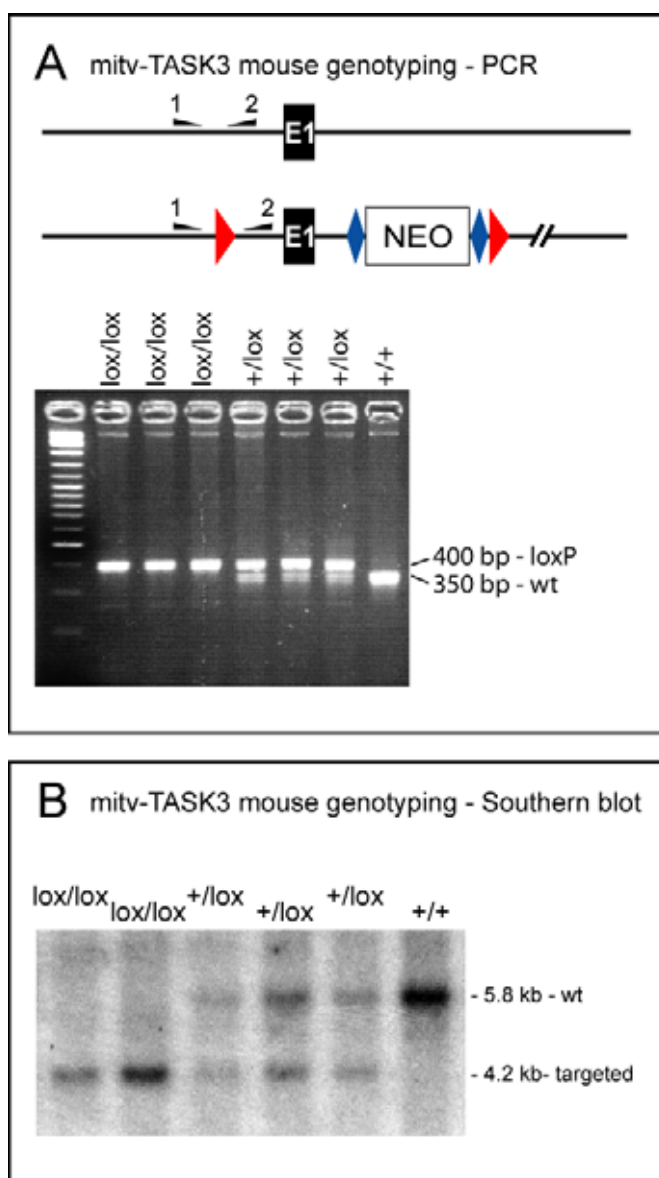


**Figure 33.** Genotyping of mitv-TASK3 mice.

**A**, genotyping strategy of mitv-TASK3 mice by PCR using primers flanking the 5' loxP site. **B**, genotyping of mitv-TASK3 mice by Southern blot by probing with 5' external probe on NcoI digested tail DNA.

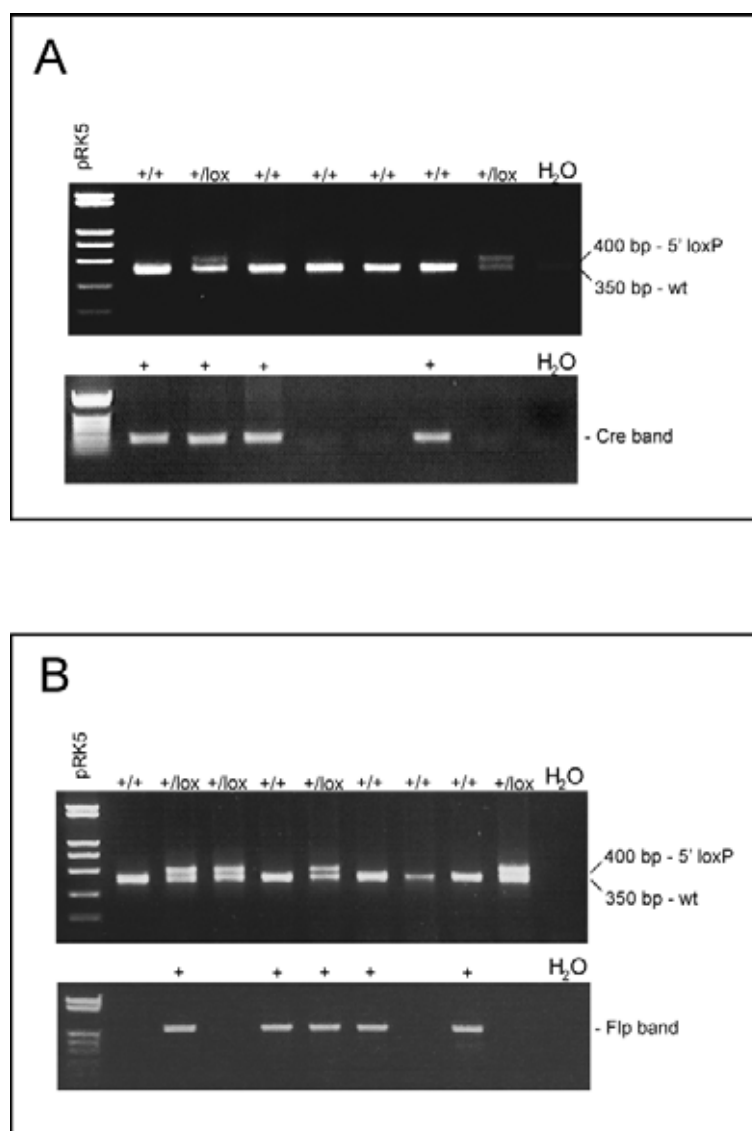


**Figure 34.** PCR genotyping of heterozygote offspring obtained by crossing *mitv-TASK3* mice with *Cre* and, respectively, *Flp* deleter mice.

PCR amplification from mouse tail DNA of heterozygote offspring obtained by **A**, crossing of *mitv-TASK3* mice with *Cre* deleter and **B**, by crossing with *Flp* deleter mice.

### 5.9. Removal of the neomycin insertion from the *mitv-TASK3* line reactivates the *TASK-3* gene

Analysis of knockout mice is optimal if the neo gene has been removed (see Discussion section 4.1 “Generation of *TASK-3* knockout mice: technical considerations”). Crossing *mitv-TASK3* mice with the *Cre* deleter strain most likely deletes part of intron 1 and inverts exon 1 and a linked *frt*-flanked neo gene (see Figure 23B). We think it is an inversion because of the 2.5 Kb *NcoI* fragment obtained with the 5' probe. My hypothesis is that one of the integrated targeting vector copies was inserted in reversed orientation. After *Cre* recombination, a pair of opposite

oriented loxP sites allowed the inversion of the floxed genomic fragment. These mice were termed “neo-TASK3 mice”.

Crossing neo-TASK3 mice with a Flp deleter strain gave mice, with the neo insertion removed, termed “floxed”-TASK3 mice”, but the TASK-3 gene was reactivated (Figure 35).

*In situ* hybridization revealed that after complete removal of the neo cassette, the TASK-3 gene becomes active (Figure 35), indicating the inhibitory effect of the multiple insertion of neomycin gene in intron 1 of the TASK-3 gene. The mRNA expression of TASK-1 and T1 genes remains unaltered compared with wild-type in this mice. It is possible that the presence of loxP and/or frr sites in opposite orientations induced the flipping of the DNA fragment containing the exon 1 during Cre and/or Flp recombination. A slight reduction of TASK-3 mRNA is observed in all regions of the brains of these animals.

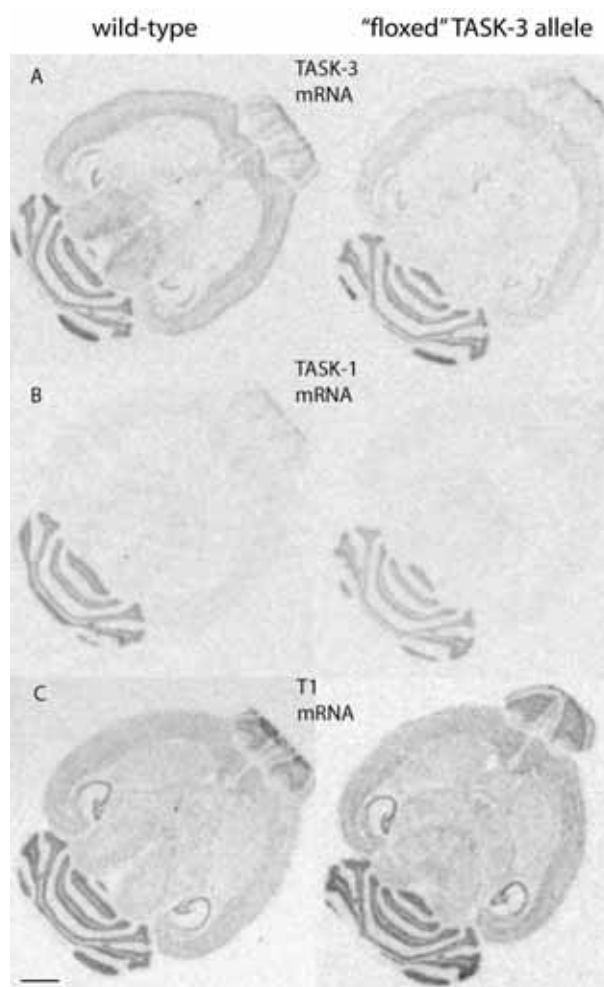


**Figure 35.** mRNA expression of TASK-3 (A), TASK-1 (B) and T1 (C) after the complete removal of the neo cassette in adult mouse brain (scale bar 2mm).

## 5.10. List of primers

### 5.10.1 Sequencing primers used for targeting vector construction

Lac:	5'-GTTTTCCCAGTCACGAC-3'
Lac reverse:	5'-CAGGAAACAGCTATGAC-3'
pL7S1:	5'-CTCTGTCCCGGCTACCGATCCTGC-3'
pL7S2:	5'-GCCACACTGGAGGCGATTAGCTGG-3'
pL7AS1:	5'-TGTGCGCTACATCTCCTACACCCC-3'
pL7AS2:	5'-GAAACAGGGTCTGTCTTAAACCTG-3'
P4TV2:	5'-TTCCGTGGGCGCAGCGGGTTCCGC-3'
P5TV2:	5'-ACCCAGGCCTGGAATGTTTCCACC-3'
P6TV2:	5'-ATTCGCAGCGCATCGCCTTCTATC-3'
P7TV2:	5'-ACCTCCTGTCACCTTAATGTCCCA-3'
P8TV2:	5'-AGGGGCATGACCTCACTCTTCCAG-3'

### 5.10.2 Sequencing primers used for mTASK-3 and mTASK-1 cDNA

T1Seq1:	5'-AGCACGGACGGAGGCAAGGTGTTC-3'
T1Seq2:	5'-GACTATGTGCGCTGCAGAAGGAC-3'
T1Seq3:	5'-GCGTCGGTGGCAGCGGCTTCCGCA-3'
T1Seq1AS:	5'-CTCGTAGCCGCCCTCGCTGAGG-3'
T1Seq2AS:	5'-GAAACCGATGAGCACCATGTTG-3'
T3Seq1:	5'-ATGCTGGCAAGGCCTTCTGTATGT-3'
T3Seq2:	5'-ATTTTGTGGCCCTGCAGGCCAAGG-3'
T3Seq3:	5'-CGATAATGTTGTTGTTACTGCTCC-3'
9AST3:	5'-AAGGCACAGGGTGCCCATGCAGGA-3'
12AST3:	5'-CGCAGAGATAGCACAGGGTTCTGC-3'

### 5.10.3 Probe primers

#### 1 Kb intronic probe

32510mTA3S:	5'-CCATCACTGTCATCACAACACTATCG-3'
33510mTA3AS:	5'-CTCACAGATCCAAAGAGATGGACC-3'

#### 5' Probe primers

PB/S: 5'-CCATGGCTAGGGACAGAGAAGATA-3'

PB/AS: 5'-TCTCATTTCCTCTCCAGCAGTA-3'

### 3' Probe primers

PA/S 5'-ATGTGTGCATGCTCTTATGCACTC-3'

PA/AS 5'-GGCCACCTAGATATGGAGAACTCA-3'

### pBluescript II SK (+) sequencing primers

T3: 5'-AATTAACCCTCACTAAAGGG-3'

T7: 5'-TAATACGACTCACTATAGGG-3'

## 5.10.4 Primers for genotyping

### CRE primers

CRE/S: 5'-GACCAGGTTCGTTCACTCATGG-3' (sense)

CRE/AS 5'-AGGCTAAGTGCCTTCTCT ACAC-3' (antisense)

### FLP primers

FLP/S: 5'-CACTGATATTGTAAGTAGTTT-3' (sense)

FLP/AS: 5'-TAGTGCGAAGTAGTGATCAGG-3' (antisense)

## 5.11 In situ hybridization oligonucleotides

**mTASK-1a**, 5'-GGT GCA CAC GAT GAG AGC CAA CGT GCG CAC ATT CTG CCG  
CTT CAT CG-3'

**mTASK-1b**, 5'-TCA CAC CGA GCT CCT GCG CTT CAT GAG GCC GCG GAA GGC  
AGC CAG-3'

**rTASK-3a** 5'-GAT GGA CTT GCG ACG GAT GTG CAG CCT GTG GTT TTC CCC GCA  
GGT GTG CAT-3'

**rTASK-3b**, 5'-GTA CTT GCC TCT GAG GCG GAC CTC TTC TGC TTT AAG TTT CTC  
CTC-3'

**mTWIK-1a**, 5'-CTC CAC CAG GCG CAC GCA CGA GCT GCC GGC CAG GGA CTG  
CAG CAT-3'

**mTWIK-1b**, 5'-GTG GTC TGC AGA GCC ATC CTC ATA GGG TGG GGA CTG GGA  
GGC CAC-3'

**mTREK-1a**, 5'-GTT CTG AGC AGC AGA CTT GGG ATC CAG CAA GTC AGG GGC  
CGC CAT-3'

**mTREK-1b**, 5'-CTT CAT GTT CTC AAT GAC AGC TAT GTC CTC ACC AGC ACA GTG TGG-3'

**mTREK-2a**, 5'-ATC CCA GTT CAC CTG CTT TCT TGG CGT CTC GAT TGG AAA TTT CAT-3'

**mTREK-2b**, 5'-ATG GCT CCC GTG GAT ACC AGG CAC GAA GAT ATG AGT GCA GAC AAA-3'

**mTHIK-2a**, 5'-TAT GGT CGA CAC CAC GGT GCC CAC GAA GTA GAA CCG AGG TCC CTT-3'

**mTHIK-2b**, 5'-CTC GGA CAG CTG CTT CTG CAG CAG CGC CAG CGA CAC CTT GTT GGA-3'

**mTHIK-1a**, 5'-GTC GTC CAT CAG TGT CAC GTT CCA TCA CCC CGT CTG TCT CTA T-3'

**mTHIK-1b**, 5'-GCT ACT TCT GGT TCC TAC CTA TCT CCA CTG GTC TCT GCC AAC CTG-3'

**mT1a**, 5'-CCA ACG TGT TTC CGC ATG CGT CCT TGG CAC CGC TTC TTG TAG TGT-3'

**mT1b**, 5'-GGC CTG TGC CCC GAG GGC CCT CAC ATG CAC GCT GGG TAA GCA AAC-3'

## 5.12 Real-time quantitative-PCR oligonucleotides

**TASK-1 forward** 5'-CGGCTTCCGCAACGTCTAT-3'

**TASK-1 reverse** 5'-TTGTACCAGAGGCACGAGCA-3'

**TASK-3 forward** 5'-GACGTGCTGAGGAACACCTACTT-3'

**TASK-3 reverse** 5'-GTGTGCATTCCAGGAGGGA-3'

**TWIK-1 forward** 5'-TGTCCTTCTCCTCCGTCCTG-3'

**TWIK-1 reverse** 5'-AGGCCACAAAAGGCTCACTTT-3'

**THIK-2 forward** 5'-GGGACTTCCCTGGAGCCTTC-3'

**THIK-2 reverse** 5'-GTCATGCCGAAACCTATGGTCG-3'

**TREK-1 forward** 5'-TTTCCTGGTGGTCGTCCTC-3'

**TREK-1 reverse** 5'-GCTGCTCCAATGCCTTGAAC-3'

**TREK-2 forward** 5'-CCGGAATTACTCTCTGGATGAAGA-3'

**TREK-2 reverse** 5'-CATGGCTGTGCTGGAGTTGT-3'

---

<b>TRAAK forward</b>	5'-CCCCAGTGAGAATCTGGCC-3'
<b>TRAAK reverse</b>	5'-GGGCACAGCCACGCTC-3'
<b>GABA<math>\alpha</math>6 forward</b>	5'-CGCCCCCTGTGGCAA-3'
<b>GABA<math>\alpha</math>6 reverse</b>	5'-TACTTGGAGTCAGAATGCACAACA-3'
<b>Cyclophylin forward</b>	5'-AGGTCCTGGCATCTTGTCCAT-3'
<b>Cyclophylin reverse</b>	5'-GAACCGTTTGTGTTTGGTCCA-3'

## 6 ABBREVIATIONS

$\alpha$	Alpha
$\alpha^{32}\text{P}$ -dCTP	Deoxycytosin triphosphate labeled with $^{32}\text{P}$ in alpha position
$\gamma^{32}\text{P}$ -ATP	Adenosine triphosphate labeled with $^{32}\text{P}$ in gamma position
$\mu$	Micro
A	Ampere
A	Alanine
AT1R	Angiotensin II type I receptor
ATP	Adenosine triphosphate
$\beta$	Beta
BAC	Bacterial artificial chromosome
bp	Base pair
BSA	Bovine serum albumin
C	Celsius
C	Cysteine
CA 1-3	Cornu ammonis
cDNA	Complementary DNA
CGC	Cerebellar granule cells
CNS	Central Nervous System
Cre	Cre recombinase
DAG	Diacylglycerol
DEPC	Diethyl pyrocarbonate
DNA	Deoxyribonucleic acid
dNTP	Deoxyribonucleotide triphosphate
DTT	Dithiothreitol
E	Glutamic acid
<i>E. coli</i>	<i>Escherichia Coli</i>
et al.	et alii
EDTA	Ethylenediamine tetraacetic acid
EGTA	Ethylene glycol-bis(2-aminoethyl)-N,N,N',N'-tetraacetic acid
ES	Embryonic Stem

---

F	Phenylalanine
Flp	Flp recombinase
$\gamma$	gamma
G proteins	signal transducing GTP-binding proteins
G418	Geneticin
GABA	$\gamma$ -aminobutyric acid
H	Histidine
HEK	Human embryonic kidney
HEPES	N-(2-Hydroxyethyl)piperazine-N'-ethanesulfonic acid
I	Current
IgG	Immunoglobulin G
$I_{K(SO)}$	“Standing outward” potassium current
IP3	Inositol-1,4,5-triphosphate
IRES	Internal Ribosome Entry Site from the encephalomyocarditis virus
K2P	Two-pore-domain potassium channel
kb	Kilobase
KCNKx	potassium channel, subfamily K, member x
KO	knock-out
L	Leucine
lacZ	$\beta$ -galactosidase
LoxP	Locus of crossing over (for) phage P
LPL	Lysophospholipids
$\mu$	micro
m	Milli
M	Methionine
M	Molar
min	minute
mRNA	Messenger RNA
nAChR	nicotinic acetylcholine receptor
NADPH	Nicotinamide adenine dinucleotide phosphate
neo	Neomycin resistance gene
ORF	Open reading frame
P	Pore domain

---

PAGE	Polyacrylamide gel electrophoresis
PBS	Phosphate-buffered saline
PCO <sub>2</sub>	Partial CO <sub>2</sub> pressure
PCR	Polymerase chain reaction
PDZ domain	Post synaptic density/disc large/zona occludens-1 homology domain
PEG	Polyethylenglycol
PFA	Paraformaldehyde
PIP <sub>2</sub>	Phosphatidyl-4,5-inositol-biphosphate
PLC	Phospholipase C
PO <sub>2</sub>	Partial O <sub>2</sub> pressure
PUFA	Polyunsaturated fatty acids
PKA	Cyclic AMP-dependent protein kinase A
PKC	Protein kinase C
PVP	Polyvinylpyrrolidone
R	Arginine
R-(+)-WIN 55,212-2	R-(+)-(2,3-dihydro-5-methyl-3-[(4-morpholinyl) methyl] pyrrol [1,2, 3-de]-1,4- benzoxazin-6-yl)(1-naphthalenyl) methanone monomethanesulfonate
RNA	Ribonucleic acid
RR	Ruthenium red
RT	Room temperature
RT-PCR	Reverse transcription coupled to polymerase chain reaction
S	Serine
SDS	Sodium-dodecyl-sulfat
T	Threonine
t	Time
TALK	<u>T</u> WIK-related <u>a</u> lkaline pH activated <u>K</u> <sup>+</sup> channel
TASK	<u>T</u> WIK-related <u>a</u> cid- <u>s</u> ensitive <u>K</u> <sup>+</sup> channel
TBE	Tris-borate buffer
TBS	Tris-buffered saline
TE	Tris/EDTA buffer
TENS	Tris-EDTA-Sodium chloride-SDS buffer

---

THIK	<u>T</u> andem pore domain <u>h</u> alothane- <u>i</u> nhibited <u>K</u> <sup>+</sup> channel
TM	<u>T</u> ransmembrane domain
TRAAK	<u>T</u> WIK- <u>r</u> elated <u>a</u> rachidonic <u>a</u> cid- <u>s</u> timulated <u>K</u> <sup>+</sup> channel
TREK	<u>T</u> WIK- <u>r</u> elated <u>K</u> <sup>+</sup> channel
TRESK	<u>T</u> WIK- <u>r</u> elated <u>s</u> pinal cord <u>K</u> <sup>+</sup> channel
TRH	<u>T</u> hyrotropin-releasing hormone
Tris	<u>T</u> ris(hydroxymethyl)aminomethane
Tris-HCl	<u>T</u> ris(hydroxymethyl)aminomethane-hydrochloride
TWIK	<u>T</u> andem of <u>P</u> domains in a <u>w</u> eak <u>i</u> nwardly rectifying <u>K</u> <sup>+</sup> channel
U	<u>U</u> nit
v	<u>V</u> olume
V	<u>V</u> aline
V	<u>V</u> oltage
V	<u>V</u> olt
W	<u>W</u> att
wt	<u>W</u> ild-type
Y	<u>Y</u> tyrosine

## 7 REFERENCES

- Aller M. I., Veale E., Linden A. M., Sandu C., Schwaninger M., Evans L., Korpi E. R., Mathie A., Wisden W. and Brickley S. G. (2005) Modifying the subunit composition of TASK channels alters the modulation of a leak conductance in cerebellar granule neurons and is associated with impaired motor performance. *J Neurosci*, in press
- Asamura K., Abe S., Imamura Y., Aszodi A., Suzuki N., Hashimoto S., Takumi Y., Hayashi T., Fassler R., Nakamura Y. and Usami S. (2005) Type IX collagen is crucial for normal hearing. *Neuroscience* 132, 493-500.
- Ashmole I., Goodwin P. A. and Stanfield P. R. (2001) TASK-5, a novel member of the tandem pore K<sup>+</sup> channel family. *Pflugers Arch* 442, 828-833.
- Assaf S. Y. and Chung S. H. (1984) Release of endogenous Zn<sup>2+</sup> from brain tissue during activity. *Nature* 308, 734-736.
- Bang H., Kim Y. and Kim D. (2000) TREK-2, a new member of the mechanosensitive tandem-pore K<sup>+</sup> channel family. *J Biol Chem* 275, 17412-17419.
- Barriere H., Belfodil R., Rubera I., Tauc M., Lesage F., Poujeol C., Guy N., Barhanin J. and Poujeol P. (2003) Role of TASK2 potassium channels regarding volume regulation in primary cultures of mouse proximal tubules. *J Gen Physiol* 122, 177-190.
- Bayliss D. A., Sirois J. E. and Talley E. M. (2003) The TASK family: two-pore domain background K<sup>+</sup> channels. *Mol Interv* 3, 205-219.
- Berg A. P., Talley E. M., Manger J. P. and Bayliss D. A. (2004) Motoneurons express heteromeric TWIK-related acid-sensitive K<sup>+</sup> (TASK) channels containing TASK-1 (KCNK3) and TASK-3 (KCNK9) subunits. *J Neurosci* 24, 6693-6702.
- Bockenhauer D., Zilberberg N. and Goldstein S. A. (2001) KCNK2: reversible conversion of a hippocampal potassium leak into a voltage-dependent channel. *Nat Neurosci* 4, 486-491.
- Boyd D. F., Millar J. A., Watkins C. S. and Mathie A. (2000) The role of Ca<sup>2+</sup> stores in the muscarinic inhibition of the K<sup>+</sup> current I<sub>K(SO)</sub> in neonatal rat cerebellar granule cells. *J Physiol* 529 Pt 2, 321-331.
- Brickley S. G., Revilla V., Cull-Candy S. G., Wisden W. and Farrant M. (2001) Adaptive regulation of neuronal excitability by a voltage-independent potassium conductance. *Nature* 409, 88-92.
- Brown L. D., Kim K. M., Nakajima Y. and Nakajima S. (1993) The role of G protein in muscarinic depolarization near resting potential in cultured hippocampal neurons. *Brain Res* 612, 200-209.
- Buchholz F., Angrand P. O. and Stewart A. F. (1996) A simple assay to determine the functionality of Cre or FLP recombination targets in genomic manipulation constructs. *Nucleic Acids Res* 24, 3118-3119.
- Buckler K. J. (1997) A novel oxygen-sensitive potassium current in rat carotid body type I cells. *J Physiol* 498 ( Pt 3), 649-662.
- Buckler K. J., Williams B. A. and Honoré E. (2000) An oxygen-, acid- and anaesthetic-sensitive TASK-like background potassium channel in rat arterial chemoreceptor cells. *J Physiol* 525, 135-142.
- Buluwela L., Forster A., Boehm T. and Rabbitts T. H. (1989) A rapid procedure for colony screening using nylon filters. *Nucleic Acids Res* 17, 452.
- Byrne J. H. and Kandel E. R. (1996) Presynaptic facilitation revisited: state and time dependence. *J Neurosci* 16, 425-435.

- Callahan R., Labunskiy D. A., Logvinova A., Abdallah M., Liu C., Cotten J. F. and Yost C. S. (2004) Immunolocalization of TASK-3 (KCNK9) to a subset of cortical neurons in the rat CNS. *Biochem Biophys Res Commun* 319, 525-530.
- Capecchi M. R. (2005) Gene targeting in mice: functional analysis of the mammalian genome for the twenty-first century. *Nat Rev Genet* 6, 507-512.
- Chapman C. G., Meadows H. J., Godden R. J., Campbell D. A., Duckworth M., Kelsell R. E., Murdock P. R., Randall A. D., Rennie G. I. and Gloger I. S. (2000) Cloning, localisation and functional expression of a novel human, cerebellum specific, two pore domain potassium channel. *Brain Res Mol Brain Res* 82, 74-83.
- Chavez R. A., Gray A. T., Zhao B. B., Kindler C. H., Mazurek M. J., Mehta Y., Forsayeth J. R. and Yost C. S. (1999) TWIK-2, a new weak inward rectifying member of the tandem pore domain potassium channel family. *J Biol Chem* 274, 7887-7892.
- Chemin J., Girard C., Duprat F., Lesage F., Romey G. and Lazdunski M. (2003) Mechanisms underlying excitatory effects of group I metabotropic glutamate receptors via inhibition of 2P domain K<sup>+</sup> channels. *Embo J* 22, 5403-5411.
- Chemin J., Patel A., Duprat F., Zanzouri M., Lazdunski M. and Honoré E. (2005) Lysophosphatidic acid-operated K<sup>+</sup> channels. *J Biol Chem* 280, 4415-4421.
- Cibulsky S. M. and Sather W. A. (1999) Block by ruthenium red of cloned neuronal voltage-gated calcium channels. *J Pharmacol Exp Ther* 289, 1447-1453.
- Clarke C. E., Veale E. L., Green P. J., Meadows H. J. and Mathie A. (2004) Selective block of the human 2-P domain potassium channel, TASK-3, and the native leak potassium current, IKSO, by zinc. *J Physiol* 560, 51-62.
- Cope D. W., Wulff P., Oberto A., Aller M. I., Capogna M., Ferraguti F., Halbsguth C., Hoeger H., Jolin H. E., Jones A., McKenzie A. N., Ogris W., Poeltl A., Sinkkonen S. T., Vekovischeva O. Y., Korpi E. R., Sieghart W., Sigel E., Somogyi P. and Wisden W. (2004) Abolition of zolpidem sensitivity in mice with a point mutation in the GABA<sub>A</sub> receptor gamma2 subunit. *Neuropharmacology* 47, 17-34.
- Cotten J. F., Zou H. L., Liu C., Au J. D. and Yost C. S. (2004) Identification of native rat cerebellar granule cell currents due to background K channel KCNK5 (TASK-2). *Brain Res Mol Brain Res* 128, 112-120.
- Crawley J. N. (2000) What's wrong with my mouse? Behavioral phenotyping of transgenic and knockout mice., Wiley-Liss, Weinheim.
- Czirjak G., Fischer T., Spat A., Lesage F. and Enyedi P. (2000) TASK (TWIK-related acid-sensitive K<sup>+</sup> channel) is expressed in glomerulosa cells of rat adrenal cortex and inhibited by angiotensin II. *Mol Endocrinol* 14, 863-874.
- Czirjak G. and Enyedi P. (2002a) Formation of functional heterodimers between the TASK-1 and TASK-3 two-pore domain potassium channel subunits. *J Biol Chem* 277, 5426-5432.
- Czirjak G. and Enyedi P. (2002b) TASK-3 dominates the background potassium conductance in rat adrenal glomerulosa cells. *Mol Endocrinol* 16, 621-629.
- Czirjak G. and Enyedi P. (2003) Ruthenium red inhibits TASK-3 potassium channel by interconnecting glutamate 70 of the two subunits. *Mol Pharmacol* 63, 646-652.
- Czirjak G., Toth Z. E. and Enyedi P. (2004) The two-pore domain K<sup>+</sup> channel, TRESK, is activated by the cytoplasmic calcium signal through calcineurin. *J Biol Chem* 279, 18550-18558.
- Decher N., Maier M., Dittrich W., Gassenhuber J., Bruggemann A., Busch A. E. and Steinmeyer K. (2001) Characterization of TASK-4, a novel member of the pH-sensitive, two-pore domain potassium channel family. *FEBS Lett* 492, 84-89.
- Doyle D. A., Morais Cabral J., Pfuetzner R. A., Kuo A., Gulbis J. M., Cohen S. L., Chait B. T. and MacKinnon R. (1998) The structure of the potassium channel: molecular basis of K<sup>+</sup> conduction and selectivity. *Science* 280, 69-77.

- Dray A., Forbes C. A. and Burgess G. M. (1990) Ruthenium red blocks the capsaicin-induced increase in intracellular calcium and activation of membrane currents in sensory neurones as well as the activation of peripheral nociceptors in vitro. *Neurosci Lett* 110, 52-59.
- Duprat F., Lesage F., Fink M., Reyes R., Heurteaux C. and Lazdunski M. (1997) TASK, a human background K<sup>+</sup> channel to sense external pH variations near physiological pH. *Embo J* 16, 5464-5471.
- Eisenstein M. (2004) A (positive) blot on his record. *Nature Methods* 1, 90.
- Evans M. J. and Kaufman M. H. (1981) Establishment in culture of pluripotential cells from mouse embryos. *Nature* 292, 154-156.
- Feinberg A. P. and Vogelstein B. (1983) A technique for radiolabeling DNA restriction endonuclease fragments to high specific activity. *Anal Biochem* 132, 6-13.
- Fink M., Duprat F., Lesage F., Reyes R., Romey G., Heurteaux C. and Lazdunski M. (1996) Cloning, functional expression and brain localization of a novel unconventional outward rectifier K<sup>+</sup> channel. *Embo J* 15, 6854-6862.
- Fink M., Lesage F., Duprat F., Heurteaux C., Reyes R., Fosset M. and Lazdunski M. (1998) A neuronal two P domain K<sup>+</sup> channel stimulated by arachidonic acid and polyunsaturated fatty acids. *Embo J* 17, 3297-3308.
- Franklin K. B. J. and Paxinos G. (1997) *The Mouse Brain in Stereotaxic Coordinates*, Academic Press, San Diego.
- Franks N. P. and Lieb W. R. (1994) Molecular and cellular mechanisms of general anaesthesia. *Nature* 367, 607-614.
- Franks N. P. and Honoré E. (2004) The TREK K2P channels and their role in general anaesthesia and neuroprotection. *Trends Pharmacol Sci* 25, 601-608.
- Frederickson C. J. (1989) Neurobiology of zinc and zinc-containing neurons. *Int Rev Neurobiol* 31, 145-238.
- Gabriel A., Abdallah M., Yost C. S., Winegar B. D. and Kindler C. H. (2002) Localization of the tandem pore domain K<sup>+</sup> channel KCNK5 (TASK-2) in the rat central nervous system. *Brain Res Mol Brain Res* 98, 153-163.
- Gerstin K. M., Gong D. H., Abdallah M., Winegar B. D., Eger E. I., 2nd and Gray A. T. (2003) Mutation of KCNK5 or Kir3.2 potassium channels in mice does not change minimum alveolar anesthetic concentration. *Anesth Analg* 96, 1345-1349.
- Girard C., Duprat F., Terrenoire C., Tinel N., Fosset M., Romey G., Lazdunski M. and Lesage F. (2001) Genomic and functional characteristics of novel human pancreatic 2P domain K<sup>+</sup> channels. *Biochem Biophys Res Commun* 282, 249-256.
- Girard C., Tinel N., Terrenoire C., Romey G., Lazdunski M. and Borsotto M. (2002) p11, an annexin II subunit, an auxiliary protein associated with the background K<sup>+</sup> channel, TASK-1. *Embo J* 21, 4439-4448.
- Goldstein S. A., Price L. A., Rosenthal D. N. and Pausch M. H. (1996) ORK1, a potassium-selective leak channel with two pore domains cloned from *Drosophila melanogaster* by expression in *Saccharomyces cerevisiae*. *Proc Natl Acad Sci U S A* 93, 13256-13261.
- Goldstein S. A., Bockenhauer D., O'Kelly I. and Zilberberg N. (2001) Potassium leak channels and the KCNK family of two-P-domain subunits. *Nat Rev Neurosci* 2, 175-184.
- Gray A. T., Winegar B. D., Leonoudakis D. J., Forsayeth J. R. and Yost C. S. (1998) TOK1 is a volatile anesthetic stimulated K<sup>+</sup> channel. *Anesthesiology* 88, 1076-1084.
- Gray A. T., Zhao B. B., Kindler C. H., Winegar B. D., Mazurek M. J., Xu J., Chavez R. A., Forsayeth J. R. and Yost C. S. (2000) Volatile anesthetics activate the human tandem pore domain baseline K<sup>+</sup> channel KCNK5. *Anesthesiology* 92, 1722-1730.

- Gruss M., Bushell T. J., Bright D. P., Lieb W. R., Mathie A. and Franks N. P. (2004) Two-pore-domain K<sup>+</sup> channels are a novel target for the anesthetic gases xenon, nitrous oxide, and cyclopropane. *Mol Pharmacol* 65, 443-452.
- Gu W., Schlichthorl G., Hirsch J. R., Engels H., Karschin C., Karschin A., Derst C., Steinlein O. K. and Daut J. (2002) Expression pattern and functional characteristics of two novel splice variants of the two-pore-domain potassium channel TREK-2. *J Physiol* 539, 657-668.
- Gutman G. A., Chandy K. G., Adelman J. P., Aiyar J., Bayliss D. A., Clapham D. E., Covarriubias M., Desir G. V., Furuichi K., Ganetzky B., Garcia M. L., Grissmer S., Jan L. Y., Karschin A., Kim D., Kuperschmidt S., Kurachi Y., Lazdunski M., Lesage F., Lester H. A., McKinnon D., Nichols C. G., O'Kelly I., Robbins J., Robertson G. A., Rudy B., Sanguinetti M., Seino S., Stuehmer W., Tamkun M. M., Vandenberg C. A., Wei A., Wulff H. and Wymore R. S. (2003) International Union of Pharmacology. XLI. Compendium of voltage-gated ion channels: potassium channels. *Pharmacol Rev* 55, 583-586.
- Hammond C. (2001) Cellular and Molecular Neurobiology. Second edition, Academic Press.
- Han J., Truell J., Gnatenco C. and Kim D. (2002) Characterization of four types of background potassium channels in rat cerebellar granule neurons. *J Physiol* 542, 431-444.
- Hartness M. E., Lewis A., Searle G. J., O'Kelly I., Peers C. and Kemp P. J. (2001) Combined antisense and pharmacological approaches implicate hTASK as an airway O<sub>2</sub> sensing K<sup>+</sup> channel. *J Biol Chem* 276, 26499-26508.
- Heurteaux C., Guy N., Laigle C., Blondeau N., Duprat F., Mazzuca M., Lang-Lazdunski L., Widmann C., Zanzouri M., Romey G. and Lazdunski M. (2004) TREK-1, a K<sup>+</sup> channel involved in neuroprotection and general anesthesia. *Embo J* 23, 2684-2695.
- Hille B. (2001) Ion Channels of Excitable Membranes. Third edition, Sinauer Associates, Inc.
- Hirano M., Imaizumi Y., Muraki K., Yamada A. and Watanabe M. (1998) Effects of ruthenium red on membrane ionic currents in urinary bladder smooth muscle cells of the guinea-pig. *Pflugers Arch* 435, 645-653.
- Hsu K., Seharaseyon J., Dong P., Bour S. and Marban E. (2004) Mutual functional destruction of HIV-1 Vpu and host TASK-1 channel. *Mol Cell* 14, 259-267.
- Iturriaga R. and Alcayaga J. (2004) Neurotransmission in the carotid body: transmitters and modulators between glomus cells and petrosal ganglion nerve terminals. *Brain Res Brain Res Rev* 47, 46-53.
- Jezzini S. H. and Moroz L. L. (2004) Identification and distribution of a two-pore domain potassium channel in the CNS of *Aplysia californica*. *Brain Res Mol Brain Res* 127, 27-38.
- Jones A., Korpi E. R., McKernan R. M., Pelz R., Nusser Z., Makela R., Mellor J. R., Pollard S., Bahn S., Stephenson F. A., Randall A. D., Sieghart W., Somogyi P., Smith A. J. and Wisden W. (1997) Ligand-gated ion channel subunit partnerships: GABA<sub>A</sub> receptor alpha6 subunit gene inactivation inhibits delta subunit expression. *J Neurosci* 17, 1350-1362.
- Jurd R., Arras M., Lambert S., Drexler B., Sieghart R., Crestani F., Zaugg M., Vogt K. E., Ledermann B., Antkowiak B. and Rudolph U. (2003) General anesthetic actions in vivo strongly attenuated by a point mutation in the GABA(A) receptor beta3 subunit. *Faseb J* 17, 250-252.
- Kandel E. R., Schwartz J. H. and Jessell T. M. (2000) Principles of Neural Sciences. Fourth edition, McGraw-Hill Companies, Inc.
- Kang D., Mariash E. and Kim D. (2004a) Functional expression of TRESK-2, a new member of the tandem-pore K<sup>+</sup> channel family. *J Biol Chem* 279, 28063-28070.
- Kang D., Han J., Talley E. M., Bayliss D. A. and Kim D. (2004b) Functional expression of TASK-1/TASK-3 heteromers in cerebellar granule cells. *J Physiol* 554, 64-77.
- Kanjhan R., Anselme A. M., Noakes P. G. and Bellingham M. C. (2004) Postnatal changes in TASK-1 and TREK-1 expression in rat brain stem and cerebellum. *Neuroreport* 15, 1321-1324.

- Karschin C., Wischmeyer E., Preisig-Muller R., Rajan S., Derst C., Grzeschik K. H., Daut J. and Karschin A. (2001) Expression pattern in brain of TASK-1, TASK-3, and a tandem pore domain K<sup>+</sup> channel subunit, TASK-5, associated with the central auditory nervous system. *Mol Cell Neurosci* 18, 632-648.
- Kennard L. E., Chumbley J. R., Ranatunga K. M., Armstrong S. J., Veale E. L. and Mathie A. (2005) Inhibition of the human two-pore domain potassium channel, TREK-1, by fluoxetine and its metabolite norfluoxetine. *Br J Pharmacol* 144, 821-829.
- Ketchum K. A., Joiner W. J., Sellers A. J., Kaczmarek L. K. and Goldstein S. A. (1995) A new family of outwardly rectifying potassium channel proteins with two pore domains in tandem. *Nature* 376, 690-695.
- Kim D., Fujita A., Horio Y. and Kurachi Y. (1998) Cloning and functional expression of a novel cardiac two-pore background K<sup>+</sup> channel (cTBAK-1). *Circ Res* 82, 513-518.
- Kim D. and Gnatenco C. (2001) TASK-5, a new member of the tandem-pore K<sup>+</sup> channel family. *Biochem Biophys Res Commun* 284, 923-930.
- Kim D. (2003) Fatty acid-sensitive two-pore domain K<sup>+</sup> channels. *Trends Pharmacol Sci* 24, 648-654.
- Kim Y., Bang H. and Kim D. (2000) TASK-3, a new member of the tandem pore K<sup>+</sup> channel family. *J Biol Chem* 275, 9340-9347.
- Kim Y., Bang H., Gnatenco C. and Kim D. (2001a) Synergistic interaction and the role of C-terminus in the activation of TRAAK K<sup>+</sup> channels by pressure, free fatty acids and alkali. *Pflugers Arch* 442, 64-72.
- Kim Y., Gnatenco C., Bang H. and Kim D. (2001b) Localization of TREK-2 K<sup>+</sup> channel domains that regulate channel kinetics and sensitivity to pressure, fatty acids and pH. *Pflugers Arch* 442, 952-960.
- Koh S. D., Monaghan K., Sergeant G. P., Ro S., Walker R. L., Sanders K. M. and Horowitz B. (2001) TREK-1 regulation by nitric oxide and cGMP-dependent protein kinase. An essential role in smooth muscle inhibitory neurotransmission. *J Biol Chem* 276, 44338-44346.
- Larkman P. M. and Perkins E. M. (2005) A TASK-like pH- and amine-sensitive 'leak' K<sup>+</sup> conductance regulates neonatal rat facial motoneuron excitability in vitro. *Eur J Neurosci* 21, 679-691.
- Lauritzen I., Zanzouri M., Honoré E., Duprat F., Ehrengruber M. U., Lazdunski M. and Patel A. J. (2003) K<sup>+</sup>-dependent cerebellar granule neuron apoptosis. Role of task leak K<sup>+</sup> channels. *J Biol Chem* 278, 32068-32076.
- Lee Y. M., Kim B. J., Chun Y. S., So I., Choi H., Kim M. S. and Park J. W. (2005) NOX4 as an oxygen sensor to regulate TASK-1 activity. *Cell Signal* in press
- Leonoudakis D., Gray A. T., Winegar B. D., Kindler C. H., Harada M., Taylor D. M., Chavez R. A., Forsayeth J. R. and Yost C. S. (1998) An open rectifier potassium channel with two pore domains in tandem cloned from rat cerebellum. *J Neurosci* 18, 868-877.
- Lesage F., Reyes R., Fink M., Duprat F., Guillemare E. and Lazdunski M. (1996a) Dimerization of TWIK-1 K<sup>+</sup> channel subunits via a disulfide bridge. *Embo J* 15, 6400-6407.
- Lesage F., Guillemare E., Fink M., Duprat F., Lazdunski M., Romey G. and Barhanin J. (1996b) TWIK-1, a ubiquitous human weakly inward rectifying K<sup>+</sup> channel with a novel structure. *Embo J* 15, 1004-1011.
- Lesage F., Maingret F. and Lazdunski M. (2000a) Cloning and expression of human TRAAK, a polyunsaturated fatty acids-activated and mechano-sensitive K<sup>+</sup> channel. *FEBS Lett* 471, 137-140.
- Lesage F., Terrenoire C., Romey G. and Lazdunski M. (2000b) Human TREK2, a 2P domain mechano-sensitive K<sup>+</sup> channel with multiple regulations by polyunsaturated fatty acids, lysophospholipids, and Gs, Gi, and Gq protein-coupled receptors. *J Biol Chem* 275, 28398-28405.
- Lesage F. (2003) Pharmacology of neuronal background potassium channels. *Neuropharmacology* 44, 1-7.

- Linden A. M., Aller I. M., Vekovischeva O., Lepp E., Rosenberg P. H., Wisden W. and Korpi E. R. (2004) Sensitivity of K<sup>+</sup> channel TASK-1 deficient mice to anesthetics isoflurane and propofol. *Society for Neuroscience, Online Program No. 966.1*.
- Liu C., Au J. D., Zou H. L., Cotten J. F. and Yost C. S. (2004) Potent activation of the human tandem pore domain K channel TREK with clinical concentrations of volatile anesthetics. *Anesth Analg* 99, 1715-1722, table of contents.
- Liu C., Cotten J. F., Schuyler J. A., Fahlman C. S., Au J. D., Bickler P. E. and Yost C. S. (2005) Protective effects of TASK-3 (KCNK9) and related 2P K channels during cellular stress. *Brain Res* 1031, 164-173.
- Long S. B., Campbell E. B. and Mackinnon R. (2005) Crystal structure of a mammalian voltage-dependent Shaker family K<sup>+</sup> Channel. *Science*, 309, 897-903.
- Lopes C. M., Gallagher P. G., Buck M. E., Butler M. H. and Goldstein S. A. (2000) Proton block and voltage gating are potassium-dependent in the cardiac leak channel Kcnk3. *J Biol Chem* 275, 16969-16978.
- Lopes C. M., Rohacs T., Czirjak G., Balla T., Enyedi P. and Logothetis D. E. (2005) PIP2 hydrolysis underlies agonist-induced inhibition and regulates voltage gating of two-pore domain K<sup>+</sup> channels. *J Physiol* 564, 117-129.
- Lopez-Barneo J., Lopez-Lopez J. R., Urena J. and Gonzalez C. (1988) Chemotransduction in the carotid body: K<sup>+</sup> current modulated by PO<sub>2</sub> in type I chemoreceptor cells. *Science* 241, 580-582.
- Lossi L., Mioletti S. and Merighi A. (2002) Synapse-independent and synapse-dependent apoptosis of cerebellar granule cells in postnatal rabbits occur at two subsequent but partly overlapping developmental stages. *Neuroscience* 112, 509-523.
- Maingret F., Fosset M., Lesage F., Lazdunski M. and Honoré E. (1999a) TRAAK is a mammalian neuronal mechano-gated K<sup>+</sup> channel. *J Biol Chem* 274, 1381-1387.
- Maingret F., Patel A. J., Lesage F., Lazdunski M. and Honoré E. (1999b) Mechano- or acid stimulation, two interactive modes of activation of the TREK-1 potassium channel. *J Biol Chem* 274, 26691-26696.
- Maingret F., Patel A. J., Lesage F., Lazdunski M. and Honoré E. (2000) Lysophospholipids open the two-pore domain mechano-gated K<sup>+</sup> channels TREK-1 and TRAAK. *J Biol Chem* 275, 10128-10133.
- Maingret F., Patel A. J., Lazdunski M. and Honoré E. (2001) The endocannabinoid anandamide is a direct and selective blocker of the background K<sup>+</sup> channel TASK-1. *Embo J* 20, 47-54.
- Manley N. R., Barrow J. R., Zhang T. and Capecchi M. R. (2001) Hoxb2 and hoxb4 act together to specify ventral body wall formation. *Dev Biol* 237, 130-144.
- Mann-Metzer P. and Yarom Y. (1999) Electrotonic coupling interacts with intrinsic properties to generate synchronized activity in cerebellar networks of inhibitory interneurons. *J Neurosci* 19, 3298-3306.
- Marx J. (2005) Cell biology. SUMO wrestles its way to prominence in the cell. *Science* 307, 836-839.
- Mathie A. and Clarke C. E. (2002) Background potassium channels move into focus. *J Physiol* 542, 334.
- Mathie A., Clarke C. E., Ranatunga K. M. and Veale E. L. (2003) What are the roles of the many different types of potassium channel expressed in cerebellar granule cells? *Cerebellum* 2, 11-25.
- McCormick D. A. (1992) Neurotransmitter actions in the thalamus and cerebral cortex and their role in neuromodulation of thalamocortical activity. *Prog Neurobiol* 39, 337-388.
- Meadows H. J. and Randall A. D. (2001) Functional characterisation of human TASK-3, an acid-sensitive two-pore domain potassium channel. *Neuropharmacology* 40, 551-559.

- Meadows H. J., Benham C. D., Cairns W., Gloger I., Jennings C., Medhurst A. D., Murdock P. and Chapman C. G. (2000) Cloning, localisation and functional expression of the human orthologue of the TREK-1 potassium channel. *Pflugers Arch* 439, 714-722.
- Melchior F., Schergaut M. and Pichler A. (2003) SUMO: ligases, isopeptidases and nuclear pores. *Trends Biochem Sci* 28, 612-618.
- Mellor J. R., Merlo D., Jones A., Wisden W. and Randall A. D. (1998) Mouse cerebellar granule cell differentiation: electrical activity regulates the GABA<sub>A</sub> receptor alpha 6 subunit gene. *J Neurosci* 18, 2822-2833.
- Meuth S. G., Budde T., Kanyshkova T., Broicher T., Munsch T. and Pape H. C. (2003) Contribution of TWIK-related acid-sensitive K<sup>+</sup> channel 1 (TASK1) and TASK3 channels to the control of activity modes in thalamocortical neurons. *J Neurosci* 23, 6460-6469.
- Millar J. A., Barratt L., Southan A. P., Page K. M., Fyffe R. E., Robertson B. and Mathie A. (2000) A functional role for the two-pore domain potassium channel TASK-1 in cerebellar granule neurons. *Proc Natl Acad Sci U S A* 97, 3614-3618.
- Mu D., Chen L., Zhang X., See L. H., Koch C. M., Yen C., Tong J. J., Spiegel L., Nguyen K. C., Servoss A., Peng Y., Pei L., Marks J. R., Lowe S., Hoey T., Jan L. Y., McCombie W. R., Wigler M. H. and Powers S. (2003) Genomic amplification and oncogenic properties of the KCNK9 potassium channel gene. *Cancer Cell* 3, 297-302.
- Muller S., Hoege C., Pyrowolakis G. and Jentsch S. (2001) SUMO, ubiquitin's mysterious cousin. *Nat Rev Mol Cell Biol* 2, 202-210.
- Nicoll R. A., Malenka R. C. and Kauer J. A. (1990) Functional comparison of neurotransmitter receptor subtypes in mammalian central nervous system. *Physiol Rev* 70, 513-565.
- North R. A. (2000) Potassium-channel closure taken to TASK. *Trends Neurosci* 23, 234-235.
- Nusser Z., Ahmad Z., Tretter V., Fuchs K., Wisden W., Sieghart W. and Somogyi P. (1999) Alterations in the expression of GABA<sub>A</sub> receptor subunits in cerebellar granule cells after the disruption of the alpha6 subunit gene. *Eur J Neurosci* 11, 1685-1697.
- O'Kelly I., Stephens R. H., Peers C. and Kemp P. J. (1999) Potential identification of the O<sub>2</sub>-sensitive K<sup>+</sup> current in a human neuroepithelial body-derived cell line. *Am J Physiol* 276, L96-L104.
- O'Kelly I., Butler M. H., Zilberberg N. and Goldstein S. A. (2002) Forward transport. 14-3-3 binding overcomes retention in endoplasmic reticulum by dibasic signals. *Cell* 111, 577-588.
- Olsen E. N., Arnold H. H., Rigby P. W. and Wold B. J. (1996) Know your neighbors: three phenotypes in null mutants of myogenic bHLH gene MRF4. *Cell* 85, 1-4.
- Pardo L. A., del Camino D., Sanchez A., Alves F., Bruggemann A., Beckh S. and Stuhmer W. (1999) Oncogenic potential of EAG K<sup>+</sup> channels. *Embo J* 18, 5540-5547.
- Patel A. J., Honoré E., Maingret F., Lesage F., Fink M., Duprat F. and Lazdunski M. (1998) A mammalian two pore domain mechano-gated S-like K<sup>+</sup> channel. *Embo J* 17, 4283-4290.
- Patel A. J., Honoré E., Lesage F., Fink M., Romey G. and Lazdunski M. (1999) Inhalational anesthetics activate two-pore-domain background K<sup>+</sup> channels. *Nat Neurosci* 2, 422-426.
- Patel A. J., Maingret F., Magnone V., Fosset M., Lazdunski M. and Honoré E. (2000) TWIK-2, an inactivating 2P domain K<sup>+</sup> channel. *J Biol Chem* 275, 28722-28730.
- Patel A. J. and Honoré E. (2001a) Properties and modulation of mammalian 2P domain K<sup>+</sup> channels. *Trends Neurosci* 24, 339-346.
- Patel A. J., Lazdunski M. and Honoré E. (2001b) Lipid and mechano-gated 2P domain K<sup>+</sup> channels. *Curr Opin Cell Biol* 13, 422-428.

- Pei L., Wiser O., Slavin A., Mu D., Powers S., Jan L. Y. and Hoey T. (2003) Oncogenic potential of TASK3 (Kcnk9) depends on K<sup>+</sup> channel function. *Proc Natl Acad Sci U S A* 100, 7803-7807.
- Pham C. T., MacIvor D. M., Hug B. A., Heusel J. W. and Ley T. J. (1996) Long-range disruption of gene expression by a selectable marker cassette. *Proc Natl Acad Sci U S A* 93, 13090-13095.
- Plant L. D., Kemp P. J., Peers C., Henderson Z. and Pearson H. A. (2002) Hypoxic depolarization of cerebellar granule neurons by specific inhibition of TASK-1. *Stroke* 33, 2324-2328.
- Plant L. D., Rajan S. and Goldstein S. A. (2005) K2P channels and their protein partners. *Curr Opin Neurobiol* 15, 326-333.
- Rajan S., Wischmeyer E., Xin Liu G., Preisig-Muller R., Daut J., Karschin A. and Derst C. (2000) TASK-3, a novel tandem pore domain acid-sensitive K<sup>+</sup> channel. An extracellular histidine as pH sensor. *J Biol Chem* 275, 16650-16657.
- Rajan S., Wischmeyer E., Karschin C., Preisig-Muller R., Grzeschik K. H., Daut J., Karschin A. and Derst C. (2001) THIK-1 and THIK-2, a novel subfamily of tandem pore domain K<sup>+</sup> channels. *J Biol Chem* 276, 7302-7311.
- Rajan S., Preisig-Muller R., Wischmeyer E., Nehring R., Hanley P. J., Renigunta V., Musset B., Schlichthorl G., Derst C., Karschin A. and Daut J. (2002) Interaction with 14-3-3 proteins promotes functional expression of the potassium channels TASK-1 and TASK-3. *J Physiol* 545, 13-26.
- Rajan S., Plant L. D., Rabin M. L., Butler M. H. and Goldstein S. A. (2005) Sumoylation silences the plasma membrane leak K<sup>+</sup> channel K2P1. *Cell* 121, 37-47.
- Rekling J. C., Funk G. D., Bayliss D. A., Dong X. W. and Feldman J. L. (2000) Synaptic control of motoneuronal excitability. *Physiol Rev* 80, 767-852.
- Reyes R., Duprat F., Lesage F., Fink M., Salinas M., Farman N. and Lazdunski M. (1998) Cloning and expression of a novel pH-sensitive two pore domain K<sup>+</sup> channel from human kidney. *J Biol Chem* 273, 30863-30869.
- Rodriguez C. I., Buchholz F., Galloway J., Sequerra R., Kasper J., Ayala R., Stewart A. F. and Dymecki S. M. (2000) High-efficiency deleter mice show that FLPe is an alternative to Cre-loxP. *Nat Genet* 25, 139-140.
- Rogers D. C., Fisher E. M., Brown S. D., Peters J., Hunter A. J. and Martin J. E. (1997) Behavioral and functional analysis of mouse phenotype: SHIRPA, a proposed protocol for comprehensive phenotype assessment. *Mamm Genome* 8, 711-713.
- Rudolph U. and Antkowiak B. (2004) Molecular and neuronal substrates for general anaesthetics. *Nat Rev Neurosci* 5, 709-720.
- Salinas M., Reyes R., Lesage F., Fosset M., Heurteaux C., Romey G. and Lazdunski M. (1999) Cloning of a new mouse two-P domain channel subunit and a human homologue with a unique pore structure. *J Biol Chem* 274, 11751-11760.
- Salkoff L., Butler A., Fawcett G., Kunkel M., McArdle C., Paz-y-Mino G., Nonet M., Walton N., Wang Z. W., Yuan A. and Wei A. (2001) Evolution tunes the excitability of individual neurons. *Neuroscience* 103, 853-859.
- Sambrook J. and Russell D. (2000) *Molecular cloning: A laboratory Manual*. Third edition, Cold Spring Harbor Laboratory Press.
- Sano Y., Inamura K., Miyake A., Mochizuki S., Kitada C., Yokoi H., Nozawa K., Okada H., Matsushime H. and Furuichi K. (2003) A novel two-pore domain K<sup>+</sup> channel, TRESK, is localized in the spinal cord. *J Biol Chem* 278, 27406-27412.
- Saper C. B. and Sawchenko P. E. (2003) Magic peptides, magic antibodies: guidelines for appropriate controls for immunohistochemistry. *J Comp Neurol* 465, 161-163.

- Schrader L. A. and Tasker J. G. (1997) Modulation of multiple potassium currents by metabotropic glutamate receptors in neurons of the hypothalamic supraoptic nucleus. *J Neurophysiol* 78, 3428-3437.
- Schweitzer P., Madamba S. G. and Siggins G. R. (1998) Somatostatin increases a voltage-insensitive K<sup>+</sup> conductance in rat CA1 hippocampal neurons. *J Neurophysiol* 79, 1230-1238.
- Single F. N., Rozov A., Burnashev N., Zimmermann F., Hanley D. F., Forrest D., Curran T., Jensen V., Hvalby O., Sprengel R. and Seeburg P. H. (2000) Dysfunctions in mice by NMDA receptor point mutations NR1(N598Q) and NR1(N598R). *J Neurosci* 20, 2558-2566.
- Sirois J. E., Lei Q., Talley E. M., Lynch C., 3rd and Bayliss D. A. (2000) The TASK-1 two-pore domain K<sup>+</sup> channel is a molecular substrate for neuronal effects of inhalation anesthetics. *J Neurosci* 20, 6347-6354.
- Smithies O. (2005) Many little things: one geneticist's view of complex diseases. *Nat Rev Genet* 6, 419-425.
- Talley E. M., Lei Q., Sirois J. E. and Bayliss D. A. (2000) TASK-1, a two-pore domain K<sup>+</sup> channel, is modulated by multiple neurotransmitters in motoneurons. *Neuron* 25, 399-410.
- Talley E. M., Solorzano G., Lei Q., Kim D. and Bayliss D. A. (2001) CNS distribution of members of the two-pore-domain (KCNK) potassium channel family. *J Neurosci* 21, 7491-7505.
- Talley E. M. and Bayliss D. A. (2002) Modulation of TASK-1 (Kcnk3) and TASK-3 (Kcnk9) potassium channels: volatile anesthetics and neurotransmitters share a molecular site of action. *J Biol Chem* 277, 17733-17742.
- Talley E. M., Sirois J. E., Lei Q. and Bayliss D. A. (2003) Two-pore-domain (KCNK) potassium channels: dynamic roles in neuronal function. *Neuroscientist* 9, 46-56.
- Thompson J. D., Higgins D. G. and Gibson T. J. (1994) CLUSTAL W: improving the sensitivity of progressive multiple sequence alignment through sequence weighting, position-specific gap penalties and weight matrix choice. *Nucleic Acids Res* 22, 4673-4680.
- Uusi-Oukari M., Heikkilä J., Sinkkonen S. T., Makela R., Hauer B., Homanics G. E., Sieghart W., Wisden W. and Korpi E. R. (2000) Long-range interactions in neuronal gene expression: evidence from gene targeting in the GABA(A) receptor beta2-alpha6-alpha1-gamma2 subunit gene cluster. *Mol Cell Neurosci* 16, 34-41.
- Vega-Saenz de Miera E., Lau D. H. P., Zhadina M., Pountney D., Coetzee W. A. and Rudy B. (2001) KT3.2 and KT3.3, two novel human two-pore K<sup>+</sup> channels closely related to TASK-1. *J Neurophysiol* 86, 130-142.
- Vekovischeva O. Y., Aitta-Aho T., Echenko O., Kankaanpää A., Seppala T., Honkanen A., Sprengel R. and Korpi E. R. (2004) Reduced aggression in AMPA-type glutamate receptor GluR-A subunit-deficient mice. *Genes Brain Behav* 3, 253-265.
- Wang H., Zhang Y., Cao L., Han H., Wang J., Yang B., Nattel S. and Wang Z. (2002) HERG K<sup>+</sup> channel, a regulator of tumor cell apoptosis and proliferation. *Cancer Res* 62, 4843-4848.
- Warth R., Barriere H., Meneton P., Bloch M., Thomas J., Tauc M., Heitzmann D., Romeo E., Verrey F., Mengual R., Guy N., Bendahhou S., Lesage F., Poujeol P. and Barhanin J. (2004) Proximal renal tubular acidosis in TASK2 K<sup>+</sup> channel-deficient mice reveals a mechanism for stabilizing bicarbonate transport. *Proc Natl Acad Sci U S A* 101, 8215-8220.
- Washburn C. P., Sirois J. E., Talley E. M., Guyenet P. G. and Bayliss D. A. (2002) Serotonergic raphe neurons express TASK channel transcripts and a TASK-like pH- and halothane-sensitive K<sup>+</sup> conductance. *J Neurosci* 22, 1256-1265.
- Watkins C. S. and Mathie A. (1996) A non-inactivating K<sup>+</sup> current sensitive to muscarinic receptor activation in rat cultured cerebellar granule neurons. *J Physiol* 491, 401-412.
- Wei A., Jegla T. and Salkoff L. (1996) Eight potassium channel families revealed by the *C. elegans* genome project. *Neuropharmacology* 35, 805-829.

- White B. H., Osterwalder T. P., Yoon K. S., Joiner W. J., Whim M. D., Kaczmarek L. K. and Keshishian H. (2001) Targeted attenuation of electrical activity in *Drosophila* using a genetically modified K<sup>+</sup> channel. *Neuron* 31, 699-711.
- Williams B. A. and Buckler K. J. (2004) Biophysical properties and metabolic regulation of a TASK-like potassium channel in rat carotid body type 1 cells. *Am J Physiol Lung Cell Mol Physiol* 286, L221-230.
- Williams-Simons L. and Westphal H. (1999) EIIaCre - utility of a general deleter strain. *Transgenic Res* 8, 53-54.
- Winegar B. D., Owen D. F., Yost C. S., Forsayeth J. R. and Mayeri E. (1996) Volatile general anesthetics produce hyperpolarization of *Aplysia* neurons by activation of a discrete population of baseline potassium channels. *Anesthesiology* 85, 889-900.
- Wisden W., Parker E. M., Mahle C. D., Grisel D. A., Nowak H. P., Yocca F. D., Felder C. C., Seeburg P. H. and Voigt M. M. (1993) Cloning and characterization of the rat 5-HT5B receptor. Evidence that the 5-HT5B receptor couples to a G protein in mammalian cell membranes. *FEBS Lett* 333, 25-31.
- Wisden W. and Morris B. J. (1994) *In situ* hybridisation with synthetic oligonucleotide probes. In: *In situ* hybridisation protocols for the brain, W. Wisden and B.J. Morris editors, London: Academic Press
- Wood K. A., Dipasquale B. and Youle R. J. (1993) *In situ* labeling of granule cells for apoptosis-associated DNA fragmentation reveals different mechanisms of cell loss in developing cerebellum. *Neuron* 11, 621-632.
- Wu S. N., Jan C. R. and Li H. F. (1999) Ruthenium red-mediated inhibition of large-conductance Ca<sup>2+</sup>-activated K<sup>+</sup> channels in rat pituitary GH3 cells. *J Pharmacol Exp Ther* 290, 998-1005.
- Yamamoto Y., Kummer W., Atoji Y. and Suzuki Y. (2002) TASK-1, TASK-2, TASK-3 and TRAAK immunoreactivities in the rat carotid body. *Brain Res* 950, 304-307.
- Young L. J., Nilsen R., Waymire K. G., MacGregor G. R. and Insel T. R. (1999) Increased affiliative response to vasopressin in mice expressing the V1a receptor from a monogamous vole. *Nature* 400, 766-768.